Mémoire

Auteur : Read, Colin
Promoteur(s) : Martin, John
Faculté : Faculté des Sciences
Diplôme : Master en sciences physiques, à finalité approfondie
Année académique : 2022-2023
URI/URL : http://hdl.handle.net/2268.2/17875

Faculty of Science
Department of Physics

Fighting Decoherence with Dynamical Decoupling

Author : Colin READ
Supervisor : Prof. John MARTIN

Master's thesis submitted in the partial fulfillment of the requirements for the Master's degree in Physical Science.

Academic year 2022-2023

Acknowledgment

I would like to express my sincere gratitude to my supervisor, Prof. John Martin, for his invaluable guidance, expertise and incredible support throughout the year. His constant availability and willingness to provide invaluable insights allowed me to work under the best conditions. I would also like to extend my utmost appreciation to Baptiste Debeckers for his incredible help and insights which have been instrumental to the outcome of my research.

My deepest appreciation goes to the members of my reading committee, Prof. Thierry Bastin, Prof. Matthieu Verstraete and Prof. Geoffroy Lumay. I wish each and every one of them a reading as enjoyable as possible.

I also wish to thanks my family and my friends for their unwavering support, patience and encouragement throughout the entire year as well as the four previous years of my academic journey.

Contents

Introduction **9**

1 Decoherence **15**
1.1 Closed quantum system . . . 15
1.2 Open quantum system . . . 16
1.3 The spin-boson model . . . 17
1.4 Calculation of the time-evolution operator . . . 18
1.4.1 Ohmic spectral density . . . 23
1.4.2 Lorentzian spectral density . . . 24
1.5 Adding dissipation . . . 26
1.5.1 NMQSD and HOPS . . . 27
1.5.2 Decoherence using HOPS . . . 32
1.6 Discussion . . . 38

2 General Theory of Dynamical Decoupling **39**
2.1 Dynamics of a system under periodic driving . . . 39
2.2 Desired average Hamiltonian . . . 41
2.3 Control field design . . . 42
2.4 Summary . . . 43
2.5 Examples . . . 44
2.5.1 Carr-Purcell-Meiboom-Gill . . . 44
2.5.2 XY4 . . . 44
2.6 Discussion . . . 45
2.7 Cayley graph . . . 46

3 Selective Dynamical Decoupling **49**
3.1 CPMG . . . 49
3.1.1 Analytical derivation of the system's dynamics . . . 50
3.1.2 Performance of the sequence . . . 52
3.2 Optimizing the pulses temporal location . . . 58
3.2.1 Uhrig dynamical decoupling . . . 61
3.2.2 Locally optimized dynamical decoupling . . . 65
3.2.3 Optimized noise filtration through dynamical decoupling . . . 70
3.2.4 Optimized bandwidth-adapted dynamical decoupling . . . 72
3.3 Benchmarking HOPS in the context of dynamical decoupling . . . 73
3.3.1 Impact of the negative frequencies on the relative performances of DD sequences . . . 75

4 Maximal Dynamical Decoupling **79**
4.1 XY4 . . . 81
4.2 Concatenated dynamical decoupling . . . 82
4.3 Quadratic dynamical decoupling . . . 84

5 Some Important Results in the Field of Dynamical Decoupling **87**
5.1 Dynamical decoupling using bounded control strength 87
5.1.1 Proof that dynamical decoupling occurs with non-ideal pulses 87
5.1.2 Discussion 90
5.2 Errors in the control field 91

Conclusion **97**

A Moving to the Rotating Frame **103**

B Exponential of Pauli Operators **105**

C Magnus Expansion **107**

D Locally Optimized Dynamical Decoupling for More than Four Pulses **109**

E Convergence of the HOPS Method **115**
E.1 Dephasing qubit 115
E.2 Maximal dynamical decoupling sequences 117

List of Acronyms

A great number of acronyms are introduced throughout this Master's thesis. This section regroups every one of them, presented in alphabetical order. For each one, we write what the acronym stands for as well as a brief definition or explanation on the matter.

BADD Bandwidth-Adapted Dynamical Decoupling. Sequence obtained by minimization of the infidelity with a minimal pulse separation as a constraint.

CDD Concatenated Dynamical Decoupling. DD sequences created by concatenating two smaller sequences.

CPMG Carr-Purcell-Meiboom-Gill. The first DD sequence, consisting of equidistant spin-flips and aiming at suppressing pure dephasing.

DD Dynamical Decoupling. An Hamiltonian Engineering schemes that averages out a specific part of the Hamiltonian using a specific sequence of pulses.

DFS Decoherence-Free Subspaces. Subspace of the total Hilbert space unaffected by decoherence up to a global phase factor.

HOPS Hierarchy Of Pure States. A reformulation of the NMQSD equation which aims at avoiding the computational cost resulting from the functional derivative that appear in the equation.

KDD Knill Dynamical Decoupling. Sequence of composite pulses constructed to increase the robustness of XY4 to systematic errors in the control field.

LODD Locally Optimized Dynamical Decoupling. Sequence obtained by minimization of the infidelity using a minimization algorithm.

MAXDD Maximal Dynamical Decoupling. DD strategy which aims at averaging out all possible dynamics.

NMQSD Non-Markovian Quantum State Diffusion. A stochastic method used to study non-markovian dynamics of a quantum system interacting with a bosonic field.

OFDD Optimized Noise Filtration Dynamical Decoupling. Sequence obtained by minimization of the integral over the filter function using a minimization algorithm.

QDD Quadratic Dynamical Decoupling. Sequence analytically constructed by concatenation of UDD sequences.

QEC Quantum Error Correction. Strategy to correct quantum errors after they occurred by detecting them (using measurement schemes) and figuring out the correct recovery operation.

QEM Quantum Error Mitigation. Strategy to avoid quantum errors. Some examples of such schemes are DFS and DD.

SD Spectral Density. A distribution that characterizes how much a quantum system is coupled to each frequency of the bosonic bath that models the environment.

SELDD Selective Dynamical Decoupling. DD strategy which aims at averaging out specific dynamics, leaving some useful dynamics left for computation purposes.

SELKDD Selective Knill Dynamical Decoupling. sequence of composite pulses constructed to increase the robustness of CPMG to systematic errors in the control field.

UDD Uhrig Dynamical Decoupling. Sequence of non-equidistant pulses which achieves the highest possible filtering for low frequencies.

URDD Universally Robust Dynamical Decoupling. Sequence constructed by optimizing the phase of the pulses in order to increase the robustness.

XY4 This does not really stand for something. XY4 is a sequence composed of spin-flips and phase-flips and is the first MAXDD strategy constructed.

Introduction

It is a well-known fact that quantum mechanics allows quantum systems to be in coherent superposition of states. Let us take a two-level system to explain what is meant by this statement. This system possesses two levels of energy and thus two basis states: a ground state $|g\rangle$ of lesser energy and an excited state $|e\rangle$ of higher energy. Classically, the system can only be in one of the two states. The classical *state space* of the system then consists of the two basis states $|g\rangle$ and $|e\rangle$. Quantum physics, however, allows for a much bigger state space that we call the *Hilbert space*. According to quantum physics, any linear combination of these two states, provided that the norm of the state $|\psi\rangle$ is equal to 1, is a perfectly valid state of the quantum system. That is, the most general state of a two-level quantum system can be written as $|\psi\rangle = \alpha\,|g\rangle + \beta\,|e\rangle$ with α and β two complex numbers that satisfy the condition $|\alpha|^2 + |\beta|^2 = 1$. These states are called *coherent superposition of states*. The particularity of these superposed quantum states is that they hold *hidden* quantum information in the complex numbers α and β. In fact, measuring the system would result in the state $|g\rangle$ being measured with probability $|\alpha|^2$ or $|e\rangle$ with probability $|\beta|^2$. After the measurement, the state will either collapse to $|g\rangle$ or $|e\rangle$ and the information stored in α and β will be destroyed. This hidden quantum information can thus not be directly measured, and hence can be considered *hidden* to our reality, but definitely bear verifiable consequences which can be exploited. The discussion above takes as an example the most elementary building block for the storage and processing of quantum information, a two-level quantum system that we call a *quantum bit*, or *qubit*, but a similar discussion can be made with an arbitrary d-level quantum system with $d > 2$; we then talk of *qudit*.

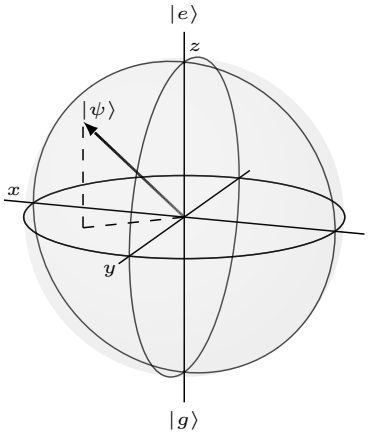

Figure 1: The so-called *Bloch sphere* provides a nice geometrical representation of the state of a qubit $|\psi\rangle = \cos(\theta/2)\,|e\rangle + e^{i\varphi}\sin(\theta/2)\,|g\rangle$ where the parameters α, β have been traded with the polar and azimuthal angles θ and φ. This figure was created using the LaTeXpackage *blochsphere*.

Let us now consider two qubits instead of one. Classically, four states are allowed: $|g_1g_2\rangle$, $|g_1e_2\rangle$, $|e_1g_2\rangle$ and $|e_1e_2\rangle$. Quantum mechanically, as in the previous case, the state space is much bigger and all coherent superpositions of these four states are valid. This allows for strange but interesting states such as the Bell state $|\psi\rangle = \frac{1}{\sqrt{2}}(|g_1g_2\rangle + |e_1e_2\rangle)$. As in the previous case, a measurement on the first qubit would result in

the state $|g_1\rangle$ or $|e_1\rangle$ being measured with probability $\frac{1}{2}$. However, after the measurement, the total state will either collapse to $|g_1g_2\rangle$ or $|e_1e_2\rangle$ depending on the result, which leads to the strange conclusion that a measurement on the first qubit has instantaneously affected the second qubit. This leads to correlation between the measurement of the first and second qubit that would not occur if the system was treated classically: the two qubits are said to be *entangled* and, similarly, the quantum state is called an entangled state. Quantum entanglement is a strange property that has no counterpart in classical physics.

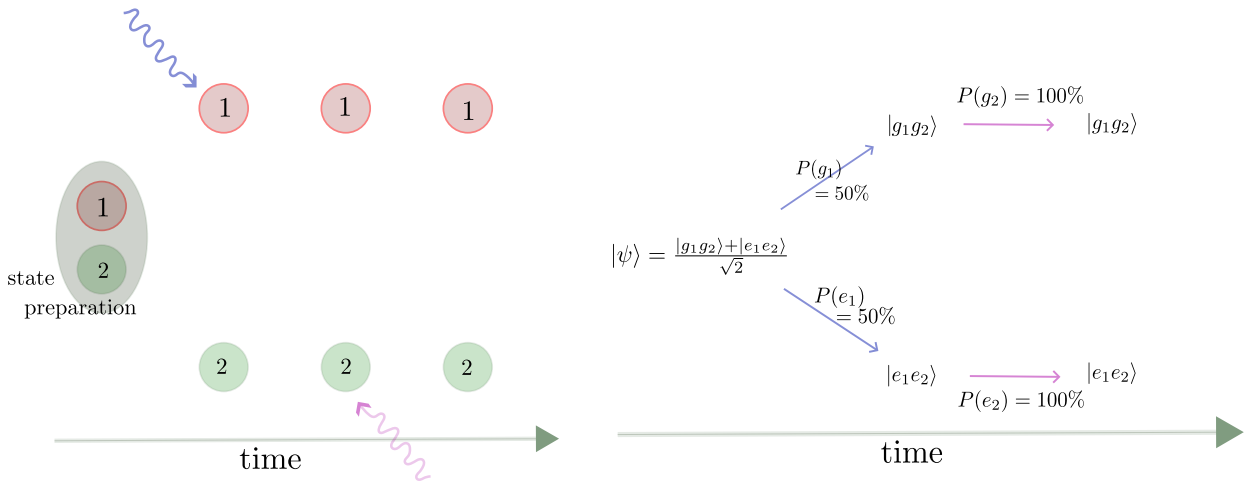

Figure 2: Representation of the non-classical correlation between two consecutive measurements of entangled qubits. When the first qubit is measured, there is a 50% chance for the ground state or the excited state to be measured and the wave function collapses to either $|g_1g_2\rangle$ or $|e_1e_2\rangle$ depending on the outcome. Because of this wave function collapse, the probabilities of each outcome of the measurement on the second qubit is affected by the outcome of the first measurement.

Those so-called entangled states are now commonly used to enable new scientific advances and the creation of new quantum technologies; many fields of research are taking advantage of entanglement and therefore depend on the reliability on which those states can be prepared, maintained and controlled [1,2]. Such areas of research are, for instance, the fields of quantum metrology, where highly non-classical states are used to perform precision measurements [3–5], or quantum cryptography [6,7]. But one of the most famous field of study relying on entanglement of quantum systems is certainly quantum information processing [8], which makes use of entangled states to perform computation with quantum algorithms that offer significant speed up over their classical counterparts.

However, those non-classical states of quantum systems on which various quantum technologies rely are unstable due to unwanted interaction with their environment. Because of the undesirable coupling between the system and its environment, quantum states degrade from a coherent superposition of states to a mixture of states, destroying the quantum information stored in the system as well as the useful entanglement properties. We say that the quantum system *relaxes*. If the relaxation occurs due to dissipation of energy, we say that the relaxation is *longitudinal* and the relaxation rate is characterized by the relaxation time T_1. On the other hand, if the relaxation occurs due to *pure dephasing*, that is without dissipation of energy, the relaxation is *transverse* and characterized by a relaxation time T_2. This process is called *decoherence* [9–11] and critically limits the performance of current quantum technologies. Qubits of a quantum computer become unreliable after a certain time, causing the proliferation of errors throughout the computation, for instance. Accordingly, the relaxation times T_1 and T_2 are two of the fundamental quantities that characterize the quality of a qubit implementation. Some promising qubit implementations and the maximal longevity obtained with such implementations are summarized in Fig.3. This coherence loss due to unwanted coupling stands as a huge obstacle for all technology that makes use of quantum information and quantum entanglement and great efforts have been made to address this problem. Numerous schemes have been developed in the

past decades to extend the lifetime of qubits and qudits. The two main strategies to fight decoherence are *Quantum Error Correction* and *Quantum Error Mitigation*.

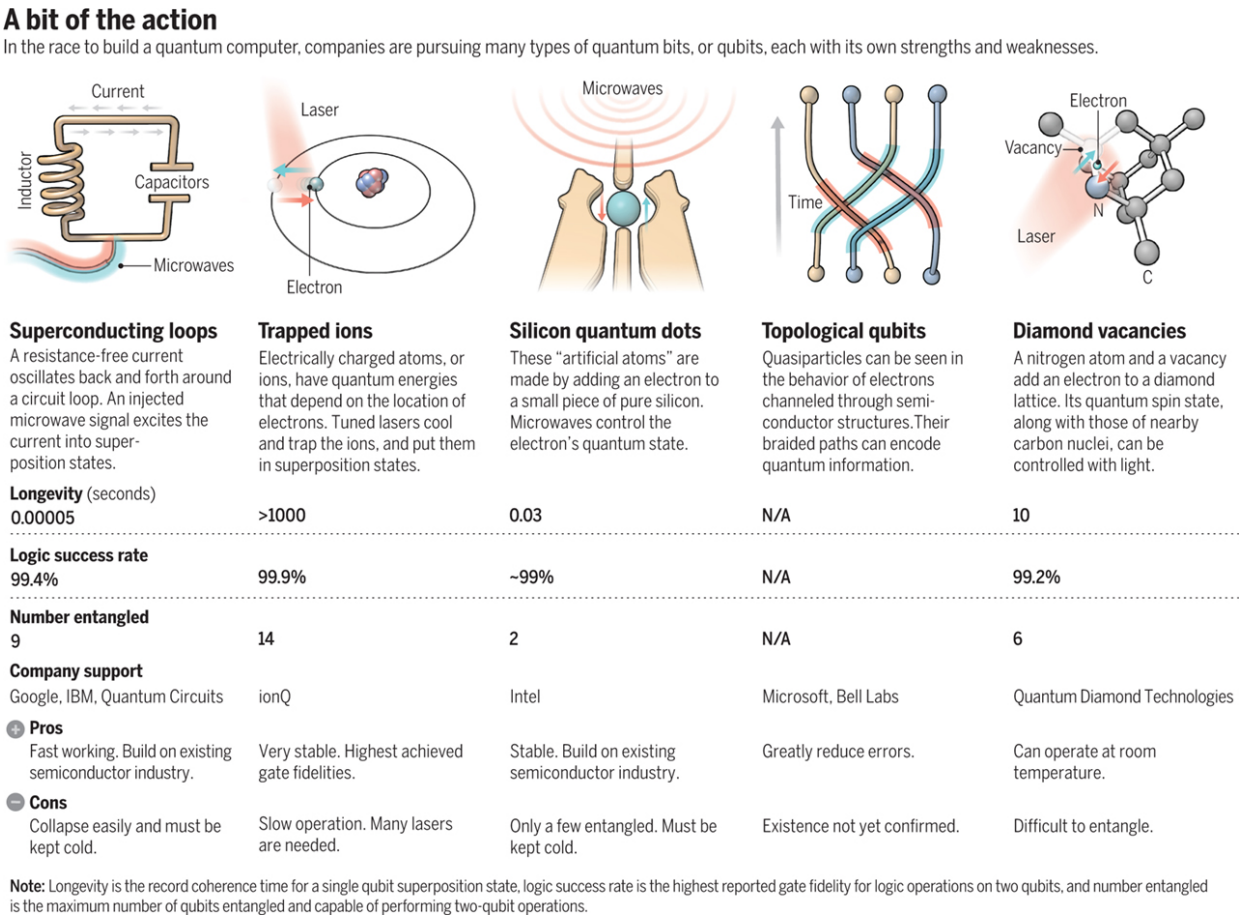

Figure 3: Presentation of some qubit implementation and the maximum coherence time achieved. Figure taken from Ref. [12].

Quantum Error Correction (QEC) [8,13–15] aims at correcting errors *after* they occurred and is believed to be the key to achieve arbitrary long and accurate quantum computation. It consists in encoding a logical qubit (or qudit) into several physical qubits (or qudits) in such a way that, when an error occurs, it is possible to detect that error and apply the necessary operation to correct it and retrieve the initial quantum state. However, a Quantum Error Correction Code can only correct so many errors at a time and quickly becomes overwhelmed by the proliferation of errors, due to both decoherence and imperfect quantum control over the system. A major result in the field of QEC was the demonstration of the *threshold theorem*, which shows that arbitrary long and accurate computation is, in principle, possible using quantum error correction codes provided that the physical error rate is below a certain threshold, which value depends on various parameters [15]. However, the computational cost of the relevant QEC scheme is usually extremely high[1] and the error rate should be lowered even further than the threshold in order to implement the necessary QEC code in practice. It is thus fundamental to develop schemes to mitigate errors, hence the development of Quantum Error Mitigation schemes.

As its name indicates, Quantum Error Mitigation (QEM) aims at mitigating errors instead of correcting

[1]For example, using a specific QEC code architecture called the surface codes, a single logical qubit should be encoded into 10^4 physical qubits in order to achieve arbitrary long computation if the error rate per qubit is in the order of 0.1% [16]; current prototypes of quantum computers only consist of a few hundred qubits for the most advanced ones.

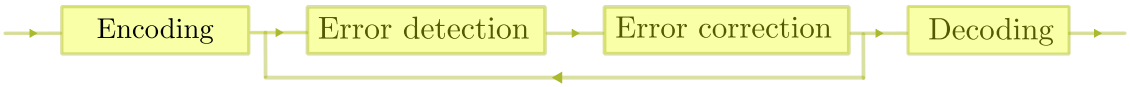

Figure 4: Representation of a QEC protocol.

them after they happened. Two fundamentally different QEM strategies are Decoherence-Free Subspaces (DFS) [17, 18] and Dynamical Decoupling (DD). A DFS scheme makes use of symmetries in the interaction Hamiltonian between the system and the environment and consists in encoding the qubits or qudits in a subspace of the total Hilbert space which rests unaffected (up to a global phase factor) by the errors resulting from the interaction Hamiltonian. This elegant approach to QEM is appealing because after the encoding procedure, no further control or resource is required. Quantum computation can then safely be performed as long as the state of the system stays in this specific subspace. However, this approach only works if the interaction Hamiltonian is known and if it exhibits enough symmetries to construct that subspace. If either of these two conditions is not satisfied, other schemes are needed, such as Dynamical Decoupling (DD) which is the subject of this Master's thesis.

Dynamical Decoupling is a technique inspired by Spin Echo in Nuclear Magnetic Resonance (NMR) [19] and consists in averaging out the unwanted terms in the Hamiltonian by the application of a sequence of *pulses*. It was first introduced in 1998 when Lorenza Viola and Seth Lloyd showed that, by applying a series of spin-flip to a qubit, it was possible to average out the term of the Hamiltonian responsible for pure dephasing [20]. They showed that, in principle, arbitrary long lifetime could be achieved simply by increasing the frequency at which these spin-flips are applied. A year later, L. Viola developed a general theory of dynamical decoupling [21]. She demonstrated that, by choosing the proper sequence of pulses, one could average out any unwanted term in the Hamiltonian, and also showed how to construct such a sequence. This work paved the way for the development of dynamical decoupling; in the last two decades, more complex sequences were found and new techniques have emerged to construct optimized sequences with higher performances. On the experimental front, the efficacy of dynamical decoupling was proven numerous times on various implementation of qubits, such as in NV center [22, 23], trapped ions [24, 25], NMR [26, 27] or superconducting qubits [28].

The objective of this Master's thesis is twofold. The first and principal objective is to write a review of the current knowledge on dynamical decoupling. Accordingly, we will introduce different protocols developed in the past two decades in the interest of extending the lifetime of a single qubit. Each sequence will be introduced in the context of *optimizing* a previous sequence or overcoming a problem encountered by the previous protocols. We will therefore start by a presentation of the most basic DD sequence and build up to the more complex and performing ones. The ambition behind this approach is that, by the end of the reading, one would not only have been introduced to the state-of-the-art protocols of dynamical decoupling, but would also, and most importantly, understand the different optimization procedures that lead to improved protocols. The second objective is to use a state-of-the-art method for studying non-Markovian behaviors of open quantum system, called the *Hierarchy Of Pure States* (HOPS), in the context of dynamical decoupling. We will make use of an exact analytical solution for a qubit undergoing DD and decoherence to validate the results obtained from the HOPS method and bring some insight into the regime of validity of HOPS in the context of studying decoherence and dynamical decoupling. We will then offer some perspectives for future utilization of the HOPS method in this context.

This work is structured as follows. In Section 1, we develop the decoherence model used throughout the sections and demonstrate the degradation of quantum information due to the interaction Hamiltonian. This will illustrate the issue encountered in the development of quantum technologies. This section is also dedicated to the derivation of the HOPS equations and the utilization of HOPS for the analysis of a decohering qubit. We then follow the pioneering work of L. Viola [21] in Section 2 in order to explain how a DD sequence can average out part of the Hamiltonian and how to construct such a sequence. In Section 3, we start by introducing the most basic dynamical decoupling sequence. Then, we introduce a first optimization procedure and present a few interesting results. The protocols established throughout this section are designed to increase the relaxation time T_2, which means that dissipation of energy is not taken

into account just yet. In the following section, we address this issue and construct a sequence to that effect. We then present another method for increasing the performance of this new sequence. In Section 5, we then present some important sequences. Each sequence will be introduced in the context of solving a particular problem of dynamical decoupling, resulting either from the theory itself or the experimental implementation.

Chapter 1

Decoherence

As explained in the introduction, decoherence is the result of interactions between a system and its environment. When decoherence occurs, entanglement and coherence are damaged; the quantum properties of a quantum system are destroyed. Decoherence is thus believed to be at the heart of the quantum-to-classical transition [29], explaining paradoxes such as Schrödinger's cat [8]. In this section, we will present a model of decoherence for a qubit interacting with a bosonic field, i.e. the spin-boson model. The objective of this section is threefold. First, this should illustrate the problem encountered when developing quantum technologies and the importance of QME and QEC schemes. Secondly, the methods presented in this section to study decoherence as well as the spin-boson model for decoherence will be used throughout this Master's thesis and it is thus important to introduce them beforehand. Finally, it is important to go through the analytical derivation of Section 1.4 as a similar derivation will be made later on in the context of studying some important dynamical decoupling sequences.

This section will start by a quick reminder (or introduction depending on how familiar you are with quantum mechanics) on how to treat closed and open quantum systems. Afterwards, we will present the spin-boson model. Once the spin-boson model is introduced, we will introduce two methods for studying the dynamics of a qubit, those two methods being used throughout this Master's thesis. The first method will consist in an analytical derivation of the time-evolution operator and will be used when only pure dephasing is taken into account (that is when no dissipation of energy occurs), while the second method consists of the derivation of a stochastic equation for which a numerical solver is already implemented in the OQLiège Julia library. The second method will be introduced in the context of adding dissipation effects to the model.

1.1 Closed quantum system

In quantum mechanics, the dynamics of a closed quantum system is entirely determined by its Hamiltonian. For a given system with an Hamiltonian H_S (which can certainly be time-dependent), a specific Hilbert space $\mathcal{H}_S$ will contain all valid quantum states $|\psi\rangle$. By solving the Schrödinger equation

$$i\hbar\frac{d}{dt}|\psi(t)\rangle = H_S(t)\,|\psi(t)\rangle \tag{1.1}$$

with respect to an initial condition $|\psi(t_0)\rangle$, one can find the time evolution of the system's state, $|\psi(t)\rangle$. The system's state will then follow a path in the Hilbert space, this path being determined by the Hamiltonian. In order to find $|\psi(t)\rangle$, one can define the *time-evolution operator* $U(t,t_0)$. The time-evolution operator is a unitary operator whose job is to give the state $|\psi(t)\rangle$ when applied to the state $|\psi(t_0)\rangle$. This means that we want $U(t,t_0)$ to satisfy

$$U(t,t_0)\,|\psi(t_0)\rangle = |\psi(t)\rangle \tag{1.2}$$

and

$$U^\dagger(t,t_0)\,|\psi(t)\rangle = |\psi(t_0)\rangle\,. \tag{1.3}$$

By plugging this into the Schrödinger equation, we find that the equation becomes

$$i\hbar\frac{d}{dt}U(t,t_0) = H_S(t)U(t,t_0) \tag{1.4}$$

for which the solution is given by

$$U(t,t_0) = \mathcal{T}_{\leftarrow}\exp\Big\{\frac{-i}{\hbar}\int_{t_0}^{t} H_S(t')dt'\Big\}. \tag{1.5}$$

The factor $\mathcal{T}_{\leftarrow}$ in Eq.(1.5) is called the *time-ordering operator*: its job is to ensure that every operator is applied in chronological order when $U(t,t_0)$ is applied to $|\psi(t_0)\rangle$. For a closed quantum system, all we need to do is to calculate the time-evolution operator in order to study the dynamics of the system. Once the time-evolution operator is known, one can find $|\psi(t)\rangle$ and then calculate the expectation value of any operator A acting on the Hilbert space of the system using

$$\langle A\rangle_{\psi} = \langle\psi(t)|\, A\,|\psi(t)\rangle\,. \tag{1.6}$$

Another way to proceed is by defining the *density operator* $\rho(t) = |\psi(t)\rangle\langle\psi(t)|$. It is straightforward to show that the density operator at time t can be found using

$$\rho(t) = |\psi(t)\rangle\langle\psi(t)| = U(t,t_0)\,|\psi(t_0)\rangle\langle\psi(t_0)|\,U^{\dagger}(t,t_0) = U(t,t_0)\rho(t_0)U^{\dagger}(t,t_0). \tag{1.7}$$

Deriving this equation with respect to time leads to the Liouville von-Neumann equation which is essentially the equivalent of the Schrödinger equation when dealing with density operators instead of wave functions:

$$\frac{d}{dt}\rho(t) = \frac{-i}{\hbar}[H_S(t),\rho(t)]. \tag{1.8}$$

The density operator will be particularly useful when dealing with open quantum system. Instead of calculating the wave function and expectation values using Eq.(1.6), one can find the density operator and calculate expectation values by tracing over the system using the equation

$$\langle A\rangle_{\rho} = \mathrm{Tr}\,[A\rho]. \tag{1.9}$$

1.2 Open quantum system

Suppose that a system of interest S is interacting with an environment B, where B stands for the *bath* that models the environment. Considering the system and the environment altogether, we have a closed system whose Hamiltonian can be written as

$$H = H_S\otimes\mathbb{1}_B + \mathbb{1}_S\otimes H_B + H_{SB} \tag{1.10}$$

where H_S and H_B are the Hamiltonian of the system and the bath respectively and H_{SB} is the interaction Hamiltonian that couples the system to its environment. We could now define $\rho_{\mathrm{tot}}(t)$ as the total density operator and solve the Liouville von-Neuman equation. However, the bath generally possesses a large number of degrees of freedom, which makes this procedure an inefficient way to tackle the problem. The spin-boson model of the environment, for instance, has an infinite number of degrees of freedom which thus leads to a density operator $\rho_{\mathrm{tot}}(t)$ of infinite size. Additionally, the dynamics of the bath is not necessarily relevant as we would like to focus on the system of interest and we thus need a way to get rid of the unwanted information about the dynamics of the bath such that we can reduce the size of the problem as much as possible.

This is typically done by defining the *reduced* density operator of the system as

$$\rho_S(t) = \mathrm{Tr}_B\,[\rho_{\mathrm{tot}}(t)] \tag{1.11}$$

where the total density operator is traced over the degrees of freedom of the bath. By defining the reduced density operator as such, one can find that the expectation value of any operator A acting only on the system can now be calculated using

$$\langle A \rangle_{\rho_{\text{tot}}} = \langle A \rangle_{\rho_S} = \text{Tr}_S \left[A \rho_S \right] \tag{1.12}$$

instead of Eq.(1.9). The useful information about the system is thus stored in the reduced density operator which contains all the information necessary to calculate the expectation values of any operator acting on the Hilbert space of the system. Instead of computing the total density operator, one now only needs to find the reduced density operator.

A common method to study the dynamics of open quantum systems is through the derivation of a *Quantum Master Equation* (QME). Basically, it consists in developping the Liouville von-Neumann equation, Eq.(1.8), for the reduced density operator. When dealing with Markovian behaviors, that is when the system and bath's dynamics is assumed to be independent from its past states, a QME is relatively easy to find [11]. However, this approximation is valid when considering the system's dynamics on a timescale much larger than the correlation time of the environment, which is not a valid approximation when studying dynamical decoupling, as we shall see later on. In order to study dynamical decoupling, we need to account for some non-Markovian dynamics which calls for more complex methods. Non-Markovian QME are considerably harder to derive, but some work on dynamical decoupling showed that DD effects can be accounted for by using a Redfield equation [28, 30], where the Markov approximation is not entirely made and some non-Makrovian behaviors is thus accounted for.

In order to describe non-Markovian behaviors for systems where non-Markovian QME cannot be easily derived, a different method to study open quantum systems is through *Stochastic Simulation Methods* [11]. It consists of realizing independent runs of a stochastic process and calculate the desired expectation values by statistical means. One such method is the Hierarchy Of Pure States (HOPS) [31] which was recently implemented in the Uliège Quantum Optics Julia library by Baptiste Debecker. It is an exact method created to study non-Markovian behaviors of a quantum system interacting with a bosonic bath. In this Master's thesis, the HOPS method will be used to study the more complex dynamical decoupling sequences and environment models.

For the most simple systems, one can decide to calculate directly the time-evolution operator and use it to find the different components of $\rho_S(t)$. This approach can be used to study the simplest sequences of dynamical decoupling as well as the most basic model of decoherence. In this section, we will use this approach to study the exact dynamics of a qubit undergoing pure dephasing. Later on, a similar derivation of $U(t, t_0)$ will be used to study two sequences of pulses designed for that same model.

1.3 The spin-boson model

The spin-boson model describes the dynamics of a two-level system, i.e. a qubit, interacting with a bath which consists of an infinite number of bosonic field modes. This model allows for the analysis of important properties of decoherence because of its exact analytical solution and has been extensively studied because of that [9, 11, 32–34]. Using this model, we can study the purest form of decoherence: pure dephasing without dissipation of energy. By changing the coupling strength with the different modes of the bosonic field (or equivalently by changing the spectral density, as we will se later on), it is possible to reproduce different properties of decoherence. Trapped ion and superconducting circuits have been used recently to simulate the spin-boson model with different spectral density, including the Ohmic spectral density [35,36] and Lorentzian spectral density [37] that we will focus on.

The spin-boson model is characterized by a total Hamiltonian of the system+bath given by

$$H = \underbrace{\frac{\hbar\omega_0}{2}\sigma_z}_{\equiv H_S} \otimes \mathbb{1}_B + \mathbb{1}_S \otimes \underbrace{\sum_k \hbar\omega_k b_k^\dagger b_k}_{\equiv H_B} + \underbrace{\hbar\sigma_z \otimes \sum_k \left(g_k b_k^\dagger + g_k^* b_k \right)}_{\equiv H_{SB}}, \tag{1.13}$$

with H_S and H_B the Hamiltonian of the system and bath respectively and H_{SB} the interaction Hamiltonian. In this expression, g_k is the coupling constant between the mode k of the bosonic bath and the system and

b_k (resp. $b_k^\dagger$) is the annihilation (resp. creation) operator of the mode k. Because we are dealing with a *bosonic* bath, the operators b_k and $b_k^\dagger$ satisfy the commutation relations

$$[b_q, b_k] = 0 = \left[b_q^\dagger, b_k^\dagger\right] \tag{1.14}$$

and

$$\left[b_q, b_k^\dagger\right] = \delta_{qk}. \tag{1.15}$$

The system Hamiltonian H_S is characterized by a transition angular frequency ω_0 between the ground state and the excited state. Because the Pauli operator σ_z possesses eigenvalues ± 1, H_S describes a two-level system with a ground state $|1\rangle$ of energy $-\frac{\hbar}{2}\omega_0$ and an excited state $|0\rangle$ of energy $\frac{\hbar}{2}\omega_0$.[1] The bath Hamiltonian H_B, on the other hand, is a typical Hamiltonian for a bosonic bath made of an infinite number of modes k of frequency ω_k. In order to lighten the notations, we will from now on omit the tensor product '$\otimes$' as well as the identity operators from Eq.(1.13) and simply write

$$H = H_S + H_B + H_{SB}. \tag{1.16}$$

In order to study this model, different methods can be used. First, we will present an analytical method. Two approximations will be made during the derivation. The first one consists in assuming that the initial state is a separable product state, such that there is no entanglement at t_0 between the system and the bath. Mathematically, we have $\rho_{\text{tot}}(t_0) = \rho(t_0) \otimes \rho_B(t_0)$. Secondly, we assume that the environment is at thermal equilibrium at $t = t_0$, $\rho_B(t_0) = \rho_B = \frac{1}{Z_B} e^{-\beta H_B}$ with Z_B the partition function of the bath. After the analytical derivation, we will show how to take dissipation into account and why another method should be used when a dissipative term is added.

1.4 Calculation of the time-evolution operator

In order to calculate the time-evolution operator, we first need to switch to the rotating frame with respect to $H_S + H_B$ in order to simplify the Schrödinger equation. For those who are a bit rusty with the rotating frame, a detailed explanation on how (and why it is advantageous) to move to the rotating frame can be found in Appendix A. In order to move to the corresponding rotating frame, we use for the unitary operator the time-evolution operator corresponding to the Hamiltonian $H_S + H_B$, given by

$$U(t) = \mathcal{T}_{\leftarrow} \exp\left\{-\frac{i}{\hbar}\int_0^t (H_S + H_B)dt'\right\}. \tag{1.17}$$

Since $H_S + H_B$ is time independent, it commutes with itself at all times t and we can remove the time ordering operator. We are left with

$$U(t) = \exp\left\{-\frac{i}{\hbar}(H_S + H_B)t\right\} = \exp\left\{-\frac{i}{\hbar}H_S t\right\} \exp\left\{-\frac{i}{\hbar}H_B t\right\} \tag{1.18}$$

because H_S and H_B commute. For the last equality, it can be proved that the exponential can be split if the two operators commute with each other by using the Baker-Campbell-Hausdorff formula. The proof was done explicitly in Ref. [38]. The effective Hamiltonian in the rotating frame is thus expressed as

$$\begin{aligned}
\tilde{H}_{SB}(t) &= U^\dagger(t) H_{SB} U(t) \\
&= \left(\exp\left\{+\frac{i}{\hbar}H_S t\right\} \exp\left\{+\frac{i}{\hbar}H_B t\right\}\right) \hbar\sigma_z \sum_k \left(g_k b_k^\dagger + g_k^* b_k\right) \left(\exp\left\{-\frac{i}{\hbar}H_S t\right\} \exp\left\{-\frac{i}{\hbar}H_B t\right\}\right) \\
&= \hbar e^{i\frac{\omega_0}{2}\sigma_z} \sigma_z e^{-i\frac{\omega_0}{2}\sigma_z} \sum_k e^{i\sum_q \omega_q b_q^\dagger b_q t} \left(g_k b_k^\dagger + g_k^* b_k\right) e^{-i\sum_q \omega_q b_q^\dagger b_q t}.
\end{aligned} \tag{1.19}$$

[1] It is worth to point out that a different convention assigns the state $|0\rangle$ to the lower energy state and $|1\rangle$ to the higher energy state. However, in quantum computation, assigning $|1\rangle$ and $|0\rangle$ the other way around is quite common.

Because the exponential of the Pauli operator σ_z can be expressed as (see Appendix B for the proof)

$$\exp\Big\{i\frac{\omega_0}{2}\sigma_z\Big\} = \cos\Big(\frac{\omega_0}{2}\Big)\mathbb{1} + i\sin\Big(\frac{\omega_0}{2}\Big)\sigma_z, \tag{1.20}$$

it is straightforward to see that the exponential $\exp\big\{i\frac{\omega_0}{2}\sigma_z\big\}$ satisfy the commutation relation[2]

$$\Big[\exp\Big\{i\frac{\omega_0}{2}\sigma_z\Big\}, \sigma_z\Big] = 0. \tag{1.21}$$

Using this commutation relation, one can simplify Eq.(1.19) and write

$$\tilde{H}_{SB}(t) = \hbar\sigma_z \sum_k e^{i\sum_q \omega_q b_q^\dagger b_q t}\Big(g_k b_k^\dagger + g_k^* b_k\Big)e^{-i\sum_q \omega_q b_q^\dagger b_q t}. \tag{1.22}$$

The next step is to use the similarity transform formula developed in [38] for bosonic systems, which read, for all $a \in \mathbb{C}$,

$$e^{ab_k^\dagger b_k t} b_k^\dagger e^{-ab_k^\dagger b_k t} = e^{at} b_k^\dagger, \tag{1.23a}$$

$$e^{ab_k^\dagger b_k t} b_k e^{-ab_k^\dagger b_k t} = e^{-at} b_k. \tag{1.23b}$$

It can also be proved that the annihilation and creation operators b_k and $b_k^\dagger$ satisfy the commutation relations

$$\Big[e^{ab_k^\dagger b_k t}, b_q^\dagger\Big] = 0, \tag{1.24a}$$

$$\Big[e^{ab_k^\dagger b_k t}, b_q\Big] = 0, \tag{1.24b}$$

when $q \neq k$. Using Eq.(1.23) and Eq.(1.24), we can greatly simply Eq.(1.22) which now reads

$$\tilde{H}_{SB}(t) = \hbar\sigma_z \sum_k \Big(g_k e^{i\omega_k t} b_k^\dagger + g_k^* e^{-i\omega_k t} b_k\Big). \tag{1.25}$$

This effective Hamiltonian now governs the dynamics of the system in the rotating frame and we can thus calculate the corresponding time-evolution operator

$$\tilde{U}(t, t_0) = \mathcal{T}_{\leftarrow} \exp\Big\{\frac{-i}{\hbar}\int_{t_0}^{t} \tilde{H}_{SB}(t')dt'\Big\}. \tag{1.26}$$

In order to eliminate the time ordering operator, we can expand the time-evolution operator as a Magnus series (see Appendix C for an introduction to the Magnus expansion) which leads to

$$\tilde{U}(t, t_0) = \exp\{\Omega(t)\} = \exp\Big\{\sum_{k=0}^{\infty} \Omega_k(t)\Big\} \tag{1.27}$$

with the first two terms of the Magnus series $\Omega(t)$ given by

$$\Omega_0(t) = \frac{-i}{\hbar}\int_{t_0}^{t} dt' \tilde{H}_{SB}(t'),$$
$$\Omega_1(t) = \frac{1}{2}\Big(\frac{-i}{\hbar}\Big)^2 \int_{t_0}^{t} dt_1 \int_{t_0}^{t_1} dt_2 \Big[\tilde{H}_{SB}(t_1), \tilde{H}_{SB}(t_2)\Big].$$

One can show that the commutation relations of the operators b_k and $b_k^\dagger$, Eq.(1.14) and (1.15), lead to the commutator $\Big[\tilde{H}_{SB}(t_1), \tilde{H}_{SB}(t_2)\Big]$ being equal to some factor times the identity operator, which leads

[2]Note that any analytic function f of an operator A commutes with A. This can be proved by expanding $f(A)$ as a Taylor series and realize that A^n commutes with A for all powers n. This property is thus not unique to the Pauli operators.

to the first term of the Magnus series being equal to a global phase factor that we can eliminate without approximation. The following terms of the Magnus series consisting of higher orders of the commutator, they will all cancel out, which leaves the term $\Omega_0(t)$ as the only survivor of the Magnus expansion (up to a global phase factor). The time-evolution operator is thus given by

$$\tilde{U}(t,t_0) = \exp\Big\{\frac{-i}{\hbar}\int_{t_0}^{t}\tilde{H}_{SB}(t')dt'\Big\}. \tag{1.28}$$

Calculating the integral leads to

$$\begin{aligned}\tilde{U}(t,t_0) &= \exp\left\{\frac{\sigma_z}{2}\sum_k\left[\frac{2g_k}{\omega_k}\Big(1-e^{i\omega_k(t-t_0)}\Big)e^{i\omega_k t_0}b_k^\dagger - h.c.\right]\right\}\\ &\equiv \exp\left\{\frac{\sigma_z}{2}\sum_k\Big[\alpha_k(\Delta t)e^{i\omega_k t_0}b_k^\dagger - h.c.\Big]\right\}\end{aligned} \tag{1.29}$$

where 'h.c.' means the *Hermitian conjugate* of the first term in bracket and where we have defined

$$\alpha_k(\Delta t) = \frac{2g_k}{\omega_k}\big(1-e^{i\omega_k\Delta t}\big) \tag{1.30}$$

with $\Delta t = t - t_0$. We then define the operator $B(t,t_0) = \sum_k\Big(\alpha_k(\Delta t)e^{i\omega_k t_0}b_k^\dagger - h.c.\Big)$ acting on the bath such that the time-evolution operator can be written in the simplified form

$$\tilde{U}(t,t_0) = \exp\Big\{-\frac{\sigma_z}{2}\otimes B(t,t_0)\Big\}. \tag{1.31}$$

The time evolution of the system in the rotating frame is entirely determined by the operator Eq.(1.31) and includes all dynamics that result from the interaction Hamiltonian. Decoherence can therefore be studied by calculating the components of the reduced density operator in the rotating frame, $\tilde{\rho}_S(t)$, which is given by

$$\tilde{\rho}_S(t) = \mathrm{Tr}\Big[\tilde{U}(t,t_0)\tilde{\rho}_{\mathrm{tot}}(t_0)\tilde{U}^\dagger(t,t_0)\Big]. \tag{1.32}$$

Translated in the rotating frame, the assumptions described previously on the initial state and on the state of the environment lead to

$$\tilde{\rho}_{\mathrm{tot}}(t_0) = \tilde{\rho}_S(t_0)\otimes\tilde{\rho}_B(t_0) \tag{1.33}$$

with

$$\begin{aligned}\tilde{\rho}_B(t_0) &= {}^{\frac{i}{\hbar}H_B(t_0-t_0)}\,\rho_B e^{\frac{-i}{\hbar}H_B(t_0-t_0)}\\ &= \rho_B(t_0).\end{aligned}$$

We can then focus on specific components of the 2×2 matrix $\tilde{\rho}(t)$ by calculating

$$\tilde{\rho}_{ij}(t) = \langle i|\,\mathrm{Tr}_B\Big[\tilde{U}(t_0,t)(\tilde{\rho}(t_0)\otimes\rho_B)\tilde{U}^\dagger(t_0,t)\Big]\,|j\rangle\,. \tag{1.34}$$

We choose the represent the reduced density operator in the computational basis $\{|0\rangle, |1\rangle\}$ where $|0\rangle$ (resp. $|1\rangle$) is the eigenstate of eigenvalue $+1$ (resp. -1) of the Pauli operator σ_z. One can then show that the time-evolution operator applied to the states $|0\rangle$ and $|1\rangle$ results in the following operators acting on the environment:

$$\begin{aligned}\tilde{U}(t_0,t)\,|0\rangle &= \exp\Big\{-\frac{1}{2}B(t,t_0)\Big\}\,|0\rangle & \langle 0|\,\tilde{U}(t_0,t) &= \langle 0|\exp\Big\{-\frac{1}{2}B(t,t_0)\Big\}\\ \tilde{U}(t_0,t)\,|1\rangle &= \exp\Big\{\frac{1}{2}B(t,t_0)\Big\}\,|1\rangle & \langle 1|\,\tilde{U}(t_0,t) &= \langle 1|\exp\Big\{\frac{1}{2}B(t,t_0)\Big\}.\end{aligned}$$

It is then possible to calculate the components $\tilde{\rho}_{ij}$ using Eq.(1.34) and the relations above. We will do the explicit calculation for the off-diagonal component $\tilde{\rho}_{10}(t)$, but the derivation of the other components can be done similarly. We have

$$\begin{aligned}
\tilde{\rho}_{10}(t) &= \langle 1| \operatorname{Tr}_B \left[\tilde{U}(t_0,t)(\tilde{\rho}(t_0)\otimes\rho_B)\tilde{U}^\dagger(t_0,t)\right]|0\rangle \\
&= \langle 1|\tilde{\rho}(t_0)|0\rangle \operatorname{Tr}_B\left[\exp\left\{\frac{1}{2}B\right\}\rho_B\exp\left\{\frac{1}{2}B\right\}\right] \\
&= \tilde{\rho}_{10}(t_0)\operatorname{Tr}_B\left[\rho_B\exp\left\{\frac{1}{2}B\right\}\exp\left\{\frac{1}{2}B\right\}\right] \\
&= \tilde{\rho}_{10}(t_0)\operatorname{Tr}_B\left[\rho_B\exp\left\{\sum_k\left(\alpha_k(\Delta t)e^{i\omega_k t_0}b_k^\dagger - h.c.\right)\right\}\right]
\end{aligned}$$

where the cyclicity of the trace was used to gather the operators $\exp\{B/2\}$ on the right-hand side in the bracket. The trace $\operatorname{Tr}[\rho_B\exp\{B\}]$ is the expectation value of $\exp\{B\}$ in the environment state ρ_B and we can then write[3]

$$\operatorname{Tr}_B\left[\rho_B\exp\left\{\sum_k\left(\alpha_k(\Delta t)e^{i\omega_k t_0}b_k^\dagger - h.c.\right)\right\}\right] = \prod_k\left\langle\exp\left\{\alpha_k(\Delta t)e^{i\omega_k t_0}b_k^\dagger - h.c.\right\}\right\rangle_{\rho_{B,k}} \tag{1.35}$$

where $\langle\cdot\rangle_{\rho_{B,k}}$ is the expectation value for the thermal mode $\rho_{B,k} = \frac{1}{Z_B}e^{-\beta\hbar\omega_k b_k^\dagger b_k}$. This function is known as the Wigner characteristic function of the bath mode k and is a common function in quantum optics [9, 11]. It has a nice analytical expression given by

$$\left\langle\exp\left\{\alpha_k(\Delta t)e^{i\omega_k t_0}b_k^\dagger - h.c.\right\}\right\rangle_{\rho_{B,k}} = \exp\left\{-\frac{1}{2}|\alpha_k(\Delta t)|^2\coth\left(\frac{\hbar\omega_k}{2k_BT}\right)\right\}. \tag{1.36}$$

Putting everything together, we come up with the simple expression for the off-diagonal component

$$\tilde{\rho}_{10}(t) \equiv \tilde{\rho}_{10}(t_0)e^{-\Gamma(t)} \tag{1.37}$$

where we have defined the *decoherence function* $\Gamma(t)$ as

$$\boxed{\Gamma(t) = \frac{1}{2}\sum_k|\alpha_k(\Delta t)|^2\coth\left(\frac{\hbar\omega_k}{2k_BT}\right)}. \tag{1.38}$$

Using the definition of $\alpha_k(\Delta t)$, we finally obtain

$$\boxed{\Gamma(t) = 4\sum_k\frac{|g_k|^2}{\omega_k^2}[1-\cos(\omega_k\Delta t)]\coth\left(\frac{\hbar\omega_k}{2k_BT}\right)}. \tag{1.39}$$

A similar derivation for the other components of the reduced density matrix gives us the following result :

$$\tilde{\rho}_S(t) = \begin{pmatrix}\tilde{\rho}_{00}(t_0) & \tilde{\rho}_{01}(t_0)e^{-\Gamma(t)}\\ \tilde{\rho}_{10}(t_0)e^{-\Gamma(t)} & \tilde{\rho}_{11}(t_0)\end{pmatrix}. \tag{1.40}$$

In the reduced density matrix, the off-diagonal elements correspond to the *coherences*. The decoherence function is a real positive function, which means that the coherences decay exponentially with time. The

[3]Because of the commutation relation $\left[b_k, b_q^\dagger\right] = [b_k, b_q] = \left[b_k^\dagger, b_q^\dagger\right] = 0$ for $q \neq k$, the exponential of the sum over all modes can be expressed as a product over all modes of an exponential.

decay of the off-diagonal elements then corresponds to a loss of coherence where a pure, coherent superposition of state is degraded over time into a mixture of state.

Remark. Switching back from the rotating frame to the Schrödinger representation adds an additional phase factor $\exp\{i\omega_0 t\}$ to the off-diagonal components of the reduced density matrix. Because the argument of the exponential is imaginary, it does not produce any loss of coherence. This factor originates from the system Hamiltonian H_S and generates oscillations of the off-diagonal component at the frequency ω_0.

In order to study the decoherence function, we can switch to the continuum limit in order to have an expression of $\Gamma(t)$ as an integral over all frequencies ω of the bath instead of a sum over all the modes by defining the *Spectral Density*[4] (SD)

$$J(\omega) = 4\sum_k |g_k|^2 \delta(\omega - \omega_k), \tag{1.41}$$

which leads to

$$\boxed{\Gamma(t) = \int_0^\infty d\omega \frac{J(\omega)}{\omega^2}[1 - \cos(\omega\Delta t)] \coth\left(\frac{\omega}{2k_B T}\right)}. \tag{1.42}$$

which is the main result of this section. The decoherence function therefore only depends on the temperature T and the spectral density of the bath $J(\omega)$. The spectral density describes entirely the influence of the environment on the system. It basically states 'how much' the system couples with each frequency of the bosonic field. The choice of $J(\omega)$ will depend on the environment that we wish to model. Two common choices are the *Ohmic* spectral density and the *Lorentzian* spectral density. These spectral densities will be introduced shortly. It is however preferable to introduce the different quantities describing decoherence in our model beforehand.

A first quantity of interest is $1 - \exp(-\Gamma(t))$ which quantifies how much coherence is lost at time t. This quantity is independent on the initial state of the system and entirely depends on the spectral density and the temperature. Equivalently, $\exp(-\Gamma(t))$ represents how much coherence is left.

The quantity usually used in quantum information processing to quantify the reliability of qubits and qudits is the *quantum fidelity* [39, 40], which is essentially a measure of *how close* two quantum states are. In the context of quantum information storage, this would characterize how close a quantum state at time t is to the initial quantum state at time t_0. In the context of this Master's thesis, we consider a quantum system in a *pure* quantum state $|\psi(t_0)\rangle$ which suddenly undergoes decoherence at time t_0, that is the system is closed for times below t_0. In that case, the quantum fidelity at time t is given by

$$\mathcal{F}(\rho(t), |\psi(t_0)\rangle\langle\psi(t_0)|) = \langle\psi(t_0)|\rho(t)|\psi(t_0)\rangle. \tag{1.43}$$

Considering a qubit in the most general pure state $|\psi(t_0)\rangle = \alpha|0\rangle + \beta|1\rangle$, with $|\alpha|^2 + |\beta|^2 = 1$, and the reduced density matrix Eq.(1.40) with $\tilde{\rho}(t_0) = \rho(t_0) = |\psi(t_0)\rangle\langle\psi(t_0)|$, we can calculate the quantum fidelity as follows

$$\begin{aligned}\mathcal{F}(\tilde{\rho}(t), |\psi(t_0)\rangle\langle\psi(t_0)|) &= (\alpha^*\langle 0| + \beta^*\langle 1|)\tilde{\rho}(t)(\alpha|0\rangle + \beta|1\rangle) \\ &= |\alpha|^2\tilde{\rho}_{00}(t) + |\beta|^2\tilde{\rho}_{11}(t) + \alpha^*\beta\tilde{\rho}_{01}(t) + \alpha\beta^*\tilde{\rho}_{10}(t) \\ &= |\alpha|^4 + |\beta|^4 + 2|\alpha|^2|\beta|^2 e^{-\Gamma(t)}.\end{aligned} \tag{1.44}$$

Because of the normalisation condition, we have

$$\begin{aligned}\mathcal{F}(\tilde{\rho}(t), |\psi(t_0)\rangle\langle\psi(t_0)|) &= |\alpha|^4 + |\beta|^4 + 2|\alpha|^2|\beta|^2 e^{-\Gamma(t)} \\ &\leq |\alpha|^4 + |\beta|^4 + 2|\alpha|^2|\beta|^2 \\ &= \left(|\alpha|^2 + |\beta|^2\right)^2 = 1.\end{aligned}$$

[4]It should be noted that there exists different conventions to the definition of the spectral density which differ in the value of the factor that appears in Eq.(1.41). We used the same definition as in Ref. [20] by choosing a factor 4 in front of the sum. Another common choice is to replace this factor by a factor π, this convention being the one used by Baptise Debecker in the implementation of the HOPS method in the OQLiège Julia library. In order to match the analytical results with the numeric results using the HOPS method, we should then add a multiplicative factor $4/\pi$ to our definition of the spectral density.

The fidelity is therefore a real number in the interval $[0, 1]$ and the objective of quantum error mitigation schemes is to keep the fidelity as close to 1 as possible during the computation. Usually, a high fidelity between 99% and 99.99% or higher is required [41]. Equivalently, we can define the *infidelity* as $1 - \mathcal{F}$ which we aim to reduce.

1.4.1 Ohmic spectral density

The Ohmic spectral density is characterized by a coupling that increases linearly with ω until it reaches a cut-off frequency ω_c beyond which it is equal to zero. It is common to use a decreasing exponential in order to implement a smooth cut-off instead of an infinitely sharp cut-off. It is thus given by

$$J_o(\omega) = \alpha\omega e^{-\omega/\omega_c} \tag{1.45}$$

where α characterizes the overall coupling strength. Because the spectral density is a frequency, α is an adimensionnal parameter. This function peaks at $\omega = \omega_c$ with a value of $\alpha\frac{\omega_c}{e}$.

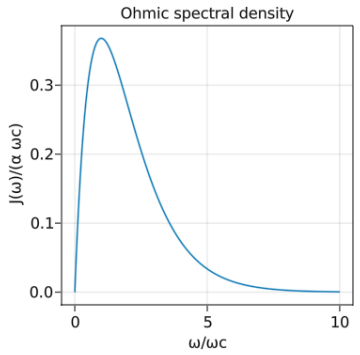

Figure 1.1: Ohmic spectral density for any parameter α and ω_c.

The choice of the Ohmic spectral density as a decoherence model throughout the paper is motivated by its utilisation in some pioneering works on dynamical decoupling [20, 41]. Using the same spectrum makes it possible to verify some of our results with previous works. The coherence loss $1 - \exp\{-\Gamma(t)\}$ and infidelity $1 - \mathcal{F}$ are plotted in FIG. 1.2 for a temperature of $k_BT/\hbar\omega_c = 10^{-2}$ which is considered the *low temperature regime* [20] where quantum fluctuations are responsible for the decoherence of the quantum system. We used the entangled state $|\psi(t_0)\rangle = \frac{1}{\sqrt{2}}(|0\rangle + |1\rangle)$ to compute the infidelity. Because the infidelity and the coherence loss behave exactly the same way[5], we will from now on only plot the coherence loss in order to avoid redundant plots.

For $\hbar\omega_c \gg k_BT$, the decoherence function has a nice analytical solution [11] given by

$$\Gamma(t) \approx \frac{\alpha}{2}\ln\left(1 + \omega_c^2 t^2\right) + \alpha\ln\left[\frac{\sinh\left(t\frac{k_BT}{\hbar\pi}\right)}{t\frac{k_BT}{\hbar\pi}}\right]. \tag{1.46}$$

There are clearly two timescales appearing in this expression: a *thermal* characteristic time $\tau_\beta = \frac{\hbar\pi}{k_BT}$ and a *vacuum* characteristic time $\tau_c = \frac{1}{\omega_c}$. Because $\hbar\omega_c \gg k_BT$, we have $\tau_c \ll \tau_\beta$. For $\omega_c t \ll 1 \ll \frac{\pi\hbar\omega_c}{k_BT}$, a series expansion reveals that the decoherence function is given by

$$\Gamma(t) \approx \frac{\alpha}{2}\omega_c^2 t^2 + \frac{\alpha}{6}\left(\frac{k_BT}{\pi\hbar}\right)^2 t^2. \tag{1.47}$$

[5]One can see from Eq. (1.44) that the fidelity decreases with the exponential factor that appears in the coherences $\rho_{01}(t)$ and $\rho_{10}(t)$. The only difference between the two expressions is dependence on the initial state.

Because $\hbar\omega_c \gg k_B T$, the thermal term can be neglected compared to the vacuum term, revealing a simple expression

$$\Gamma(t) \approx \frac{\alpha}{2}\omega_c^2 t^2. \tag{1.48}$$

This means that below the characteristic time τ_c, the coherence loss obeys the exponential law

$$\rho_{01}(t)/\rho_{01}(t_0) = e^{-\frac{\alpha}{2}\omega_c^2 t^2}, \tag{1.49}$$

and we now understand that ω_c is the characteristic frequency indicating the timescale at which a qubit looses its coherence.

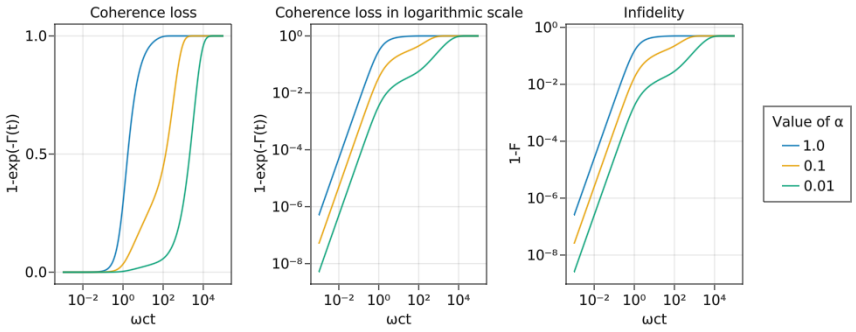

Figure 1.2: Coherence loss and infidelity as a function of the dimensionless parameter $\omega_c t$ for different orders of magnitude of the coupling strength and a temperature of $k_B T/\omega_c = 10^{-2}$. Because we are interested in the *high fidelity regime*, it makes sense to always plot these quantities in the logarithmic scale in the following sections, when it is possible.

It is clear that quantum information can only be stored with high fidelity for a timescale smaller than $\tau_c \sim \frac{1}{\omega_c}$, which is called the *correlation time* of the environment. ω_c, on the other hand, is the *characteristic frequency* of the decoherence process. For a coupling strength α equal to 1 and 0.1, a qubit can only be stored with a fidelity higher than 99% for a fraction of the correlation time. Lower coupling strengths can improve the lifetime of the qubit, but not drastically.

1.4.2 Lorentzian spectral density

The Lorentzian spectral density has, as its name indicates, the shape of a Lorentzian centered at some frequency ω_c. A parameter κ characterizes the width of the distribution. It is given by

$$J_L(\omega) = \frac{4}{\pi}\frac{g\kappa}{2}\frac{\kappa}{(\omega-\omega_c)^2+\kappa^2} \tag{1.50}$$

where g serves the same purpose as α for the Ohmic SD, except that this time g is not adimensional and has the unit of a frequency. This function peaks at $\omega = \omega_c$ with a value of $\frac{4}{\pi}\frac{g}{2}$.

The motivation behind the choice of the Lorentzian spectral density in this Master's thesis is twofold. First, as we will see later on, the HOPS method that will be used when dissipation should be added is only implemented for a Lorentzian spectral density. Secondly, it will be interesting to see how qubits with different spectral densities will differ in how they react to a dynamical decoupling protocol.

First, we should find the characteristic frequencies describing the decoherence process of a Lorentzian density. In order to do that, we performed a series expansion around $t = 0$ and considered once again the low temperature regime in order to leave out the thermal contribution, which leads to

$$\Gamma(t) = \int_0^\infty d\omega \frac{g\kappa^2}{2}\frac{1}{\kappa^2+(\omega-\omega_c)^2}\frac{1-\cos(\omega t)}{w^2} \approx \int_0^\infty d\omega \frac{g\kappa^2}{2}\frac{1}{\kappa^2+(\omega-\omega_c)^2}\frac{t^2}{2} = \frac{1}{8}g\kappa t^2(\pi + 2\arctan(\omega_c/\kappa)). \tag{1.51}$$

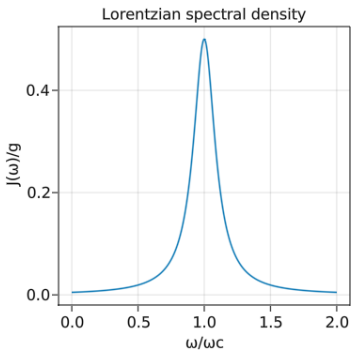

Figure 1.3: Lorentzian spectral density for $\omega_c/\kappa = 10$.

For a Lorentzian centered at $\omega_c \gg \kappa$, this leads to the nice analytical expression

$$\Gamma(t) \approx \frac{\pi}{4} g\kappa t^2. \tag{1.52}$$

We thus have the same exponential law as in the Ohmic case, except that the characteristic frequency ω_c is replaced by the frequency $\sqrt{g\kappa}$. However, this expression is only valid in the limit $t \to 0$: a series expansion of $(1 - \cos(\omega t)$ to the second order reveals that the integral does not converge over the range of frequency $[0, \infty[$. This issue did not occur in the Ohmic case because the integration had a nice analytical solution on which a series expansion was more easily done.

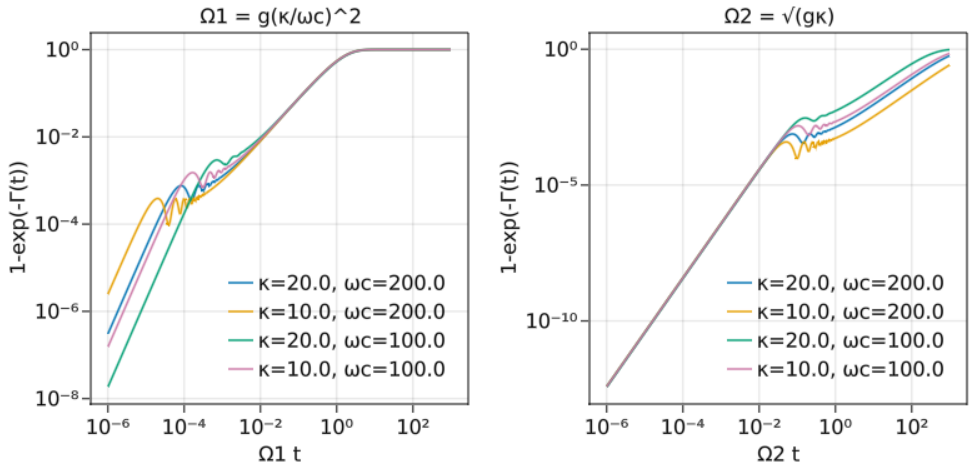

Figure 1.4: Coherence loss for the Lorentzian spectral density using different parameters.

In order to see if the characteristic frequency $\sqrt{g\kappa}$ really relates to the coherence time of the qubit, we plotted the coherence loss for different values of κ and ω_c (see FIG. 1.4) and intended to empirically find the relevant timescales. We find two characteristic frequencies Ω_1 and Ω_2. Ω_1 relates to the coherence time of the system, indicating the timescale at which the qubit totally loses its coherence, which is given by

$$\tau_1 = \frac{1}{\Omega_1} = \frac{\omega_c^2}{g\kappa^2}. \tag{1.53}$$

It thus corresponds the relevant timescale when studying decoherence produced by a Lorentzian SD. Mind

that these calculations have been done at zero temperature, thus considering $\coth\left(\frac{\hbar\omega}{k_B T}\right) = 1$.[6] The second characteristic frequency $\Omega_2 = \sqrt{g\kappa}$ is the one analytically derived above.

In order to see how the spectral density affects a dynamical decoupling procedure, one can, by tunning the Lorentzian parameters, design a Lorentzian spectral density which leads to the same decoherence time as a Ohmic spectral density. In order to do that, we first use the same value for the parameter ω_c in both spectral densities. Then, we get the value of g such that both spectral densities peak at almost the same value: because the peaks match by choosing $g = \frac{\pi}{2e}\alpha\omega_c \equiv \gamma$, we chose a value of g/γ equal to 0.8 and 1.5. Then, we varied the value of the parameter κ and plotted the coherence loss corresponding to the tuned Lorentzian and the Ohmic SD in order to find the value of κ for which the qubit with Lorentzian SD and Ohmic SD have the same decoherence properties[7]. Doing so, we construct two spectral densities of corresponding coherence time $\sim 1/\omega_c$ (see Fig. 1.5). The decoherence rate for the Lorentzian SD's seem to differ from the Ohmic one for times $t > 1/\omega_c$ but perfectly match with the Ohmic one at smaller times. Because we are interested in the high fidelity regime, we will consider that these three spectrum yield the same decoherence properties in the regime of interest. In conclusion, we have constructed two new spectral densities that yield similar decoherence properties but with different distributions.

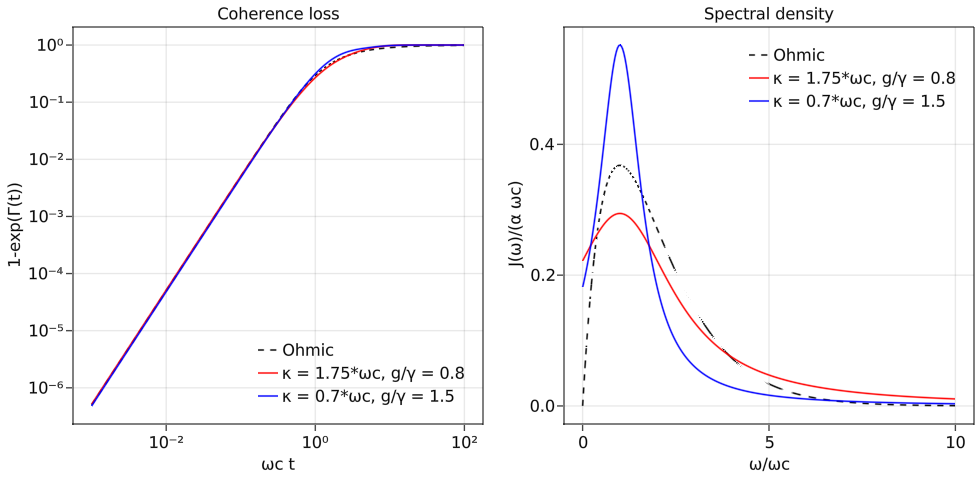

Figure 1.5: Three spectral densities of similar coherence time but with different distributions.

1.5 Adding dissipation

In the previous section, we have only considered a *purely dephasing* qubit in the spin-boson model. In this model, no dissipation is taken into account, which means that the population of the excited state is not affected by the interaction with the environment. When dissipation is taken into account, the decoherence process of a qubit can be considered as resulting from two relaxation processes, that is a *transverse relaxation* due to pure dephasing and a *longitudinal relaxation* due to dissipation [8]. These two processes are characterized by a relaxation time T_1 and T_2 for the longitudinal and transverse relaxation times respectively. Because T_1 is generally greater than T_2, pure dephasing is usually the physical process limiting the storage of quantum information with high fidelity. The superconducting qubit of IBM [42], for example, typically have a longitudinal relaxation time several times greater than the transverse relaxation time.

[6] Because the Lorentzian SD will mainly be used with HOPS and because HOPS is implemented at zero temperature, it makes sense to study them at zero temperature to begin with.

[7] The decoherence properties will never match completely, but we wish the coherence losses to match in the regime of interest, that is for low infidelity where quantum information can still be used reliably.

Neglecting dissipation may however not be a valid approximation and it may be necessary to take it into account in certain situations. According to Ref. [32], in order to incorporate dissipative dynamics, one should add a tunneling term $\Delta_0\sigma_x$ to the system's Hamiltonian in Eq.(1.13), with Δ_0 a characteristic frequency which gives the timescale of the dissipation. Another way to incorporate dissipation would be to add an interaction Hamiltonian of the form $\hbar\sigma_x \otimes \sum_k \left(g_k b_k^\dagger + g_k^* b_k\right)$ which, for a system Hamiltonian $H_S = \hbar\frac{\omega_0}{2}\sigma_z$ with $\omega_0 = \omega_c$ and using a Lorentzian SD, leads to the well known and extensively studied James-Cummings model on resonance [11, 43] and is approximated by the interaction Hamiltonian $\hbar\sum_k \left(g_k\sigma_- b_k^\dagger + g_k^*\sigma_+ b_k\right)$ using $\sigma_+ = |1\rangle\langle 0|$ and $\sigma_- = |0\rangle\langle 1|$.

Adding dissipative that way may not seem that complicated, but it actually prohibits an analytical derivation such as the one worked through in the previous section. In order to study the dynamics of a qubit undergoing both dephasing and dissipation, one needs more complex methods such as a Quantum Master Equation (QME) or a stochastic simulation method. Because QME are deterministic equations whereas stochastic simulations are, as their name indicates, stochastic, QME might seem like to way to go in order to study our dissipative system without having to calculate statistical means. However, QME are only easy to derive for time-independent Hamiltonian and Markovian systems, that is when we can make the approximation that the system's dynamics does not depend on its history, i.e. when all memory effects are neglected and the dynamics at time t do not depend on the system's state at time $t' < t$. Unfortunately, Dynamical Decoupling is non-Markovian, which makes the derivation of a QME a hard endeavor.

Fortunately, a stochastic method called the *Hierarchy Of Pure States* (HOPS) [31] was recently implemented in the OQLiège Julia Library by B. Debecker and allows us to deal with non-Markovian behaviors and time-dependent Hamiltonian. The HOPS method is a numerically exact method designed to calculate the dynamics of a system interacting with a bosonic field. It is a clever reformulation of a method called *Non-Markovian Quantum State Diffusion* (NMQSD) [44] where the interaction with the environment is encapsulated in a stochastic term of a Schrödinger equation. The equation is then solved a certain number of times and the reduced density matrix is calculated by averaging over all trajectories. In order to understand the different parameters of the simulation as well as the underlying mechanism of the solver, we dedicated the next subsection to the derivation of the NMQSD and HOPS equations. We also attempt to provide some insight into the numerical implementation of HOPS. In the following subsection, HOPS will then be used to replicate the analytical results for the purely dephasing qubit and dissipation will eventually be taken into account.

1.5.1 NMQSD and HOPS

In order to understand the HOPS method, one must first go through the derivation of the NMQSD equation. Accordingly, we will first derive the NMQSD equation. We will explain how the reduced density matrix is constructed by calculating numerous times the solution of a stochastic equation, driven by a stochastic process which is entirely described by the *correlation function*, the equivalent of the spectral density in the time domain. Once the ideas behind NMQSD are explained and the equation is derived, HOPS will be introduced.

Non-Markovian Quantum State Diffusion

Let us start with a general Hamiltonian of a system interacting with a bosonic field

$$H = H_S + \hbar\sum_k \left(g_k^* L b_k^\dagger + g_k L^\dagger b_k\right) + \sum_k \hbar\omega_k b_k^\dagger b_k \tag{1.54}$$

with H_S the system Hamiltonian which may or may not be time-dependent. In this equation, L is the operator of the interaction Hamiltonian that acts on the system. It may or may not be hermitian. Notice that, if $H_S = \hbar\frac{\omega_0}{2}\sigma_z$, choosing $L = L^\dagger = \sigma_z$ leads to the purely dephasing qubit model and choosing $L = \sigma_-$ leads to the James-Cummings model. Moving to the rotating frame with respect to $H_B = \sum_k \hbar\omega_k b_k^\dagger b_k$ leads

to the Hamiltonian

$$\begin{aligned} H(t) &= H_S + \hbar \sum_k \left(g_k^* L b_k^\dagger e^{i\omega_k t} + g_k L^\dagger b_k e^{-i\omega_k t} \right) \\ &\equiv H_S + L B^\dagger(t) + L^\dagger B(t) \end{aligned} \tag{1.55}$$

where we defined $B(t) = \hbar \sum_k g_k e^{-i\omega_k t} b_k$ as the bath operator. Considering the system and environment altogether, the total wave function can be calculated by solving the Schrödinger equation

$$i\hbar \partial_t \left| \Psi(t) \right\rangle = H(t) \left| \Psi(t) \right\rangle . \tag{1.56}$$

The idea is then to make use use of the so-called *Bargmann coherent states* [45] of the bosonic field. A Bargmann coherent state of the mode k of the bath is defined as

$$\left| z_k \right\rangle = \exp\left(z_k b_k^\dagger \right) \left| 0_k \right\rangle \tag{1.57}$$

with z_k a complex number and $|0_k\rangle$ the ground state of the mode k. This definition leads to the three interesting properties

$$\frac{1}{\pi} \int d^2 z_k \exp\left(-|z_k|^2 \right) \left| z_k \right\rangle \left\langle z_k \right| = \mathbb{1}_k, \tag{1.58a}$$

$$b_k \left| z \right\rangle = z_k \left| z \right\rangle , \tag{1.58b}$$

$$b_k^\dagger \left| z \right\rangle = \frac{\partial}{\partial z_k} \left| z \right\rangle , \tag{1.58c}$$

defining $|z\rangle = |z_1\rangle \otimes \cdots \otimes |z_k\rangle \otimes \cdots \otimes |z_N\rangle$ with $N \to \infty$ the number of modes in the bosonic field. Eq.(1.58a) is especially interesting as it leads to

$$\begin{aligned} \left| \Psi(t) \right\rangle = \mathbb{1} \left| \Psi(t) \right\rangle &= \frac{1}{\pi^N} \int d^2 z \exp\left(-|z|^2 \right) \left\langle z | \Psi(t) \right\rangle \left| z \right\rangle \\ &\equiv \frac{1}{\pi^N} \int d^2 z \exp\left(-|z|^2 \right) \left| \psi(t, z^*) \right\rangle \left| z \right\rangle \end{aligned} \tag{1.59}$$

when we extend it to the N modes of the bosonic field and define $|\psi(t, z^*)\rangle = \langle z|\Psi(t)\rangle$ as the system's state relative to the bath state $|z\rangle$. Because it is constructed by projecting the entire state onto the bath state $|z\rangle$, this wave function exists in the Hilbert space of the system. Notice first that the knowledge of the state $|\psi(t, z^*)\rangle$ for all z^* is sufficient to construct the entire wave function. Secondly, calculating the reduced density matrix using Eq.(1.58a) leads to

$$\begin{aligned} \rho_S(t) &= \mathrm{Tr}_B \left[\left| \Psi(t) \right\rangle \left\langle \Psi(t) \right| \right] \\ &= \int d^2 z \frac{\exp\left(-|z|^2 \right)}{\pi^N} \left| \psi(t, z^*) \right\rangle \left\langle \psi(t, z^*) \right| . \end{aligned} \tag{1.60}$$

This integral can be calculated using a Monte Carlo integration [46]. As a reminder, the Monte Carlo integration method, in its simplest form, consists in estimating the integral

$$I = \int dx f(x) h(x) \tag{1.61}$$

by calculating the average of the function $h(x)$,

$$\overline{h} = \frac{1}{N} \sum_{n=1}^{N} h(x_n), \tag{1.62}$$

using $X = (x_1, \ldots x_N)$ a random sample generated from the distribution $f(x)$. Considering the Monte Carlo integration to solve Eq.(1.60), one can construct the reduced density matrix by averaging $|\psi(t, z^*)\rangle \langle\psi(t, z^*)|$

over a certain number of trajectories, using for the random variable z^* a complex Gaussian distribution. We finally have

$$\rho_S(t) \approx \frac{1}{n_{\text{traj}}} \sum_{n=1}^{n_{\text{traj}}} |\psi(t, z_n^*)\rangle \langle\psi(t, z_n^*)| \tag{1.63}$$

with n_{traj} the number of trajectories and $Z = \left(z_1^*, \dots z_{n_{\text{traj}}}^*\right)$ a random sample generated by the complex Gaussian distribution $\exp\left(-|z|^2\right)/\pi^N$.

Now, we may try to find an equation for $|\psi(t, z^*)\rangle$ by projecting the Schrödinger equation Eq.(1.56) onto the bath state $|z\rangle$. This leads to

$$i\hbar\partial_t \langle z|\Psi(t)\rangle = H_S \langle z|\Psi(t)\rangle + L \langle z| B^\dagger(t) |\Psi(t)\rangle + L^\dagger \langle z| B(t) |\Psi(t)\rangle \tag{1.64}$$

where the terms $\langle z| B^\dagger(t) |\Psi(t)\rangle$ and $\langle z| B(t) |\Psi(t)\rangle$ can be calculated using the properties $\langle z| b_k^\dagger = z_k^* \langle z|$ and $\langle z| b_k = \frac{\partial}{\partial z_k^*} \langle z|$ which result from Eq.(1.58b) and Eq.(1.58c). Eq.(1.64) now reads

$$\begin{aligned} i\hbar\partial_t |\psi(t, z^*)\rangle &= H_S |\psi(t, z^*)\rangle + \hbar L \sum_k g_k^* z_k^* e^{i\omega_k t} |\psi(t, z^*)\rangle + \hbar L^\dagger \sum_k g_k^* e^{i\omega_k t} \frac{\partial}{\partial z_k^*} |\psi(t, z^*)\rangle \\ &= H_S |\psi(t, z^*)\rangle + i\hbar L\eta^*(t, z^*) |\psi(t, z^*)\rangle + \hbar L^\dagger \sum_k g_k^* e^{i\omega_k t} \frac{\partial}{\partial z_k^*} |\psi(t, z^*)\rangle \end{aligned} \tag{1.65}$$

where we defined in the last line

$$\eta^*(t, z^*) = -i \sum_k g_k^* z_k^* e^{i\omega_k t}. \tag{1.66}$$

We can rewrite $\frac{\partial}{\partial z_k^*}$ as

$$\frac{\partial}{\partial z_k^*} = \int ds \frac{\partial \eta^*(s, z^*)}{\partial z_k^*} \frac{\delta}{\delta \eta^*(s, z^*)} \tag{1.67}$$

using the chain rule for functional derivatives and calculate the derivative $\frac{\partial \eta^*(s,z^*)}{\partial z_k^*} = -ig_k^* e^{i\omega_k s}$. This leads to

$$i\partial_t |\psi(t, z^*)\rangle = \frac{1}{\hbar} H_S |\psi(t, z^*)\rangle + iL\eta^*(t, z^*) |\psi(t, z^*)\rangle - iL^\dagger \int ds \sum_k |g_k|^2 e^{-i\omega_k(t-s)} \frac{\delta}{\delta \eta^*(s, z^*)} |\psi(t, z^*)\rangle . \tag{1.68}$$

It is clear that the last term containing the integral over time will be the non-Markovian term containing all the memories of the system's history. In order to preserve causality, $|\psi(t, z^*)\rangle$ must be independent of $\eta^*(s)$ for all $s > t$, which means that $\frac{\delta}{\delta \eta^*(s,z^*)} |\psi(t, z^*)\rangle = 0$ for $s > t$. That being said, the upper limit of the integral can be set to be equal to t. We also consider a pure initial state $|\Psi(t = 0)\rangle = |\phi_0\rangle \otimes |0\rangle$ with $|0\rangle$ the ground state of the environment at zero temperature, which means that the system's state at $t = 0$ is independent of $\eta^*(s)$ for all s. Particularly, $\frac{\delta}{\delta \eta^*(s,z^*)} |\psi(t = 0, z^*)\rangle = 0$ for all $s < 0$. This means that all states $|\psi(t, z^*)\rangle$ for $t > 0$ will also be independent of $\eta^*(s)$ for $s < 0$. Having that in mind, the lower limit of the integral can be set to 0, which means that the memory term can be integrated over $[0, t]$ instead of the entire axis.

Noticing that z^* only appear through $\eta^*(t, z^*)$, we can write the equation as

$$\partial_t |\psi[\eta^*(t)]\rangle = \left[-\frac{i}{\hbar} H_S + L\eta^*(t) - L^\dagger \int_0^t ds \sum_k |g_k|^2 e^{-i\omega_k(t-s)} \frac{\delta}{\delta \eta^*(s)} \right] |\psi[\eta^*(t)]\rangle . \tag{1.69}$$

Recalling the previous sections, one element of this equation should seem familiar: the sum $\sum_k |g_k|^2$ appearing in the memory term. We find that

$$\begin{aligned}\sum_k |g_k|^2 e^{-i\omega_k(t-s)} &= \frac{1}{\pi}\int_0^\infty d\omega\pi \sum_k |g_k|^2 \delta(\omega-\omega_k) e^{-i\omega(t-s)} \\ &= \frac{1}{\pi}\int_0^\infty d\omega J(\omega) e^{-i\omega(t-s)} \\ &\equiv \alpha(t-s)\end{aligned} \tag{1.70}$$

where we defined the spectral density[8] as $J(\omega) = \pi\sum_k |g_k|^2\delta(\omega-\omega_k)$ as well as the *correlation function*

$$\alpha(\tau) = \sum_k |g_k|^2 e^{-i\omega_k\tau} = \frac{1}{\pi}\int_0^\infty d\omega J(\omega) e^{-i\omega\tau}. \tag{1.71}$$

While the spectral density encapsulates all the information on the influence of the environment on the system's dynamics in the frequency domain, the correlation function does the exact same thing in the time domain. Plugging the definition of the correlation function in Eq.(1.69), we find the *Non-Markovian Quantum State Difusion* (NMQSD) equation,

$$\boxed{\partial_t |\psi[\eta^*(t)]\rangle = \left[-\frac{i}{\hbar}H_S + L\eta^*(t) - L^\dagger \int_0^t ds\alpha(t-s)\frac{\delta}{\delta\eta^*(s)}\right]|\psi[\eta^*(t)]\rangle}. \tag{1.72}$$

Because the equation must be solved for a (large) sample of the random variable z^* using a Gaussian distribution and because z^* only appears through $\eta^*(t)$, the NMQSD equation is a stochastic equation driven by a Gaussian stochastic process $\eta^*(t)$. Because it is Gaussian, the entire stochastic process is described by the statistical moments $\mathcal{M}[\eta^*(t)]$, $\mathcal{M}[\eta(t)\eta(s)]$ and $\mathcal{M}[\eta(t)\eta^*(s)]$ using the statistical mean

$$\mathcal{M}[\cdot] = \frac{1}{\pi^N}\int d^2z \exp\left(-|z|^2\right)[\cdot]. \tag{1.73}$$

Calculating the moments introduced above, one finds that the only non-zero moment is the variance

$$\mathcal{M}[\eta(t)\eta^*(s)] = \alpha(t-s), \tag{1.74}$$

which means that the stochastic process is entirely characterized by the correlation function. The idea of the NMQSD method is then the following: (i) generate a sample of n_{traj} functions $\eta^*(t)$ using a complex distribution entirely characterized by the variance $\alpha(t)$, (ii) for each element of the sample, solve Eq.(1.72) and finally (iii) construct the reduced density matrix by averaging the n_{traj} solutions.

The hiccup with this approach is that it involves a functional derivative, which is not an easy operation to perform numerically. The HOPS method was created specifically to overcome that issue.

Hierarchy Of Pure States

As stated in the previous section, a functional derivative is not an easy operation to implement numerically. In order to avoid dealing with such derivatives, it is possible to define a set of *auxiliary states*. Let us first write again the NMQSD equation below for convenience,

$$\partial_t |\psi[\eta^*(t)]\rangle = \left[-\frac{i}{\hbar}H_S + L\eta^*(t) - L^\dagger \int_0^t ds\alpha(t-s)\frac{\delta}{\delta\eta^*(s)}\right]|\psi[\eta^*(t)]\rangle\,. \tag{1.75}$$

[8]Notice that the definition of the spectral density is not quite the same as in the last section; various convention are used for its definition. The convention used for the implementation of HOPS in OQLiège is the one with a factor π in front of the sum. Because another convention was used for the analytical derivation, i.e. the convention used by L. Viola in Ref. [20] with a factor 4, we should be careful when comparing the analytical results with numeric results from HOPS: when the results from the two different methods will be compared, an appropriate factor must be added.

In order to remove the functional derivative of Eq.(1.75), we define the *first auxiliary state* $\left|\psi^{(1)}(t)\right\rangle$ as

$$\left|\psi^{(1)}(t)\right\rangle = \int_0^t \alpha(t-s)\frac{\delta}{\delta\eta^*(s)}\left|\psi^{(0)}(t)\right\rangle \equiv D_t\left|\psi^{(0)}(t)\right\rangle \tag{1.76}$$

where we use the notation $\left|\psi^{(0)}(t)\right\rangle$ for the 'main' state, i.e. the one that appears in Eq.(1.75) and define the operator D_t for convenience. Using this definition, the NMQSD now reads

$$\partial_t\left|\psi^{(0)}(t)\right\rangle = \left[-iH_S + L\eta^*(t)\right]\left|\psi^{(0)}(t)\right\rangle - L^\dagger\left|\psi^{(1)}(t)\right\rangle \tag{1.77}$$

Instead of a functional derivative, the NMQSD equation now includes an auxiliary state that we need to calculate. In order to do that, we calculate the derivative of this first auxiliary state. This leads to

$$\partial_t\left|\psi^{(1)}(t)\right\rangle = (\partial_t D_t)\left|\psi^{(0)}(t)\right\rangle + D_t\partial_t\left|\psi^{(0)}(t)\right\rangle. \tag{1.78}$$

The two terms can be calculated separately which leads to a nice equation if we use a specific correlation function, namely the correlation function of a single-mode

$$\alpha(\tau) = ge^{-\omega\tau}, \quad \omega \in \mathbb{C},\ \tau \geq 0. \tag{1.79}$$

Remark. While this may seem like a rather restrictive assumption, this particular correlation function actually corresponds to the correlation function of a Lorentzian spectral density. Moreover, it is also possible to derive HOPS using a multi-mode correlation function of the form $\alpha(\tau) = \sum_j g_j e^{-\omega_j\tau}$ which can be used to approximate any spectral density. We will consider the single-mode in the rest of the derivation for simplicity.

Noticing that $\partial_t D_t = -\omega D_t$ for the single-mode function correlation, that we have the commutation relation $[D_t, \eta^*(t)] = \alpha(0)$ and defining the *second auxiliary state* through $D_t D_t\left|\psi^{(0)}(t)\right\rangle \equiv D_t^2\left|\psi^{(0)}(t)\right\rangle \equiv \left|\psi^{(2)}(t)\right\rangle$, we find the following equation for the first auxiliary state,

$$\partial_t\left|\psi^{(1)}(t)\right\rangle = \left[-\frac{i}{\hbar}H_S + L\eta^*(t) - \omega\right]\left|\psi^{(1)}(t)\right\rangle + L\alpha(0)\left|\psi^{(0)}(t)\right\rangle - L^\dagger\left|\psi^{(2)}(t)\right\rangle. \tag{1.80}$$

Similarly, the functional derivative that appears in the equation of the first auxiliary state was removed by introducing yet another auxiliary state. The derivation of the equation Eq.(1.80) can be repeated for the second auxiliary state; as one might expect, a *third auxiliary state* will appear in the equation in order to remove once again the functional derivative. Repeating this process an infinite number of times, we find the following equation for the kth auxiliary state,

$$\boxed{\partial_t\left|\psi^{(k)}(t)\right\rangle = \left[-\frac{i}{\hbar}H_S + L\eta^*(t) - k\omega\right]\left|\psi^{(k)}(t)\right\rangle + kL\alpha(0)\left|\psi^{(k-1)}(t)\right\rangle - L^\dagger\left|\psi^{(k+1)}(t)\right\rangle}. \tag{1.81}$$

This equation can be proven by induction, i.e. by assuming that it is true for $k' = k$ and showing that it is true for $k' = k+1$. Mathematically speaking, we have traded a single differential equation involving a functional derivative for an infinite number of coupled differential equations. This was done by constructing a so-called *hierarchy of pure states* in which the state $\left|\psi^{(0)}(t)\right\rangle$ is the physical state while additional states are fictitious states created to account for memory effects, i.e. for non-Markovian behaviors. In practice, we can truncate the set of equations by choosing $k_{\max}$ the number of auxiliary states. $k_{\max}$ should be chosen high enough to ensure that the solution is converged. Eq.(1.81) forms the *single-mode linear HOPS equations.*

Numerically, one first has to specify the number of auxiliary states ($\rightarrow k_{\max}$), the number of trajectories ($\rightarrow n_{\text{traj}}$) and the timestep ($\rightarrow dt$) for the numerical integration of the HOPS equation. For each trajectory, a random function $\eta^*(t)$ (i.e. a random noise) is generated with a stochastic process with a variance given by the correlation function. In OQLiège, the noise is implemented with an Ornstein Uhlenbeck process. Once

the noise is generated, the system of coupled differential equations is solved and the reduced density matrix is constructed by averaging over the set of trajectories.

A few remarks are in order. First, as it has already been stated, Eq. (1.81) is only valid for a single-mode correlation function. A multi-mode HOPS equation can be derived, but HOPS is only implemented for a single-mode correlation function at the moment in OQLiège. This means that, currently, only a certain type of spectral density can be studied using HOPS, that is Lorentzian spectral densities. Secondly, the linear HOPS equation derived above is not quite the HOPS equation implemented in OQLiège; instead, the non-linear HOPS equation is used, which is more efficient in terms of the number of trajectories needed to obtain a converged solution. Non-linear HOPS is the equivalent of linear HOPS but starting the derivation from non-linear NMQSD [47] instead of the NMQSD equation derived in this section. However, because the derivation of the non-linear NMQSD is far more tricky and because the objective of this section was only to provide some insight into the mechanism of the HOPS method, we did not work out the demonstration of non-linear HOPS. The single-mode non-linear HOPS equation is given by

$$\boxed{\partial_t \left|\psi^{(k)}(t)\right\rangle = \left[-\frac{i}{\hbar}H_S + L\overline{\eta}^*(t) - k\omega\right]\left|\psi^{(k)}(t)\right\rangle + kL\alpha(0)\psi_t^{(k-1)} - \left(L^\dagger - \left\langle L^\dagger\right\rangle_t\right)\left|\psi^{(k+1)}(t)\right\rangle}. \tag{1.82}$$

with

$$\overline{\eta}^*(t) = \eta^*(t) + \int_0^t ds\alpha^*(t-s)\left\langle L^\dagger\right\rangle_s. \tag{1.83}$$

where the stochastic process is shifted according to a term dependent on the correlation function in order to optimize the sampling and reduce the number of trajectories needed to approximate well enough the reduced density matrix.

It also should be noted that only a certain type of Lorentzian can be studied in the single-mode implementation of HOPS, that is Lorentzian with most of their spectral density localized in the positive axis of the frequencies. This is due to the fact that a Lorentzian spectral density corresponds to the correlation function of Eq.(1.79) only if we can make the approximation

$$\alpha(\tau) = \frac{1}{\pi}\int_0^\infty d\omega J(\omega)e^{-i\omega\tau} \approx \frac{1}{\pi}\int_{-\infty}^\infty d\omega J(\omega)e^{-i\omega\tau} = \frac{g\kappa}{2}e^{-(\kappa - i\omega_c)\tau}. \tag{1.84}$$

If a significant part of the distribution is located in the negative frequencies, then the approximation cannot be made and the spectral density does not correspond to a single-mode correlation function.

1.5.2 Decoherence using HOPS

Before using HOPS with dissipation added into the mix, it is necessary to validate the HOPS method by comparing the results for the single purely dephasing qubit with the analytical results introduced previously. In order to do that, we will calculate the off-diagonal component $\rho_{01}(t)$ of the reduced density matrix using the analytical derivation and HOPS. Because HOPS takes an initial state as an input, we decided to choose an initial state $|\psi(t=0)\rangle = \frac{1}{\sqrt{2}}(|0\rangle + |1\rangle)$ for which the density matrix consists of all components equal to $\frac{1}{2}$. Recall that $\rho_{01}(t)$ has the nice analytical expression

$$\rho_{01}(t) = \rho_{01}(t_0)e^{-\Gamma(t)} \tag{1.85}$$

with $\Gamma(t)$ the decoherence function given by

$$\Gamma(t) = \int_0^\infty d\omega g(\omega, t) \tag{1.86}$$

and $g(\omega, t)$ defined as

$$g(\omega, t) = J(\omega)\frac{1-\cos(\omega t)}{\omega^2}. \tag{1.87}$$

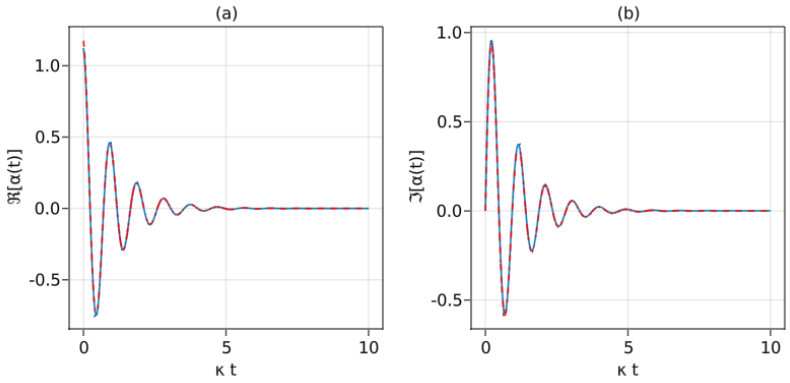

Figure 1.6: Real (a) and imaginary part (b) of the correlation function from Eq.(1.71) for the parameters $\omega_c = 10.0$, $g = 0.5$ and $\kappa = 1.5$ (blue lines) vs the single-mode from Eq.(1.79) implemented in HOPS (red). At any point in the range considered, the approximate and the real correlation function differ by less than 2×10^{-2}.

The parameters of the Lorentzian have to be chosen such that the spectral density satisfies in excellent approximation Eq.(1.84). Choosing $\omega_c = 10.0$, $g = 0.5$ and $\kappa = 1.5$, we find a correlation function (see FIG. 1.6) approximated up to 10^{-2} for all times.

Fixing these parameters, we surprisingly found that the results do not agree (see FIG. 1.7b). However, integrating $g(\omega, t)$ over the entire axis, thus including non-physical negative frequencies, we find a perfect match between the analytical function and the HOPS simulation (see FIG. 1.7a). Increasing drastically the simulation parameters $k_{\max}$, n_{traj} as well as the number of timesteps t_f/dt did not improve the agreement. This leads us to believe that a significant enough part of the spectrum is localized in the negative frequencies and that the correlation function is not approximated well enough. However, we noticed that increasing considerably the parameter ω_c did not result in any improvement either, which meant that problem lied somewhere else. In order to have a better idea of the part of the integrand that is localized in the negative

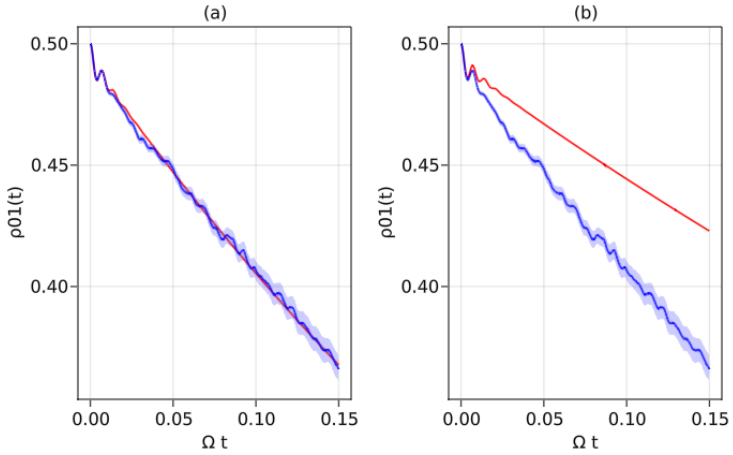

Figure 1.7: Off-diagonal component of the reduced density matrix, using HOPS (blue line) and the analytical derivation (red line). The integration over frequencies in the analytical expression was done on the positive frequencies only (b) and on the entire axis (a). We set $\Omega = g\frac{\kappa^2}{\omega_c^2}$ and the simulation parameters are set to $(k_{\max}, t_f/dt, n_{\text{traj}}) = (5,2000,400)$ with $\Omega t_f = 0.15$.

axis, we plotted $g(\omega, t)$ as a function of ω/ω_c for different times t. The results (displayed in FIG. 1.8) show that for small enough times, the integrand corresponds to a Lorentzian distribution around $\omega = \omega_c$. However, as time increases, a second peak appears at $\omega = 0$ and the part of the distribution located in the negative frequency domain becomes significant; looking at the integrand, we then see two distributions, one around $\omega = \omega_c$ and one around $\omega = 0$, the later seemingly becoming more and more significant with times while the former seems upper bounded.

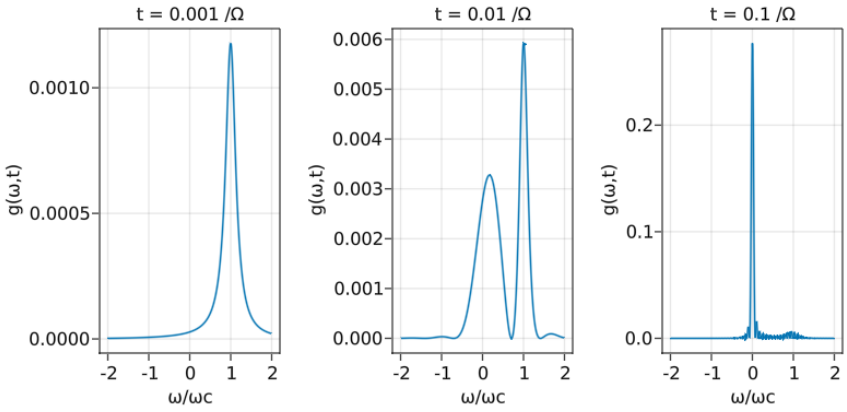

Figure 1.8: Integrand $g(\omega, t)$ as a function of the frequency for different times.

The results described above are very bothersome because it seems like the negative frequencies resulting from the single-mode correlation function, as seemingly insignificant as they can be, prohibit the analysis of decoherence. However bothersome, this is an interesting result; we came across a physical system for which the dynamics is not well taken into account with HOPS because the non-physical negative frequencies inevitably introduced by the correlation function used in HOPS have a significant impact on the dynamics. We however managed to find a regime of parameters (g, ω_c, κ) for which decoherence can be studied. We describe below the thought process which leads us to the estimation of the regime of parameters which enables the study of decoherence with HOPS.

Appropriate regime of parameters

In order to find the relevant regime of parameters, we derived two conditions that the Lorentzian must obey. The first condition on the parameters of the Lorentzian comes directly from Eq.(1.84) which states that the integration over the positive frequencies must be approximated by the integration over the entire axis. This leads to the necessary condition

$$\boxed{\omega_c \gg \kappa}. \tag{1.88}$$

The idea behind the second condition is also fairly straightforward. Basically, we want to avoid the distribution around $\omega = 0$ from building up enough significance in the relevant timescale. In order to do that, we calculated the value of $g(\omega, t)$ at $\omega = 0$ and $\omega = \omega_c$. At $\omega = \omega_c$, the value of the integrand is given by

$$g(\omega = \omega_c, t) = \frac{g\kappa^2}{2}\frac{1}{\kappa^2}\frac{1 - \cos(\omega_c t)}{\omega_c^2} = \frac{g}{2}\frac{1 - \cos(\omega_c t)}{\omega_c^2} \tag{1.89}$$

which can be upper bounded as

$$g(\omega = \omega_c, t) \leq g\frac{1}{\omega_c^2}. \tag{1.90}$$

On the other hand, $g(\omega,t)$ has a $\frac{0}{0}$ limit at $\omega=0$ because of $\frac{1-\cos(\omega t)}{\omega^2}$. However, a series expansion reveals that

$$\begin{aligned} g(\omega=0,t) &= \frac{g\kappa^2}{2}\frac{1}{\kappa^2+\omega_c^2}\left[t^2/2 - t^4\omega^2/24 + \mathcal{O}(t^6\omega^4)\right]_{\omega=0} \\ &= \frac{g\kappa^2}{2}\frac{1}{\kappa^2+\omega_c^2}\frac{t^2}{2}. \end{aligned} \tag{1.91}$$

In order to find the timescale below which the negative frequencies do not contribute significantly, we enforce the condition

$$g(\omega=0,t) \ll g(\omega=\omega_c,t) \quad \Leftrightarrow \quad t^2 \ll 4\frac{\kappa^2/\omega_c^2+1}{\kappa^2}. \tag{1.92}$$

Because $\kappa/\omega_c \ll 1$, we can neglect κ^2/ω_c^2 compared to 1 and write the final condition

$$\boxed{t \ll \frac{2}{\kappa}}. \tag{1.93}$$

This inequality indicates the timescale below which the negative frequencies resulting from HOPS do not significantly alienate the results. In other words, this indicates the strict regime of validity of the single-mode HOPS method. In the context of studying decoherence, we would like to study the dynamics on a timescale given by $\tau \sim 1/\Omega = \frac{\omega_c^2}{g\kappa^2}$ which means that the parameters of the Lorentzian must be chosen such that they satisfy the inequality

$$\frac{\omega_c^2}{g\kappa^2} \ll \frac{2}{\kappa} \tag{1.94}$$

which leads to the following condition on the coupling strength,

$$\boxed{g \gg \frac{\omega_c^2}{2\kappa}}. \tag{1.95}$$

Discussion

Besides enabling us to tune our parameters in order to use HOPS in the context of this thesis, the results above are fundamentally interesting. In order to understand why they are interesting, one should take a look at the form of the Lorentzian spectral density and its correlation function,

$$\begin{aligned} J(\omega) &= \frac{g\kappa^2}{2}\frac{1}{\kappa^2+(\omega-\omega_c)^2} \\ \alpha(\tau) &\approx \frac{g\kappa}{2}e^{-(\kappa+i\omega_c)\tau}. \end{aligned} \tag{1.96}$$

Recall that the correlation function characterizes entirely the influence of the environment on the system's dynamics. It also characterizes entirely the memory effects, i.e. the non-Markovian effects, of the interaction, which is why it appears in the memory term of the HOPS equation Eq.(1.81) and the NMQSD equation Eq.(1.72). A memory-less interaction, i.e. a Markovian interaction, corresponds to the limit $\kappa \to \infty$ [48], for which the Lorentzian tends to

$$\lim_{\kappa\to\infty} \frac{g\kappa^2}{2}\frac{1}{\kappa^2+(\omega-\omega_c)^2} = \frac{g}{2}, \tag{1.97}$$

which corresponds to a correlation function which has the form of a Dirac delta function centered at $\tau=0$. It follows that $1/\kappa$ corresponds to the *memory time*, or *correlation time* [48]. Because we demonstrated that the regime of validity of the HOPS method in this context is given by the condition $t \ll 2/\kappa$, this indicates that the negative frequencies will inevitably have a significant impact in the Markovian limit $\kappa \to \infty$. It thus seems that single-mode HOPS is a method to study non-Markovian dynamics which might not be able to retrieve the Markovian dynamics as a limiting case, at least in the context of a purely dephasing qubit; whereas most methods for studying open quantum systems rely on the Markovian limit and have trouble

incorporating non-Markovian behaviors, single-mode HOPS is a method designed to take non-Markovianity into account which encounters difficulties in the Markovian limit.

The condition Eq.(1.93) thus requires that the maximal time considered be much lower than the memory time of the interaction. In other words, in the context of the purely dephasing qubit, the negative frequencies resulting from the Lorentzian spectral density start to get enough significance in the timescale of the memory effects, thus resulting in seemingly untrustworthy results. One can wonder whether the introduction of the multiple modes in HOPS could mitigate this issue; adding modes of negative weight could possibly help mitigating the effects of the negative part of the Lorentz distributions.

In order to overcome this issue, we derived the condition Eq.(1.95) which basically consists in asking our system to undergo a decoherence process in a timescale much smaller than the memory time. We thus notice that the regime of validity of HOPS actually corresponds to the strong coupling regime. This corresponds to a strongly decohering system where the coherence time is smaller than the timescale of the non-Markovian dynamics. In other words, whereas most non-Markovian methods for studying open quantum system rely on the weak coupling approximation (e.g. the time-convolutionless projection operator technique [11]), HOPS seems to enable the analysis of decoherence mainly in the strong coupling regime.

Although a more complete and deeper discussion should be made about this result, this goes beyond the scope of this Master's thesis and future work should be dedicated to the analysis of the validity of the HOPS method in the context of the purely dephasing spin-boson model.

Dephasing and dissipation

Choosing $\kappa/\omega_c = 0.075$ and $g = 1.6\frac{\omega_c^2}{\kappa}$, we find a near perfect match between the analytical result (when integrating over the positive frequencies only) and the simulation (see FIG. 1.9). We plotted in FIG. 1.9 the fidelity and the population of the excited state $\rho_{00}(t)$ (which is supposed to stay constant when no dissipation is taken into account) for the purely dephasing qubit. Although a qualitative analysis of decoherence is possible with simulation parameters that are not highly demanding[9], larger values of n_{traj}, $k_{\max}$ and lower values of dt are required in order to simulate the dynamics with greater accuracy which increases considerably the running time of the algorithm as well as the computational memory required. Because the computer used is neither fast nor endowed with a great RAM capacity, we had to lower as much as possible the simulation parameters in order to facilitate the computation. One can find in Appendix E the procedure followed in order to find the relevant simulation parameters.

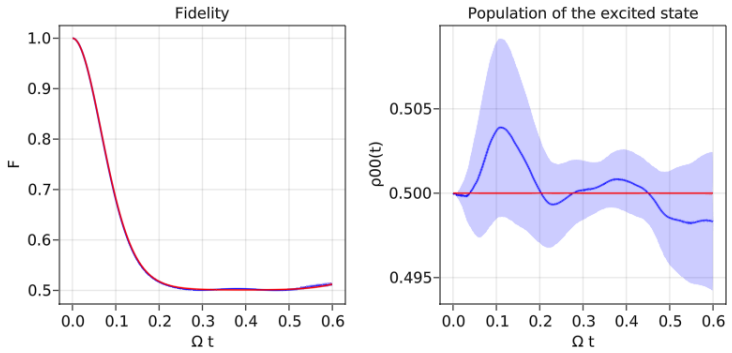

Figure 1.9: Time evolution of the coherence and the population of the excited state for a purely dephasing qubit. The simulation parameters were fixed at ($k_{\max}$, t_f/dt, n_{traj}) = (6,10000,1100) which resulted in a 80-minutes computation time on a laptop. Because the population of the excited state is supposed to stay constant at a value of 0.5, we see that these parameters lead to an error of $\sim 10^{-3}$.

[9]Typically, the parameters ($k_{\max}$, t_f/dt, n_{traj}) = (5,3000,400) result in a computation time of 6 to 8 minutes. The computation time then grows linearly with the number of trajectory and quadratically with the number of steps.

In order to take into account dissipation, we should either add a tunneling term $\Delta_0\sigma_x$ or an interaction term $\hbar\sigma_x\otimes\sum_k\left(g_k b_k^\dagger + g_k^* b_k\right)$. However, the tunneling term alone does not lead to non-unitary effects that we experience in open quantum system. Furthermore, we would prefer the dissipative term to involve a coupling to a bosonic field, because the spectral density presented previously will be very important for the analysis of dynamical decoupling protocols. It then makes sense to add the interaction term $\hbar\sigma_x\otimes\sum_k\left(g_k b_k^\dagger + g_k^* b_k\right)$. We then considered a total interaction Hamiltonian[10] of the form

$$H_{SB} = \hbar\left[\cos^2(\theta/2)\sigma_z + \sin^2(\theta/2)\sigma_x\right]\sum_k\left(g_k b_k^\dagger + g_k^* b_k\right), \tag{1.98}$$

with $\theta \in [0,\pi]$ a parameter that indicates the relative significance of the dissipative and dephasing behaviors.

The fidelity of the qubit as well as the population of the excited state and the ground state are plotted in FIG. 1.10 for $\theta = 0$, 1.2 and π. It clearly demonstrates that dissipation is taken into account with this Hamiltonian, as the population of the excited state is affected by the Hamiltonian when $\theta > 0$. The three cases considered in FIG. 1.10 yield similar behaviors in terms of fidelity, but the population of the excited state is constant for $\theta = 0$ and not constant for $\theta = 1.2$ and $\theta = \pi$. When dissipation of energy is wished to be considered in the context of dynamical decoupling, this interaction Hamiltonian will be used in HOPS. However, it should be pointed out that the ambition with the model is not to simulate a realistic experimental set-up but to highlight the decoupling properties of some dynamical decoupling protocols. Whether this type of interaction Hamiltonian describes a physical system is not the question of this Master's thesis; here, the model is merely a tool used to study dynamical decoupling. However, because the Hamiltonian of Eq.(1.98) for $\theta = 0$ and $\theta = \pi$ are known models for studying the purely dephasing qubit and the spontaneous decay (i.e. dissipation) of a qubit, it makes sense to use it in the range $\theta \in [0,\pi]$ as a tool to study the effects of dissipation and dephasing altogether. Note that it is not clear whether the dynamics represented in FIG. 1.10 for $\theta > 0$ are 'exact', in the sense that the appropriate regime of parameters derived in the previous section does not necessarily hold in the context of a dissipative qubit.

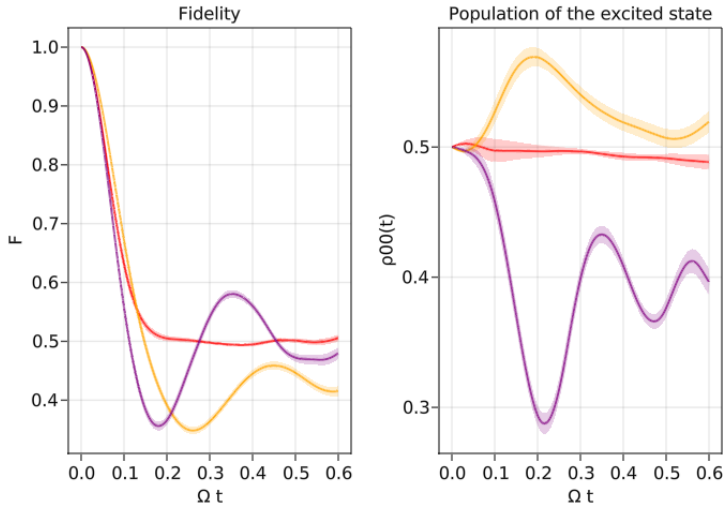

Figure 1.10: Fidelity and population of the excited state for the interaction Hamiltonian $H_{SB}(\theta)$. The simulation parameters were fixed at ($k_{\max}$, t_f/dt, n_{traj}) = (6,10000,500).

[10] I also chose a system Hamiltonian $H_s = \hbar\frac{\omega_0}{2}\sigma_z$ with $\omega_0 = \omega_c$. The motivation behind this choice is to retrieve, at $\theta = \pi$, the same dynamics as in Ref. [11] for the spontaneous decay of a two-level system.

1.6 Discussion

The results above illustrate the effect of decoherence rather well: the exponential decay of the coherence of a qubit decreases the fidelity below the relevant threshold in a certain timescale, given by $\tau \sim 1/\omega_c$ in the Ohmic model and $\tau \sim \frac{1}{g}\frac{\omega_c^2}{\kappa^2}$ in the Lorentzian model. The fundamental issue is that this time is usually rather small, leading to a small lifetime for most qubit implementations (see FIG. 3 for a summary of some promising qubit implementations and their coherence time). Higher fidelity on a greater timescale is required for any quantum technology.

In this Master's thesis, we will explore a clever technique designed to increase the lifetime of a qubit by orders of magnitude, called dynamical decoupling. In order to study the efficacy of the different sequences of dynamical decoupling, we will use as a quantum system a qubit interacting with its environment via the spin-boson model. Different methods will be used to study dynamical decoupling: an analytical derivation similar to the one made in Section 1.4 for the simplest systems (a single qubit undergoing a series of spin-flips) and numerical computation of the components of the reduced density matrix using the HOPS method for systems where no analytical derivation is possible. Depending on the method used, different spectral densities should be used. It is thus necessary to clearly state which spectral densities will be used from now on depending on the method of analysis.

Analytical solution for the time-evolution operator ? The Ohmic spectral densitiy of FIG. 1.1 for various coupling strength ($\alpha = 1.0$, 0.1 or 0.01) will be used. The Lorentzian spectral densities of FIG. 1.5 may also be used when it is interesting to compare different distributions. The timescale is, in all cases, given by $1/\omega_c$ such that all time-dependent functions will be plotted as a function of $\omega_c t$.

HOPS method necessary ? Because the HOPS method is implemented only for Lorentzian distributions almost entirely located in the positive frequency domain, only specific Lorentzians will be used when the HOPS method is applied. The timescale is given by $(g\frac{\kappa^2}{\omega_c^2})^{-1}$ and the parameters should be chosen such that the entire distribution is located in the positive frequency domain. As we have demonstrated in the previous section, the parameters $g = 1.6\frac{\omega^2}{\kappa}$, $\omega_c = 10$, $\kappa = 0.75$ can be chosen such that the negative frequencies of the spectral density do not influence the dynamics on the relevant timescale.

Chapter 2

General Theory of Dynamical Decoupling

In 1999, the authors of Ref. [21] showed that, by applying a control field on a system interacting with its environment, one could engineer the Hamiltonian in such a way that all unwanted interaction would be averaged out, therefore suppressing the unwanted dynamics generated by this Hamiltonian. In this type of Hamiltonian engineering, the objective is to design a control field that effectively implements the quantum operation

$$\mathcal{E} : \mathcal{B}(\mathcal{H}_S) \to \mathcal{B}(\mathcal{H}_S) : S \mapsto \mathcal{E}(S) = 0 \tag{2.1}$$

which acts on the Hilbert space of the system and whose job is to cancel out the unwanted operators S of the total Hamiltonian. This quantum operation can be used to suppress unwanted effects from the system Hamiltonian H_S as well as dynamics generated by the interaction Hamiltonian H_{SB}. In this section, we will follow the derivation worked out in that article in order to explain how to implement such a quantum operation using a sequence of *pulses*. Such a sequence of pulses is called a *dynamical decoupling sequence*, or DD sequence. First, we need to derive the time-evolution operator of the system+environment under periodic driving generated by a periodic control field. Then, we will be able to construct a control field such that the quantum operation Eq.(2.1) is applied.

2.1 Dynamics of a system under periodic driving

Let us consider a system of interest of Hamiltonian H_S interacting with an environment, modeled by a bath of Hamiltonian H_B. The total Hamiltonian can be expressed as

$$H = H_S + H_B + H_{SB} \tag{2.2}$$

with H_{SB} the interaction Hamiltonian containing all unwanted dynamics induced by the system-bath coupling. One can show that the most general form for the Hamiltonian is the Schmidt decomposition

$$H = \sum_\alpha S_\alpha \otimes B_\alpha \tag{2.3}$$

with S_α and B_α operators acting on the system and the bath respectively. We define the interaction space $\mathcal{I}_S \subseteq \mathcal{B}(\mathcal{H}_S)$ as the vector space of bounded linear operators spanned by the operators S_α that are originated from the interaction Hamiltonian H_{SB}, with $\mathcal{B}(\mathcal{H}_S)$ the space including all bounded linear operators acting on the state space $\mathcal{H}_S$ of the system. Now, let us choose a control algebra $\mathcal{C}_S \subseteq \mathcal{B}(\mathcal{H}_S)$. The control algebra contains all the operations that can be applied on the system to implement a DD sequence. We will implement DD by adding an extra term $H_{cf}(t) \in \mathcal{C}_S$, the 'control field', to the total Hamiltonian, so that

$$H(t) = \sum_\alpha S_\alpha \otimes B_\alpha + H_{cf}(t). \tag{2.4}$$

We will restrict ourselves to cyclic control fields such that

$$U_{cf}(t) = \mathcal{T}_{\leftarrow} e^{-\frac{i}{\hbar}\int_0^t dt' H_{cf}(t')} = U_{cf}(t+T_c) \tag{2.5}$$

with T_c the period of the control field $H_{cf}(t) = H_{cf}(t+T_c)$ and $\mathcal{T}_{\leftarrow}$ the time ordering operator. As explained previously, the time ordering operator ensures that the operators are applied in chronological order. We can now move to the rotating frame with respect to $H_{cf}(t)$, using as the unitary operator the time-evolution operator expressed in Eq.(2.5). The effective Hamiltonian in the rotating frame is thus given by

$$\tilde{H}(t) = U_{cf}^{\dagger}(t)\left[\sum_{\alpha} S_\alpha \otimes B_\alpha\right] U_{cf}(t) = \sum_{\alpha}\Big[U_{cf}^{\dagger}(t) S_\alpha U_{cf}(t)\Big] \otimes B_\alpha. \tag{2.6}$$

In the rotating frame, the time-evolution operator corresponding to this effective Hamiltonian is given by

$$\tilde{U}(t) = \mathcal{T}_{\leftarrow} e^{-\frac{i}{\hbar}\int_0^t dt' \tilde{H}(t')} \tag{2.7}$$

where we would like to eliminate the time ordering operator in order to find an analytical solution. One method to remove this operator consists using a Magnus expansion in Eq.(2.7). More information on the Magnus expansion can be found in Appendix C, but the idea is that the time ordering operator of a time-evolution operator

$$U(t) = \mathcal{T}_{\leftarrow} e^{\int_0^t dt' A(t')} \tag{2.8}$$

can be removed if we expand the argument of the exponential as a Magnus series, resulting in the operator

$$U(t) = e^{\Omega(t)} = e^{\sum_{k=0}^{\infty}\Omega_k(t)} \tag{2.9}$$

with $\Omega(t) = \sum_k \Omega_k(t)$ the Magnus series. The first three terms of the Magnus series are given in Appendix C. Using the Magnus expansion in Eq.(2.7) leads to

$$\tilde{U}(t) = \exp\Big\{-\frac{i}{\hbar}\int_0^t dt_1 \tilde{H}(t_1) - \frac{1}{2\hbar^2}\int_0^t dt_1 \int_0^{t_1} dt_2 \Big[\tilde{H}(t_1), \tilde{H}(t_2)\Big] + \dots\Big\}. \tag{2.10}$$

Because the Hamiltonian is periodic, thanks to $H_{cf}(t)$, the next step is to evaluate the expression after Nth cycles of period T_c, i.e. at time $t_N = NT_c$. This gives

$$\begin{aligned}\tilde{U}(t_N) &= \mathcal{T}_{\leftarrow} e^{-\frac{i}{\hbar}\int_0^{t_N} dt' \tilde{H}(t')} = \mathcal{T}_{\leftarrow} e^{-\frac{i}{\hbar} N \int_0^{T_c} dt' \tilde{H}(t')} \\ &= \exp\Big\{-\frac{i}{\hbar}\frac{N}{T_c}\int_0^{T_c} dt_1 \tilde{H}(t_1) T_c - \frac{1}{2\hbar^2}\frac{N}{T_c}\int_0^{T_c} dt_1 \int_0^{t_1} dt_2 \Big[\tilde{H}(t_1), \tilde{H}(t_2)\Big] T_c + \dots\Big\}\end{aligned} \tag{2.11}$$

which we can summarize with the notation

$$\tilde{U}(t_N) = \exp\Big\{-i\Big[\overline{H}^{(0)} + \overline{H}^{(1)} + \dots\Big] t_N\Big\} \tag{2.12}$$

with

$$\overline{H}^{(0)} = \frac{1}{\hbar T_c}\int_0^{T_c} dt' \tilde{H}(t') \tag{2.13a}$$

$$\overline{H}^{(1)} = \frac{1}{2\hbar^2 T_c}\int_0^{T_c} dt_1 \int_0^{t_1} dt_2 \Big[\tilde{H}(t_1), \tilde{H}(t_2)\Big] \tag{2.13b}$$

for the first terms of the Magnus series. A small enough period T_c ensures that the Magnus expansion can be approximated to only the lowest-order term $\overline{H}^{(0)}$, so we can for the purpose of this development consider the *fast control limit* which consists in considering the double limit $N \to \infty$ and $T_c \to 0$ with $t_N = NT_c$.

From a physical point of view, that would mean applying an infinite number of infinitely fast cycles during a finite time t_N. Using this assumption, we can write

$$\tilde{U}(t_N) = \exp\Big\{-i\overline{H}^{(0)}T_N\Big\}. \tag{2.14}$$

In this limit, the entire dynamics of the system will be determined by the *average Hamiltonian*

$$\overline{H}^{(0)} = \frac{1}{\hbar T_c}\int_0^{T_c} dt' \tilde{H}(t'). \tag{2.15}$$

The objective is now to design the right control field such that the average Hamiltonian does not contain any of the unwanted operators present in the interaction Hamiltonian.

2.2 Desired average Hamiltonian

In order to construct the right control field, we first need to choose a finite group of unitary operators $\mathcal{G} = \{g_j, j = 1, \dots |\mathcal{G}|\}$, i.e. operators such that $g_j g_j^\dagger = \mathbb{1}$, that generates the control algebra $\mathcal{C}_S$ with $g_1 = \mathbb{1}$. Once such a group is chosen (and we will see how to choose it based on the Hamiltonian later on), we can define the superoperator

$$\Pi_{\mathcal{G}} : \mathcal{B}(\mathcal{H}_S) \to \mathcal{B}(\mathcal{H}_S) : S \mapsto \overline{S} = \Pi_{\mathcal{G}}(S) = \frac{1}{|\mathcal{G}|}\sum_{g_j\in\mathcal{G}} g_j^\dagger S g_j \tag{2.16}$$

as the quantum operation that we want to implement using the control field, as we shall explain later on. We can prove that applying this superoperator on some operator S leads to an operator $\overline{S}$ that commutes with every operators g_j of the group $\mathcal{G}$, thereby belonging to the so-called *commutant* of $\mathcal{C}_S$, i.e. the space that contains all operators of $\mathcal{B}(\mathcal{H}_S)$ that commute with every operator of $\mathcal{C}_S$. For any unitary operators g_i, we can show that

$$\begin{aligned} g_i^\dagger \overline{S} g_i &= \frac{1}{|\mathcal{G}|}\sum_{g_j\in\mathcal{G}} g_i^\dagger g_j^\dagger S g_j g_i \\ &= \frac{1}{|\mathcal{G}|}\sum_{g_j\in\mathcal{G}} (g_j g_i)^\dagger S (g_j g_i) \\ &= \frac{1}{|\mathcal{G}|}\sum_{g_k\in\mathcal{G}} g_k^\dagger S g_k \end{aligned}$$

with $g_k = g_j g_i$. Because $\mathcal{G}$ constitutes a group, if $\{g_j, j = 1, \dots |\mathcal{G}|\}$ contains every element of $\mathcal{G}$, then so does $\{g_k = g_j g_i, j = 1, \dots |\mathcal{G}|\}$. This leads to

$$g_i^\dagger \overline{S} g_i = \overline{S} \quad \Leftrightarrow \quad \big[\overline{S}, g_i\big] = 0 \tag{2.17}$$

In fact, $\Pi_{\mathcal{G}}$ is the projector onto the commutant of $\mathcal{C}_S$; we also say that $\Pi_{\mathcal{G}}$ projects onto a subspace *invariant* under $\mathcal{G}$, also called a $\mathcal{G}$-*invariant* subspace [21]. A quantum operation such as Eq.(2.16) is also called a (quantum dynamical) *symmetrization procedure* [49]. The idea is then to implement that quantum procedure using the control field such that the averaged Hamiltonian Eq.(2.15) is equal to

$$\overline{H}^{(0)} = \Pi_{\mathcal{G}}(H) = \frac{1}{|\mathcal{G}|}\sum_\alpha\sum_j g_j^\dagger S_\alpha g_j \otimes B_\alpha = \sum_\alpha \overline{S}_\alpha \otimes B_\alpha, \tag{2.18}$$

which is of the form (2.3) but with every operator S_α replaced by their corresponding averaged operator $\overline{S}_\alpha$. An appropriate choice of the group $\mathcal{G}$ can lead to $\overline{S}_\alpha = 0$ for any unwanted operator S_α. In fact, the first

step when constructing a dynamical decoupling sequence is to find a group $\mathcal{G}$ that satisfies $\Pi_{\mathcal{G}}(S) = 0$ for all operators S of the interaction space $\mathcal{I}_S$, with $\mathcal{I}_S \subseteq \mathcal{B}(\mathcal{H}_S)$ the linear space of bounded operators spanned by the system operators present in the interaction Hamiltonian H_{SB}. If we succeed in finding such a group, that is sometimes called the *decoupling group*, then implementing the symmetrization procedure $\Pi_{\mathcal{G}}$ results in all unwanted operators being averaged out to zero.

Now that we showed that the right decoupling group can average out any unwanted operator, the objective is to understand how to implement

$$\overline{H}^{(0)} = \frac{1}{|\mathcal{G}|} \sum_j g_j^\dagger H g_j \tag{2.19}$$

from the Hamiltonian derived in Eq.(2.15),

$$\overline{H}^{(0)} = \frac{1}{\hbar T_c} \int_0^{T_c} dt' \tilde{H}(t'). \tag{2.20}$$

2.3 Control field design

This can be done using a sequence of *ideal pulses*, that is operations of infinitely short duration and infinitely great strength that implement a unitary operator that acts on the system. Such ideal pulses are also called δ-pulses. This sequence of total duration T_c consists of $|\mathcal{G}|$ pulses P_j occurring at times t_j, with the first pulse P_1 occurring at $t_1 > 0$ and the last one $P_{|\mathcal{G}|}$ at $t_{|\mathcal{G}|} = T_c$. The time-evolution operator corresponding to such a sequence is given by

$$U_{cf}(t) = \begin{cases} P_0 = \mathbb{1} & \text{if} \quad t_0 = 0 < t < t_1 \\ P_1 P_0 & \text{if} \quad t_1 \leq t < t_2 \\ \vdots & \vdots \\ P_{j-1} P_{j-2} \dots P_0 & \text{if} \quad t_{j-1} \leq t < t_j \\ \vdots & \vdots \\ P_{|\mathcal{G}|-1} P_{|\mathcal{G}|-2} \dots P_0 & \text{if} \quad t_{|\mathcal{G}|-1} \leq t < t_{|\mathcal{G}|} = T_c \end{cases} \tag{2.21}$$

with $\prod_{j=1}^{|\mathcal{G}|} P_j = \mathbb{1}$ in order to obtain a periodic control field $U_{cf}(t + T_c) = U_{cf}(t)$. This creates a step-wise constant propagator and the pulses can be chosen to design the desired propagator at each step. Therefore, choosing the pulses such that

$$g_j = P_{j-1} P_{j-2} \dots P_0, \quad j = 1, \dots |\mathcal{G}|, \tag{2.22}$$

leads to the propagator

$$U_{cf}(t) = \begin{cases} g_1 & \text{if} \, t_0 = 0 \leq t < t_1 \\ g_2 & \text{if} \, t_1 \leq t < t_2 \\ \vdots & \vdots \\ g_j & \text{if} \, t_{j-1} \leq t < t_j \\ \vdots & \vdots \\ g_{|\mathcal{G}|} & \text{if} \, t_{|\mathcal{G}|-1} \leq t < t_{|\mathcal{G}|} = T_c \end{cases} . \tag{2.23}$$

This choice leads to the propagator $U_{cf}(t)$ "visiting" every element of the decoupling group $\mathcal{G}$ during the sequence. A pulse P_j is thus used to steer the Hamiltonian $\tilde{H}(t)$ from $g_j^\dagger H g_j$ to $g_{j+1}^\dagger H g_{j+1}$. Because the pulses are *ideal*, i.e. of infinitely short duration, the switching is instantaneous. Plugging this propagator into Eq.(2.20) results in the average Hamiltonian

$$\overline{H}^{(0)} = \frac{1}{\hbar} \sum_j \tau_j g_j^\dagger H g_j \tag{2.24}$$

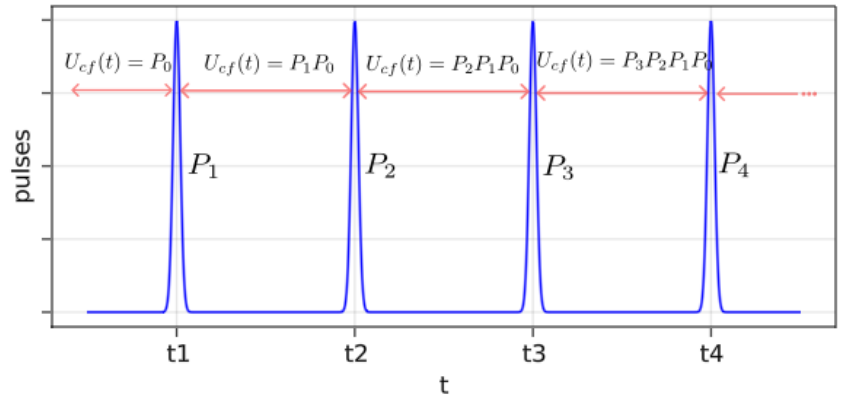

Figure 2.1: Representation of the time evolution of the propagator $U_{cf}(t)$. The pulses are represented as narrow Gaussian distributions, which in the limit of the ideal δ-pulses correspond to Dirac delta functions. Note that it is not possible to plot an operator and that this figure only aims at providing a visual representation of Eq. (2.21).

where we defined $\tau_j = \frac{t_j - t_{j-1}}{T_c}$ the dimensionless parameter that characterizes the duration of the step at which the propagator has the value g_j. It is now straightforward to verify that, by dividing the sequence into $|\mathcal{G}|$ intervals of same duration $\Delta t = T_c/|\mathcal{G}|$, hence by using equidistant pulses, the average Hamiltonian is now given by

$$\overline{H}^{(0)} = \frac{1}{\hbar}\frac{1}{|\mathcal{G}|}\sum_j g_j^\dagger H g_j \tag{2.25}$$

which is precisely the Hamiltonian of Eq.(2.19) corresponding to the quantum dynamical symmetrization procedure described previously. From the definition of the pulses, we get

$$g_{j+1} = P_j g_j, \tag{2.26}$$

which means that we can simply find the pulses needed to implement the symmetrization procedure using the relations

$$\boxed{P_j = g_{j+1} g_j^\dagger \quad \forall j = 1, \dots |\mathcal{G}| - 1}, \tag{2.27a}$$

$$\boxed{P_{|\mathcal{G}|} = g_1 g_{|\mathcal{G}|}^\dagger}. \tag{2.27b}$$

2.4 Summary

To sum up, we have explained how a Hamiltonian can be averaged out by the symmetrization procedure in Eq.(2.16) if the right decoupling group $\mathcal{G} = \{g_j\}$ is chosen. Once the relevant group is found, we have shown that a DD sequence can be implemented using a sequence of pulses $\{P_l, t_l\}$, $k = 1, \dots L$ with L the number of pulses in the sequence, where each pulse P_l is chosen according to the relations (2.27). It is worth pointing out that the construction of the pulses depends on the *path* chosen along the elements of $\mathcal{G}$, which means that there can be (and there are) more than one sequence of pulses that implements the same symmetrization procedure. Any DD sequence is entirely characterized by the decoupling group and the pulse sequence. We can now define the set of unitary operators $\Gamma = \{\gamma_\lambda\}$ as a *generating set* of $\mathcal{G}$ such that every element of $\mathcal{G}$ can be expressed as a product of elements of Γ; the elements of Γ are the *generators* of $\mathcal{G}$. Because of the construction of the pulses described in Eq.(2.27) and because $\mathcal{G}$ is a group of unitary operators, each pulse

P_l is an element of $\mathcal{G}$ and can thus be expressed as a product of the generators. We now realize that, in order to implement a pulse sequence experimentally, we only need to implement the generators γ_λ of a generating set Γ.

2.5 Examples

In this section, we will apply the theory derived in the previous section to construct two dynamical decoupling sequences. The first sequence, called the Carr-Purcell-Meiboom-Gill sequence, or *CPMG* sequence, is designed to protect a qubit against pure dephasing. The second one, the so-called $XY4$ sequence, is designed to protect a qubit against all possible errors. This includes pure dephasing as well as dissipative dynamics.

2.5.1 Carr-Purcell-Meiboom-Gill

The Hamiltonian responsible of the pure dephasing of a qubit was introduced in Section 1.3 in the context of the spin-boson interaction. The most general form of the interaction Hamiltonian of a purely dephasing qubit is given by $H_{SB} = \sigma_z \otimes B$ with B some operator acting on the environment. In this case, the unwanted system operator is σ_z and the objective is to find the decoupling group that averages it out. One such decoupling group of order $|\mathcal{G}| = 2$ is given by $\mathcal{G} = \{\mathbb{1}, \sigma_x\}$. In fact, one can easily verify that this decoupling group satisfies $\Pi_\mathcal{G}(H_{SB}) = 0$ and the explicit calculation is done below,

$$\Pi_\mathcal{G}(S = \sigma_z) = \frac{1}{2}\big[\sigma_z + \sigma_x^\dagger \sigma_z \sigma_x\big] = \frac{1}{2}\big[\sigma_z - \sigma_x^\dagger \sigma_x \sigma_z\big] = \frac{1}{2}[\sigma_z - \sigma_z] = 0. \tag{2.28}$$

where we have used the anticommutation relation $\{\sigma_x, \sigma_z\} = 0$ for the Pauli operators. Because $|\mathcal{G}| = 2$, it follows that two δ-pulses are needed in the DD sequence. Using the relations derived in Eq.(2.27), we find

$$\begin{aligned} P_1 &= \sigma_x \mathbb{1} = \sigma_x, \\ P_2 &= \mathbb{1}\sigma_x = \sigma_x. \end{aligned} \tag{2.29}$$

In the case of the CPMG sequence, the two pulses are identical and correspond to spin-flips. The generating set thus possesses one element and is given by $\Gamma = \{X\}$, using the notation $X \equiv \sigma_x$. A sequence of period T_c can then be constructed by applying two spin-flip separated by an interval of time $\Delta t = T_c/2$. This protocol can be summarized as

$$\Delta t - X - \Delta t - X. \tag{2.30}$$

The sequence mentioned above is called a *Selective* Dynamical Decoupling strategy (SELDD) because the pulse sequence has been carefully designed to average out operators belonging to a certain subspace of $\mathcal{B}(\mathcal{H}_S)$, leaving some terms of the Hamiltonian unchanged. Such SELDD can only be designed if enough information is known about the interaction with the environment and when it exhibits certain symmetries.

2.5.2 XY4

The most general interaction Hamiltonian that contains all types of errors that can occur on a qubit is given by $H_{SB} = \sum_\alpha \sigma_\alpha \otimes B_\alpha$ with $\alpha = x, y, z$. Three operators need to be averaged out, namely σ_x, σ_y and σ_z. A sufficient decoupling group is given by $\mathcal{G} = \{\mathbb{1}, \sigma_x, \sigma_y, \sigma_z\}$, as one can verify by explicitly calculating $\Pi_\mathcal{G}(\sigma_\alpha)$ for $\alpha = x, y, z$. As an example, the calculation for $\alpha = y$ can be found below:

$$\Pi_\mathcal{G}(S = \sigma_y) = \frac{1}{4}\big[\sigma_y + \sigma_x^\dagger \sigma_y \sigma_x + \sigma_y^\dagger \sigma_y \sigma_y + \sigma_z^\dagger \sigma_y \sigma_z\big] = \frac{1}{4}\big[\sigma_y - \sigma_x^\dagger \sigma_x \sigma_y + \sigma_y - \sigma_z^\dagger \sigma_z \sigma_y\big] = 0 \tag{2.31}$$

As explained previously, the construction of the pulses depend on the path chosen along the elements of $\mathcal{G}$. By choosing $g_1 = \mathbb{1}$, $g_2 = \sigma_x$, $g_3 = \sigma_y$ and $g_4 = \sigma_z$, one can find the following pulses:

$$\begin{aligned} P_1 &= \sigma_x, \\ P_2 &= \sigma_y\sigma_z = -i\sigma_z, \\ P_3 &= \sigma_z\sigma_y = -i\sigma_x, \\ P_4 &= \sigma_z. \end{aligned}$$

Up to a c-factor, this leads to the pulses $\{X, Z, X, Z\}$ where $X = \sigma_x$, $Z = \sigma_z$. This consists in a series of spin-flip and phase-flip. The generating set is thus $\Gamma = \{X, Z\}$ and the protocol can be summarized as

$$\Delta t - X - \Delta t - Z - \Delta t - X - \Delta t - Z \tag{2.32}$$

with $\Delta t = T_c/4$. This sequence is a *Maximal* dynamical decoupling strategy (MAXDD) because it averages out the all set of Pauli operators, resulting in a qubit protected against all kinds of errors.

2.6 Discussion

A few remarks relative to the theoretical development above are in order.

First, in order to obtain Eq.(2.25), we assumed τ_j identical for all j, i.e. we assumed the pulses equidistant in time. However, averaged out Hamiltonians can be obtained using DD procedures consisting of non-equidistant pulses, with $\tau_j \neq \tau_i$ for some i, j, and performance can be enhanced by designing sequences that way. The temporal location of the pulses in the sequence is a parameter that can definitely be optimized. Examples of such optimized sequences are Uhrig Dynamical Decoupling (UDD) [41, 50] and Quadratic Dynamical Decoupling (QDD) [51] which we will present in the next sections. Some algorithms used to optimize the spacing of the pulses are presented in Refs. [52–54] and will be introduced shortly. In the next chapter, we will present some interesting optimized sequences based on the optimization of the temporal location of the pulses.

Secondly, we focused in the developments above on finding a sequence of pulses that averages out the Hamiltonian as in Eq.(2.18), where each element g_j of the group $\mathcal{G}$ is 'visited' once, resulting in a sequence of $|\mathcal{G}|$ pulses. However, nothing prevents us from designing longer pulse sequences with the elements of $\mathcal{G}$ appearing more than once in Eq.(2.18). Despite the burden of having to use more pulses separated by smaller time intervals to implement that kind of sequences, such methods can be advantageous as they allow dynamical decoupling to occur using bounded strength control instead of ideal δ-pulses, as we will see later on. UDD and QDD are also examples of sequences for which every element of $\mathcal{G}$ is visited more than once in the period T_c.

Thirdly, as the fast control limit used to simplify the Magnus expansion in Eq.(2.14) can obviously not be attained experimentally, higher terms of the Magnus series will contribute to the dynamics of the system. Advanced DD sequences can be designed to achieve higher-order decoupling. We say that kth-order decoupling will be achieved when terms up to $\overline{H}^{(k-1)}$ are successfully averaged out. Using concatenation methods [55], it is possible to create *Concatenated Dynamical Decoupling* (CDD) sequences that can achieve arbitrarily high orders of decoupling. Another way to increase the order of the decoupling is to design symmetric-cycles, i.e. sequences for which $U_{cf}(T_c - t) = U_{cf}(t)$. It can be shown that such a sequence automatically leads to $\overline{H}^{(k)} = 0$ for odd k [21].

Fourthly, ideal δ-pulses are obviously not experimentally implementable; experimental set-ups lead to *realistic* pulses with bounded strength and finite duration. This issue will be addressed in Chapter 5 where we will demonstrate that dynamical decoupling can still be realized with realistic pulses.

Finally, dynamical decoupling has the side effect of reducing the control that we possess over the system. Since the whole interaction space $\mathcal{I}_S$ will be averaged out by the DD sequence, all operators belonging to that subspace will be useless for computation purposes. In fact, only the operators belonging to the commutant of $\mathcal{C}_S$ will be left unchanged by the symmetrization procedure. When a maximal DD strategy is used, no

control over the system remains. It thus seems that dynamical decoupling is fundamentally incompatible with quantum computation; while developing selective DD sequences helps in leaving some dynamics available, it seems impossible to keep full control over our system while performing dynamical decoupling. However, some clever schemes have been developed in order to overcome that problem. *Dynamically Error-Corrected Gates* (DECG) [56] can be constructed by modifying a DD sequence in such a way that, in addition to fighting decoherence, the sequence effectively implements a quantum gate. This approach is possible because of the introduction of additional pulses inside a given sequence, the design of those pulses depending greatly on the environment model used. Another approach consists in encoding a set of qubits [57], thus allowing the construction of quantum gates that commute with the DD pulses.

2.7 Cayley graph

Before moving on to the analysis of different Dynamical Decoupling sequences, it is worth spending some time explaining the concept of a *Cayley graph* in the context of dynamical decoupling [58, 59] as it provides an elegant representation of a DD sequence. So far, a specific DD sequence is characterized by a decoupling group, $\mathcal{G} = \{g_i\}$, and a sequence of pulses $P = \{P_l, t_l\}$. As stated earlier, the sequence of pulses depends on the path chosen along the elements of $\mathcal{G}$. Another way to define (and discover) a DD sequence of pulses is through the construction of a so-called Cayley graph, an elegant representation of the structure of the decoupling group. In order to construct a Cayley graph, one only needs the decoupling group $\mathcal{G}$ and a generating set Γ. Once the graph is constructed, it is trivial to find the sequence of pulses that implements the relevant symmetrization procedure.

Now let us consider a decoupling group $\mathcal{G} = \{g_i\}$ and a generating set $\Gamma = \{\gamma_\lambda\}$ and create the so-called Cayley graph of $\mathcal{G}$ with respect to Γ, $G(\mathcal{G}, \Gamma)$. One can do that by following two simple steps :

1. Assign to each element of $\mathcal{G}$ a 'vertex'.
2. Join each vertex g_i to the vertices g_j by a directed 'edge' characterized by a 'color' λ if $g_j = \gamma_\lambda g_i$.

Once these steps are completed, the only remaining task to construct a pulse sequence is to choose a cyclic path along the graph. Then, the pulse sequence is constructed by following the path, starting from the vertex corresponding to the identity and each edge corresponding to a pulse. Let us consider the simple example of one qubit for which we want to apply a maximal dynamical decoupling procedure. In this case, the decoupling group is $\mathcal{G} = \{\mathbb{1}, X, Y, Z\}$ with $X \equiv \sigma_x$, $Z \equiv \sigma_z$ and $Y = XZ$ and a generating set is $\Gamma = \{X, Z\}$, resulting in the XY4 sequence mentionned previously. Following the two steps described above, the corresponding Cayley graph is depicted in Fig. 2.2a and an example of cyclic path along this graph is represented in Fig. 2.2b. Following this path leads to the pulse sequence $X \to Z \to X \to Z$.

Cayley graphs prove useful for the task of finding a pulse sequence which uses only the pulses defined in the generating set. One simply needs to find the Cayley graph of the decoupling group with respect to the generating set containing the generators that we want to use (for example, the quantum gates that we can perform with high-fidelity) and choose one of the several cyclic paths.

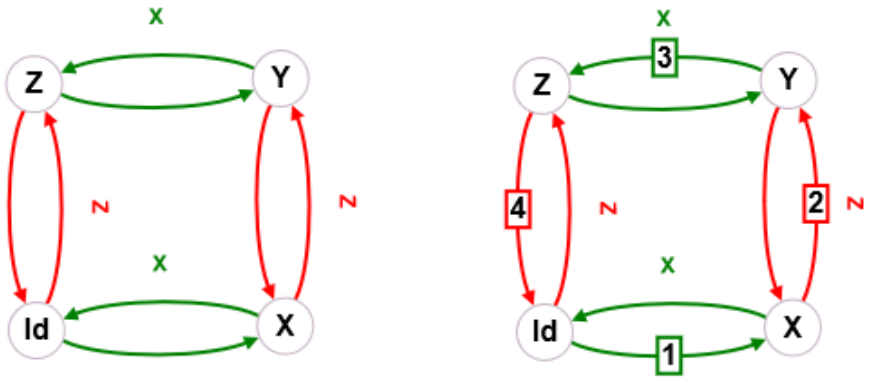

Figure 2.2: Cayley graph of $\mathcal{G} = \{\mathbb{1} \equiv Id, X, Y, Z\}$ with respect to $\Gamma = \{X, Z\}$.

Chapter 3

Selective Dynamical Decoupling

In this section, we will investigate different Selective Dynamical Decoupling (SELDD) strategies in the context of preserving the coherence of a single purely dephasing qubit interacting with a bosonic field, i.e. the spin-boson model presented in Section 1.3. We will first present the CPMG sequence, the most basic DD sequence which was introduced for the first time in Ref. [20]. Then, we will investigate different approaches to the optimization of the SELDD sequence by considering the pulses location in the sequence as a set of parameters that we can optimize over.

The spin-boson model with pure dephasing is extremely convenient because it enables an exact derivation of the time-evolution operator as well as the off-diagonal components of the reduced density matrix. This derivation will be similar to the one made in Section 1.4, except that an additional term in the system Hamiltonian will account for the control field. Because of the nice analytical solution for this system, we will be able to validate the HOPS method in the context of dynamical decoupling.

3.1 CPMG

As stated previously, the CPMG sequence is designed to average out the interaction Hamiltonian $H_{SB} = \sigma_z \otimes B$ and consists of a sequence of period T_c with two successive (ideal) spin-flips applied at $t = T_c/2$ and $t = T_c$. The protocol can be summarized by

$$CPMG \equiv \Delta t - X - \Delta t - X. \tag{3.1}$$

with $\Delta t = T_c/2$. Another way to write Eq.(3.1) is

$$CPMG \equiv U(\Delta t)XU(\Delta t)X \tag{3.2}$$

with $U(\Delta t)$ the free-evolution propagator for a duration Δt. This sequence can be implemented using the control field Hamiltonian

$$H_{cf}(t) = \frac{\pi}{2}\hbar \sum_{n=1}^{2N} \delta(t - t_p^{(n)})\sigma_x \tag{3.3}$$

where $t_p^{(n)} = t_0 + n\Delta t$ and N is the number of sequences of period T_c that we wish to apply. For a given period T_c, the parameter N will determine the total time $t_N = NT_c$, whereas for a given number of sequences N the parameter T_c will do this job.

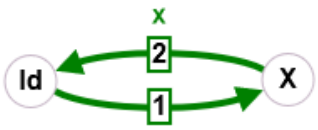

Figure 3.1: Cayley graph representation of the CPMG sequence.

3.1.1 Analytical derivation of the system's dynamics

Adding this control field to the total Hamiltonian of Eq.(1.13) leads to the Hamiltonian

$$H = \underbrace{\frac{\hbar\omega_0}{2}\sigma_z}_{\equiv H_S} + \underbrace{\frac{\pi}{2}\hbar\sum_{n=1}^{2N}\delta(t-t_p^{(n)})\sigma_x}_{\equiv H_{cf}(t)} + \underbrace{\sum_k \hbar\omega_k b_k^\dagger b_k}_{\equiv H_B} + \underbrace{\hbar\sigma_z\otimes\sum_k\left(g_k b_k^\dagger + g_k^* b_k\right)}_{\equiv H_{SB}} \tag{3.4}$$

governing the dynamics of the system. In the rotating frame with respect to $H_S + H_B$, the effective Hamiltonian governing the dynamics of the system is now given by

$$\tilde{H}(t) = \underbrace{\frac{\pi}{2}\hbar\sum_{n=1}^{2N}\delta(t-t_p^{(n)})e^{i\frac{\omega_0}{2}\sigma_z t}\sigma_x e^{-i\frac{\omega_0}{2}\sigma_z t}}_{\equiv\tilde{H}_{cf}(t)} + \underbrace{\hbar\sigma_z\otimes\sum_k\left(g_k e^{i\omega_k t}b_k^\dagger + g_k^* e^{-i\omega_k t}b_k\right)}_{\equiv\tilde{H}_{SB}(t)}. \tag{3.5}$$

Because the approximation of the ideal pulse is made, we can consider that, during a pulse, the interaction Hamiltonian $\tilde{H}_{SB}(t)$ does not contribute. We can then distinguish two propagators: the propagator of the free evolution $\tilde{U}_0(t,t_0)$ where the control field is null and the propagator of the pulse $\tilde{U}_P(t_p^{(n)})$. The total time-evolution operator of a sequence of period T_c is then given by

$$\tilde{U}_{\text{tot}}(t_0+2\Delta t,t_0) = \tilde{U}_{P_2}\tilde{U}_0(t_0+2\Delta t,t_0+\Delta t)\tilde{U}_{P_1}\tilde{U}_0(t_0+\Delta t,t_0). \tag{3.6}$$

The free-evolution propagator is essentially the same as in Section 1.4 where no control field is considered and is thus given by Eq.(1.29). The propagator is written again below for convenience,

$$\tilde{U}(t,t_0) = \exp\left\{\frac{\sigma_z}{2}\sum_k\left[\alpha_k(\Delta t)e^{i\omega_k t_0}b_k^\dagger - h.c.\right]\right\} \tag{3.7}$$

with

$$\alpha_k(\Delta t) = \frac{2g_k}{\omega_k}\left(1-e^{i\omega_k\Delta t}\right). \tag{3.8}$$

and $\Delta t = (t-t_0)$. The pulse propagator can be easily calculated and we obtain

$$\begin{aligned}
\tilde{U}_P(t_p^{(n)}) &= \lim_{\delta t\to 0}\tilde{U}_P(t_p^{(n)}-\delta t, t_p^{(n)}+\delta t)\\
&= \lim_{\delta t\to 0}\exp\left\{-i\frac{\pi}{2}\int_{t_p^{(n)}-\delta t}^{t_p^{(n)}+\delta t}\delta(t-t_p^{(n)})e^{i\frac{\omega_0}{2}\sigma_z t'}\sigma_x e^{-i\frac{\omega_0}{2}\sigma_z t'}\right\}\\
&= \exp\left\{e^{i\frac{\omega_0}{2}\sigma_z t_p^{(n)}}\left(-i\frac{\pi}{2}\sigma_x\right)e^{-i\frac{\omega_0}{2}\sigma_z t_p^{(n)}}\right\}\\
&= (-i)e^{i\frac{\omega_0}{2}\sigma_z t_p^{(n)}}\sigma_x e^{-i\frac{\omega_0}{2}\sigma_z t_p^{(n)}}
\end{aligned} \tag{3.9}$$

for the propagator corresponding to the pulse at time $t_p^{(n)}$. For the last equality, we used the property

$$e^B f(A)e^{-B} = f(e^B A e^{-B}) \tag{3.10}$$

for any two operators A and B as well as the expression of the exponential of a Pauli operator derived in Appendix B. Knowing both propagators, we can now calculate the time-evolution operator of Eq.(3.6). In order to simplify the calculation, $\mathbb{1} = \tilde{U}_{P_1}\tilde{U}_{P_1}^{\dagger}$ can be inserted between the second free evolution and the second pulse, which leads to

$$\tilde{U}_{\text{tot}}(t_0+2\Delta t,t_0) = \underbrace{\tilde{U}_{P_2}\tilde{U}_{P_1}}_{(*)}\overbrace{\tilde{U}_{P_1}^{-1}\tilde{U}_0(t_0+2\Delta t,t_0+\Delta t)\tilde{U}_{P_1}}^{(**)}\tilde{U}_0(t_0+\Delta t,t_0) \tag{3.11}$$

where the factors $(*)$ and $(**)$ are calculated separately for convenience. In order to do that, one needs to use the following relations for the exponential of a Pauli operators:

$$\left[e^{\alpha\sigma_z}, e^{\beta\sigma_z}\right] = 0 \tag{3.12a}$$

$$e^{\alpha\sigma_z} = e^{-\alpha\sigma_z}\sigma_x \tag{3.12b}$$

for all $\alpha,\beta\in\mathbb{C}$. Having that in mind, we can calculate $(*)$,

$$\begin{aligned}(*) &= -e^{i\frac{\omega_0}{2}\sigma_z(t_0+2\Delta t)}\sigma_x e^{-i\frac{\omega_0}{2}\sigma_z(t_0+2\Delta t)}e^{i\frac{\omega_0}{2}\sigma_z(t_0+\Delta t)}\sigma_x e^{-i\frac{\omega_0}{2}\sigma_z(t_0+\Delta t)}\\ &= -e^{i\frac{\omega_0}{2}\sigma_z(t_0+2\Delta t)}\sigma_x e^{-i\frac{\omega_0}{2}\sigma_z\Delta t}\sigma_x e^{-i\frac{\omega_0}{2}\sigma_z(t_0+\Delta t)}\\ &= -e^{i\frac{\omega_0}{2}\sigma_z(t_0+2\Delta t)}e^{i\frac{\omega_0}{2}\sigma_z\Delta t}\sigma_x\sigma_x e^{-i\frac{\omega_0}{2}\sigma_z(t_0+\Delta t)}\\ &= \exp\Big\{i\frac{\omega_0}{2}\sigma_z 2\Delta t\Big\},\end{aligned} \tag{3.13}$$

and $(**)$,

$$(**) = \exp\left\{-\frac{\sigma_z}{2}\sum_k\Big(\alpha_k(\Delta t)e^{i\omega_k(t_0+\Delta t)}b_k^{\dagger} - h.c.\Big)\right\}. \tag{3.14}$$

Plugging $(*)$ and $(**)$ in Eq.(3.11), we find the time-evolution operator

$$\tilde{U}_{\text{tot}}(t_1,t_0) = \exp\Big\{i\frac{\omega_0}{2}\sigma_z(t_1-t_0)\Big\}\exp\left\{\frac{\sigma_z}{2}\sum_k\left(\underbrace{\alpha_k(\Delta t)\big(1-e^{i\omega_k\Delta t}\big)}_{\equiv\eta_k(\Delta t)}e^{i\omega_k t_0}b_k^{\dagger} - h.c.\right)\right\} \tag{3.15}$$

with $t_n = t_0+2n\Delta t$ and where we defined

$$\eta_k(\Delta t) = \alpha_k(\Delta t)\big(1-e^{i\omega_k\Delta t}\big). \tag{3.16}$$

After N sequences, the propagator becomes

$$\tilde{U}_{\text{tot}}(t_N,t_0) = \tilde{U}_{\text{tot}}(t_N,t_{N-1})\dots\tilde{U}_{\text{tot}}(t_1,t_0). \tag{3.17}$$

This can be calculated using Eq.(3.15) and leads to

$$\tilde{U}_{\text{tot}}(t_N,t_0) = \exp\Big\{i\frac{\omega_0}{2}\sigma_z(t_N-t_0)\Big\}\exp\left\{\frac{\sigma_z}{2}\sum_k\left(\underbrace{\eta_k(\Delta t)\sum_{n=1}^{N}e^{2i(n-1)\omega_k\Delta t}}_{\equiv\eta_k(N,\Delta t)}e^{i\omega_k t_0}b_k^{\dagger} - h.c.\right)\right\} \tag{3.18}$$

with

$$\eta_k(N,\Delta t) = \eta_k(\Delta t)\sum_{n=1}^{N}e^{2i(n-1)\omega_k\Delta t} = \eta_k(\Delta t)\frac{1-e^{2iN\Delta t}}{1-e^{2i\Delta t}}. \tag{3.19}$$

This propagator can be compared with the propagator in Eq.(1.29). One can first notice the additional factor $\exp\{i\frac{\omega_0}{2}\sigma_z(t_N - t_0)\}$ which corresponds to the effect of the pulse sequence on the system Hamiltonian H_S. This factor will be responsible for the mitigation of the oscillations of the off-diagonal components generated from the system Hamiltonian. The other difference is the factor $\eta_k(N, \Delta t)$ that appears instead of $\alpha_k(t_N - t_0)$ (Eq.(1.30)) in the term responsible for decoherence. This corresponds to the effect of the pulse sequence on the interaction Hamiltonian. Repeating the exact same steps as in Section 1.4, we find the decoherence function

$$\boxed{\Gamma_{\text{CPMG}}(t_N) = \frac{1}{2}\sum_k |\eta_k(N, \Delta t)|^2 \coth\left(\frac{\hbar\omega_k}{2k_BT}\right)} \tag{3.20}$$

that replaces the previous decoherence function (Eq.(1.38)), corresponding to the free evolution without control field,

$$\boxed{\Gamma_0(t_N) = \frac{1}{2}\sum_k |\alpha_k(2N\Delta t)|^2 \coth\left(\frac{\hbar\omega_k}{2k_BT}\right)}. \tag{3.21}$$

In the continuum limit, Eq.(3.20) becomes

$$\begin{aligned}
\Gamma_{\text{CPMG}}(t_N) &= \frac{1}{2}\sum_k |\eta_k(N, \Delta t)|^2 \coth\left(\frac{\hbar\omega_k}{2k_BT}\right) \\
&= \frac{1}{2}\sum_k \frac{4|g_k|^2}{\omega_k^2}\left|1 - e^{i\omega_k\Delta t}\right|^4 \left|\frac{1 - e^{2iN\omega_k\Delta t}}{1 - e^{2i\omega_k\Delta t}}\right|^2 \coth\left(\frac{\hbar\omega_k}{2k_BT}\right) \\
&= \frac{1}{2}\sum_k \frac{4|g_k|^2}{\omega_k^2} 4[1 - \cos(\omega_k\Delta t)]^2 \frac{\sin^2(N\omega_k\Delta t)}{\sin^2(\omega_k\Delta t)} \coth\left(\frac{\hbar\omega_k}{2k_BT}\right) \\
&= 2\int_0^{+\infty} d\omega \frac{J(\omega)}{\omega^2}[1 - \cos(\omega\Delta t)]^2 \frac{\sin^2(N\omega\Delta t)}{\sin^2(\omega\Delta t)} \coth\left(\frac{\hbar\omega}{2k_BT}\right),
\end{aligned} \tag{3.22}$$

using

$$\begin{aligned}
\left|1 - e^{i\omega_k\Delta t}\right|^4 &= 4|1 - \cos(\omega_k\Delta t)|^2, \\
\left|\frac{1 - e^{2iN\omega_k\Delta t}}{1 - e^{2i\omega_k\Delta t}}\right|^2 &= \frac{\sin^2(N\omega_k\Delta t)}{\sin^2(\omega_k\Delta t)}.
\end{aligned} \tag{3.23}$$

All effects of the CPMG sequence on the decoherence properties are accounted for in this decoherence function.

3.1.2 Performance of the sequence

In this section, we will analyse the performances of the CPMG sequence using the decoherence function derived above. As a starting point, we will consider the fast control limit of an infinitely short sequence applied an infinite number of times. According to the results presented in the previous chapter, this should lead to all decoherence effects being suppressed and we will prove that this is indeed the case. Then, we will compare the decoherence functions with and without pulses applied in order to illustrate how performing dynamical decoupling can be.

Fast control limit

It is interesting to consider the limiting case of the fast control limit which consists in the double limit

$$\begin{cases} \Delta t & \to 0 \\ N & \to \infty \\ t_N & = t_0 + 2N\Delta t \end{cases}. \tag{3.24}$$

In order to study this limiting case, it is helpful to do a series expansion of $\eta_k(N,\Delta t)$ around $\Delta t = 0$. The function $\eta_k(N,\Delta t)$ is written below for convenience,

$$\eta_k(N,\Delta t) = \alpha_k(\Delta t)(1-e^{i\omega_k\Delta t})\frac{1-e^{2iN\Delta t}}{1-e^{2i\Delta t}} = \frac{2g_k}{\omega_k}(1-e^{i\omega_k\Delta t})^2\frac{1-e^{2iN\Delta t}}{1-e^{2i\Delta t}}. \tag{3.25}$$

Because $N\Delta t$ is a constant, the series expansion gives

$$\eta_k(N,\Delta t) = 2\frac{g_k}{\omega_k}\big(1-e^{2iN\Delta t}\big)\left[-\frac{i}{2}\omega_k\Delta t - \frac{i}{24}\omega_k^3\Delta t^3 + \mathcal{O}\big(\Delta t^5\big)\right]. \tag{3.26}$$

Using this series expansion, we can express $|\eta_k(N,\Delta t)|^2$ as

$$|\eta_k(N,\Delta t)|^2 = 2|g_k|^2[1-\cos(2N\Delta t)]\left[\Delta t^2 + \frac{1}{12}\omega_k^2\Delta t^4 + \mathcal{O}(\Delta t^6)\right] \tag{3.27}$$

which is upper bounded by

$$|\eta_k(N,\Delta t)|^2 \leq 4|g_k|^2\left[\Delta t^2 + \frac{1}{12}\omega_k^2\Delta t^4 + \mathcal{O}(\Delta t^6)\right]. \tag{3.28}$$

It then becomes clear that, in the double limit of Eq.(3.24), we have

$$|\eta_k(N,\Delta t)|^2 \to 0 \quad \forall \text{ modes } k \tag{3.29}$$

this means that in the fast control limit, decoherence is entirely suppressed and

$$\Gamma_{\text{CPMG}}(t_N) \approx 0 + \mathcal{O}(\Delta t^2) \tag{3.30}$$

Dynamical decoupling as a filter function

A first result can be obtained by comparing the parameters $|\eta_k(N,\Delta t)|^2$ and $|\alpha_k(2N\Delta t)|^2$ of the decoherence functions obtained in Eq.(3.20) and Eq.(3.21). These parameters characterize the decoherence rate induced by the mode k of the bosonic field and should be reduced in order to increase the coherence time of the qubit. We have shown previously that they can be developed as

$$|\eta_k(N,\Delta t)|^2 = 16\frac{|g_k|^2}{\omega_k^2}[1-\cos(\omega_k\Delta t)]^2\frac{\sin^2(N\omega_k\Delta t)}{\sin^2(\omega_k\Delta t)} \tag{3.31}$$

and

$$|\alpha_k(2N\Delta t)|^2 = 8\frac{|g_k|^2}{\omega_k^2}[1-\cos(\omega_k 2N\Delta t)]. \tag{3.32}$$

One can decide to compare the decoherence function by comparing these two factors for any mode k. Because the factor $8\frac{|g_k|^2}{\omega_k^2}$ appears in both terms, we will instead compare the terms

$$\alpha = \frac{|\eta_k(N,\Delta t)|^2}{8\frac{|g_k|^2}{\omega_k^2}} = 2[1-\cos(\omega_k\Delta t)]^2\frac{\sin^2(N\omega_k\Delta t)}{\sin^2(\omega_k\Delta t)} \tag{3.33}$$

and

$$\beta = \frac{|\alpha_k(2N\Delta t)|^2}{8\frac{|g_k|^2}{\omega_k^2}} = [1-\cos(\omega_k 2N\Delta t)]. \tag{3.34}$$

Using Mathematica, one easily finds that

$$\beta - \alpha = 2\cos(\omega_k\Delta t)\frac{\sin^2(N\omega_k\Delta t)}{\cos^2(\omega_k\Delta t/2)}. \tag{3.35}$$

Because $\frac{\sin^2(N\omega_k\Delta t)}{\cos^2(\omega_k\Delta t/2)} \geq 0$ for all N and for all $\omega_k\Delta t$, the sign of $\beta-\alpha$ will be entirely determined by the sign of $\cos(\omega_k\Delta t)$. This leads to the conclusion that

$$\beta - \alpha \geq 0 \quad \forall\, \omega_k\Delta t \in [0, \pi/2] \tag{3.36}$$

and, equivalently, that

$$|\eta_k(N,\Delta t)|^2 \leq |\alpha_k(2N\Delta t)|^2 \tag{3.37}$$

for all modes k satisfying

$$\omega_k\Delta t \in [0, \pi/2]. \tag{3.38}$$

In other words, for a given sequence of period $T_c = 2\Delta t$, the decoherence induced by the modes k corresponding to frequencies satisfying Eq.(3.38) will be reduced compared to the case where no pulse is applied, and that for any number of sequences N. However, the modes k corresponding to higher frequencies can result in higher decoherence rate in the presence of pulses. From this result, we understand that the sequence of pulses essentially acts as a *filter function* [52] in the decoherence function which reduces the coupling strength of the frequencies

$$\omega < \frac{\pi}{2\Delta t}. \tag{3.39}$$

In practice, Δt has to be chosen such that the highest frequency of the bath, i.e. the frequency ω_c above which the spectral density cuts off, satisfies the condition

$$\omega_c\Delta t \lesssim 1. \tag{3.40}$$

If Δt and ω_c satisfy the condition above, then the decoherence rate corresponding to each mode k will be reduced and thus so will be the overall decoherence rate. This filter function perspective of dynamical decoupling is more obvious in the continuum limit where the decoherence function is given by

$$\Gamma_{\text{CPMG}}(t_N) = 2\int d\omega \frac{J(\omega)}{\omega^2}[1-\cos(\omega\Delta t)]^2 \frac{\sin^2(N\omega\Delta t)}{\sin^2(\omega\Delta t)} \coth\left(\frac{\hbar\omega}{2k_BT}\right), \tag{3.41a}$$

$$\Gamma_0(t_N) = \int d\omega \frac{J(\omega)}{\omega^2}[1-\cos(\omega 2N\Delta t)] \coth\left(\frac{\hbar\omega}{2k_BT}\right), \tag{3.41b}$$

where we can define $f_{\text{CPMG}}(\omega\Delta t, N)$ and $f_0(\omega\Delta t, N)$ as former α and β:

$$f_{\text{CPMG}}(\omega\Delta t, N) = 2[1-\cos(\omega\Delta t)]^2 \frac{\sin^2(N\omega\Delta t)}{\sin^2(\omega\Delta t)}, \tag{3.42a}$$

$$f_0(\omega\Delta t, N) = [1-\cos(\omega 2N\Delta t)]. \tag{3.42b}$$

Putting Eq.(3.42) into Eq.(3.41) leads to

$$\Gamma_{\text{CPMG}}(t_N) = \int d\omega \frac{J(\omega)}{\omega^2} f_{\text{CPMG}}(\omega\Delta t, N) \coth\left(\frac{\hbar\omega}{2k_BT}\right), \tag{3.43a}$$

$$\Gamma_0(t_N) = \int d\omega \frac{J(\omega)}{\omega^2} f_0(\omega\Delta t, N) \coth\left(\frac{\hbar\omega}{2k_BT}\right). \tag{3.43b}$$

In this equation, the decoherence function is given by an integral over all frequencies of the spectral density over ω^2, multiplied by two factors: a factor that depends on the temperature and a filter function $f(\omega\Delta t, N)$ whose job is to filter certain frequencies.

The filter functions of Eq.(3.42) are plotted in FIG. 3.2 for increasing time. A first observation is that the filter function of the free evolution (without pulse) filters low frequencies satisfying

$$\omega t \lesssim 1 \tag{3.44}$$

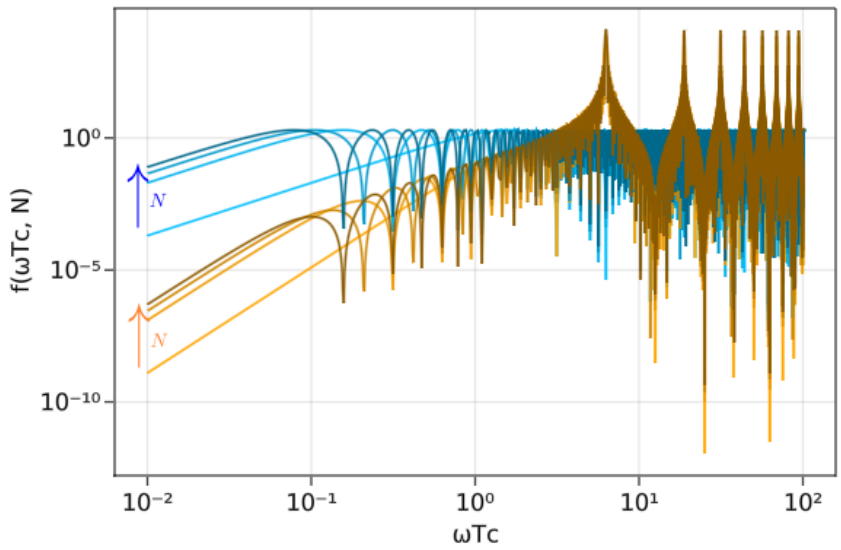

Figure 3.2: Filter functions without pulse (blue lines) and with the CPMG sequence (orange lines). The filter function was plotted for increasing number of sequences N ($N = 1$, 20, 30 and 40), corresponding to increasing time t_N, with smaller values of N corresponding to lighter tones of blue (resp. orange).

such that, as time increases, the filter function filters less and less frequencies. The value of the filter function stays however smaller or equal to 2 for all frequencies at all times. The CPMG filter function, on the other hand, exhibits different properties. Frequencies satisfying

$$\omega T_c \lesssim 2 \tag{3.45}$$

are filtered at all times, with $T_c = 2\Delta t$. The efficiency of the filter function, however, decreases as time increases. For higher frequencies, the value of the filter function can get much greater than 1, which means that the decoherence effects induced by those frequencies are increased compared to the no-pulse scenario. This means that dynamical decoupling filters all frequencies smaller than the frequency of the DD sequence while increasing the decoherence rate corresponding to higher frequencies.

Coherence loss of a qubit

Now that the filter function nature of dynamical decoupling has been presented, the actual gain in terms of fidelity (or equivalently infidelity) can be demonstrated by specifying a spectral density and choosing a sequence's period.

For an Ohmic spectral density of cut-off frequency ω_c, we can infer from the previous discussion that a sequence of period $T_c \sim 2/\omega_c$ (or shorter) is necessary to filter the relevant frequencies. We plotted in Fig. 3.3 the infidelity of a qubit of initial state $|\psi\rangle = \frac{1}{\sqrt{2}}(|0\rangle + |1\rangle)$ interacting with a bosonic bath as presented in Section 1.4 for the Ohmic spectral density for different coupling strengths. As expected, a relevant decrease of the infidelity is first observed for periods T_c satisfying

$$\omega_c \Delta t = \omega_c T_c/2 \lesssim 1, \tag{3.46}$$

while sequences of longer periods result in greater decoherence. Evidently, decreasing the period even further leads to improved performances, meaning that we are able to reach a lower infidelity for an extended period of time. The value of the infidelity that we are able to reach with a given period, however, still largely depends on the coupling strength. While periods of $T_c \sim 2/\omega_c$ are sufficient to ensure a fidelity increase

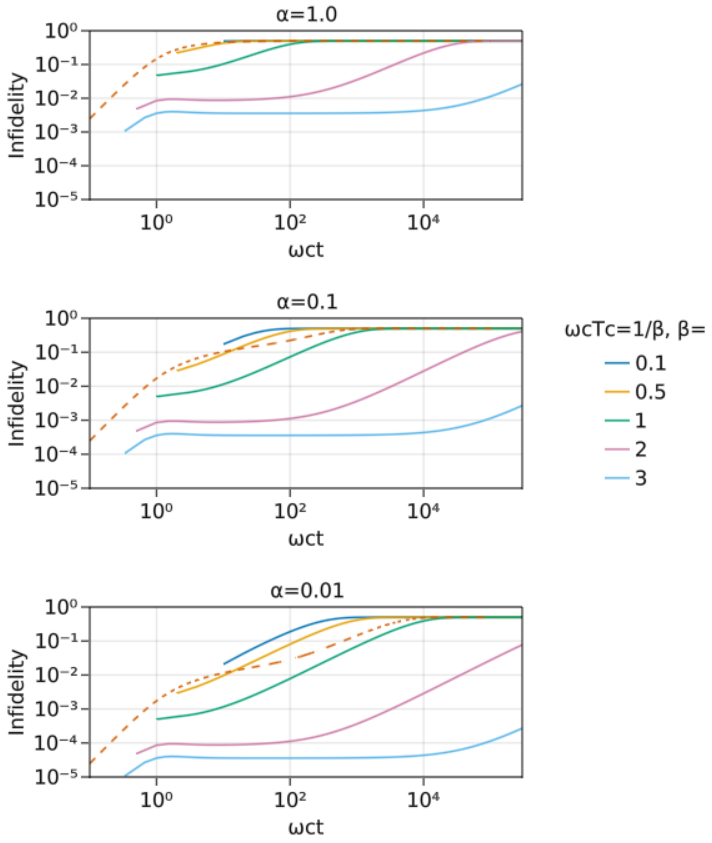

Figure 3.3: Infidelity of a qubit in the initial state $|\psi\rangle = \frac{1}{\sqrt{2}}(|0\rangle + |1\rangle)$ interacting with its environment via the spin-boson model with Ohmic spectral density described in Section 1.4, plotted for different coupling strengths ($\alpha = 1.0$, 0.1 and 0.01). The dashed line corresponds to the infidelity when no control field is applied while the solid lines correspond to the infidelity when a CPMG sequence (of period indicated in the graph legend) is applied.

compared to the free evolution, much smaller periods are necessary to attain the fidelity threshold presented previously.

Instead of fixing the period of the sequence and calculate the infidelity at times t, one can also decide to fix the number of pulses and compute the infidelity at various times t (see FIG.3.5). This will give us information about the fidelity that we can reach if the number of pulses is the limiting physical quantity that we wish to reduce. This point of view will be useful when comparing two different sequences because it will allow us to easily verify which sequence gives a superior fidelity with a lesser number of pulses.

It is interesting to reproduce FIG. 3.4 for different spectral densities which yield similar coherence times. Such spectral densities were introduced in Section 1.4 precisely for such analysis and were plotted in FIG. 1.5. In FIG. 3.5, the infidelity for a fixed number of pulses is plotted for two types of spectral densities (Ohmic SD and two Lorentzian SD's). Comparing the infidelity for both Lorentzian SD's, it first appears that the CPMG sequence is less effective for the broader Lorentzian ($g/\gamma = 0.8$, $\kappa = 175.0$); both systems yield similar coherence times without dynamical decoupling, but the coherence time increases slightly less for the broader Lorentzian when the CPMG sequence is applied. This can be explained by the filter function formalism of dynamical decoupling; we have learned from FIG. 3.2 that, for a given period T_c, frequencies lower than $2/T_c$ are filtered whereas higher frequencies can be amplified. This means that the performance of the DD sequence will depend on the form of the spectral density *beyond* the cut-off frequency ω_c. Now

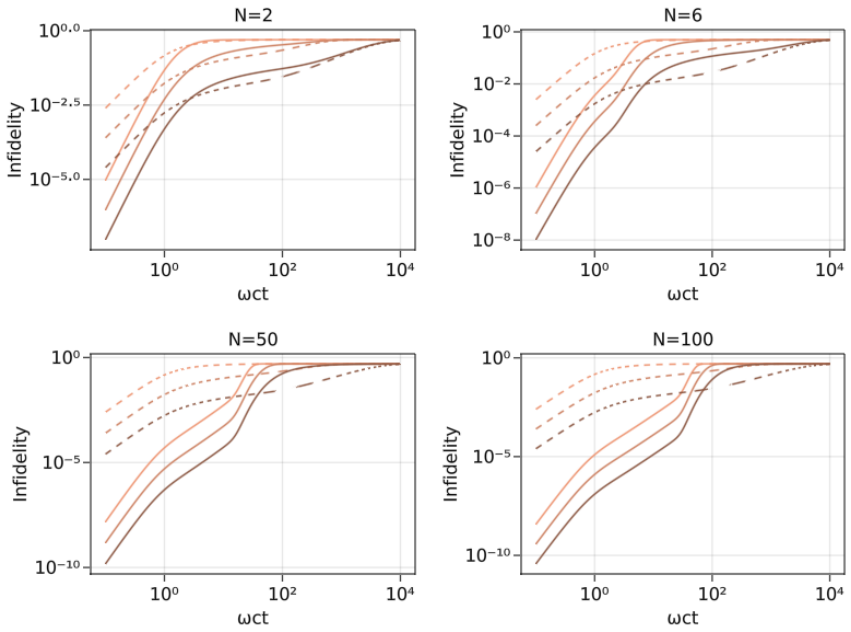

Figure 3.4: Infidelity for a fixed number of pulses (solid lines) and for the free-evolution (dashed lines). The infidelity was calculated for $\alpha = 1.0$, 0.1 and 0.01 (from top to bottom).

looking at FIG. 1.5, one can see that the Lorentzian ($g/\gamma = 1.5$, $\kappa = 70.0$) has a harder cut-off beyond the frequency ω_c. This means that for a DD sequence satisfying $T_c \lesssim 2/\omega_c$, the intervals of frequencies that are *amplified* by the DD sequence correspond to smaller values of the spectral density. A smoother cut-off hence results in reduced performances. This discussion highlights one important aspect of DD sequences: the performance of a given sequence will depend greatly on the spectral density.

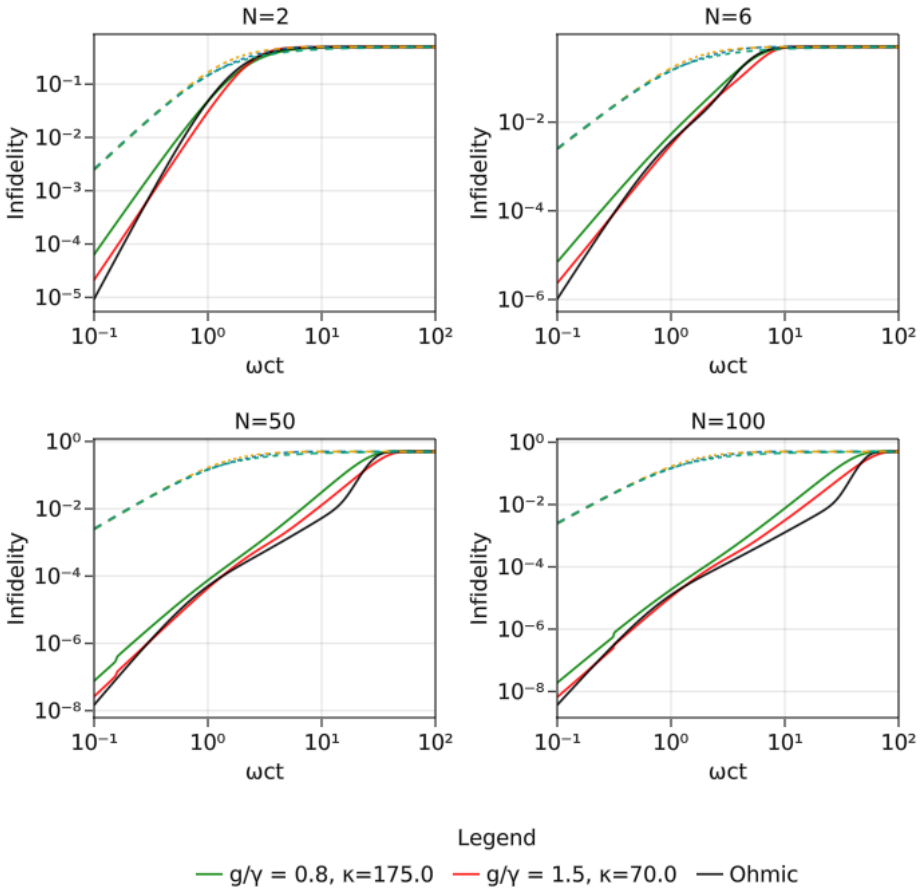

Figure 3.5: Infidelity for a fixed number of pulses (solid lines) and for the free-evolution (dashed lines). Three spectral densities introduced in Section 2.6 are studied, including the Ohmic spectral density used above. The coupling strength of the Ohmic spectral density is fixed at $\alpha_c = 1.0$ and the Lorentzian's are fixed to $g/\gamma = 0.8$ and 1.5 with $\gamma = \alpha_0 \frac{\kappa\omega_c}{e}$ as defined in Section 2.6.

3.2 Optimizing the pulses temporal location

As stated in Section 2.2, a sequence of pulses (i) does not have to consist of equidistant pulses and (ii) can visit each element of the decoupling group more than once. Having that in mind, we can try and optimize the CPMG sequence by using N non-equidistant pulses instead of two for a given period T_c. Because the control field has to be cyclic, N is an even number. The control field for one sequence, with the approximation of unbounded δ-pulses, can be modeled by the Hamiltonian

$$H_{cf}(t) = \frac{\pi}{2}\hbar \sum_{j=1}^{N} \delta(t - t_j)\sigma_x = H_{cf}(t + T_c) \tag{3.47}$$

where the positions of the pulses $\{t_j\}$ are parameters of the sequence that are yet to be fixed. Having made the approximation of unbounded δ-pulses, we can set the interaction Hamiltonian equal to zero when a pulse is applied, resulting in the following time-evolution operator,

$$\tilde{U}_{\text{tot}}(T_c, T_0) = \tilde{U}_0(t_{N+1}, t_N)\tilde{U}_P(t_N)\tilde{U}_0(t_N, t_N - 1)\tilde{U}_P(t_{N-1}) \dots \tilde{U}_P(t_2)\tilde{U}_0(t_2, t_1)\tilde{U}_P(t_1)\tilde{U}_0(t_1, t_0) \tag{3.48}$$

with

$$\tilde{U}_P(t_n) = (-i)e^{i\frac{\omega_0}{2}\sigma_z t_n}\sigma_x e^{-i\frac{\omega_0}{2}\sigma_z t_n}$$
$$\text{and} \quad \tilde{U}_0(t_{n+1}, t_n) = \exp\left\{\frac{\sigma_z}{2}\sum_k \left(\alpha_k(t_{n+1}-t_n)e^{i\omega_k t_n}b_k^\dagger - h.c.\right)\right\} \tag{3.49}$$

the expression of the pulse applied at t_n and the free-evolution in the time interval $[t_n, t_{n+1}]$ respectively. $\alpha_k(t_{n+1}-t_n)$ is defined by

$$\alpha_k(t_{n+1}-t_n) = 2\frac{g_k}{\omega_k}\left[1 - e^{i\omega_k(t_{n+1}-t_n)}\right] \tag{3.50}$$

and is independent of t_0. Equation (3.48) can be developed as

$$\begin{aligned}\tilde{U}_{\text{tot}}(T_c, t_0) &= \tilde{U}_0(t_{N+1}, t_N)\prod_{n=0}^{N-1}\tilde{U}_P(t_{n+1})\tilde{U}_0(t_{n+1}, t_n)\\ \text{(up to a c-number)} \ &= \tilde{U}_0(t_{N+1}, t_N)\prod_{n=0}^{N-1}\left(\sigma_x e^{-i\omega_0\sigma_z t_{n+1}}\exp\left\{\frac{\sigma_z}{2}\sum_k\left(\alpha_k(t_{n+1}-t_n)e^{i\omega_k t_n}b_k^\dagger - h.c.\right)\right\}\right).\end{aligned}$$

Now we can move all σ_x to the left, taking into account that as a σ_x permutes with an exponential of σ_z, the sign of the exponential is changed. As a result, the factor relative to the value $n=0$ will not change sign as it will permute with no σ_x, the one relative to $n=1$ will change sign one time as it will permute with one σ_x, the one relative to $n=2$ will change sign 2 times (resulting in no change of sign), etc. At the end of the day, we are left with the product of N Pauli matrices σ_x which is nothing but the identity operator as N is even. This results in the expression

$$\begin{aligned}\tilde{U}_{\text{tot}}(T_c, t_0) &= \tilde{U}_0(t_{N+1}, t_N)\prod_{n=0}^{N-1}\left(e^{(-1)^{n+1}i\omega_0\sigma_z t_{n+1}}\exp\left\{(-1)^n\frac{\sigma_z}{2}\sum_k\left(\alpha_k(t_{n+1}-t_n)e^{i\omega_k t_n}b_k^\dagger - h.c.\right)\right\}\right)\\ &= \left(\prod_{n=1}^{N}\exp\{(-1)^n i\omega_0\sigma_z t_n\}\right)\left(\prod_{n=0}^{N}\exp\left\{(-1)^n\frac{\sigma_z}{2}\sum_k\left(\alpha_k(t_{n+1}-t_n)e^{i\omega_k t_n}b_k^\dagger - h.c.\right)\right\}\right)\\ &= \exp\left\{\sum_{n=1}^{N}(-1)^n i\omega_0\sigma_z t_n\right\}\exp\left\{\sum_{n=0}^{N}(-1)^n\frac{\sigma_z}{2}\sum_k\left(\alpha_k(t_{n+1}-t_n)e^{i\omega_k t_n}b_k^\dagger - h.c.\right)\right\}.\end{aligned} \tag{3.51}$$

The propagator once again consists of two factors, the first one $\exp\left\{\sum_{n=1}^{N}(-1)^n i\omega_0\sigma_z t_n\right\}$ corresponding to the effect of the sequence on the system Hamiltonian H_S and the second factor corresponding to its effects on the interaction Hamiltonian. Defining

$$\mu_k(N, T_c) \equiv \sum_{n=0}^{N}(-1)^n\alpha_k(t_{n+1}-t_n)e^{i\omega_k t_n}, \tag{3.52}$$

we can write the total propagator for one period T_c as

$$\tilde{U}_{\text{tot}}(T_c, t_0) = \exp\left\{i\omega_0\sigma_z\sum_{n=1}^{N}(-1)^n t_n\right\}\exp\left\{\frac{\sigma_z}{2}\sum_k\left(\mu_k(N, T_c)e^{i\omega_k t_0}b_k^\dagger - h.c.\right)\right\}. \tag{3.53}$$

As $\alpha_k(t_{n+1}-t_n)$ does not depend on t_0 as previously mentioned, the only dependence on t_0 appears in the factor $e^{i\omega_k t_0}$. We can now calculate the total propagator after J sequences of period T_c, in a similar way as was done previously in the case of the CPMG sequence. This ultimately leads to

$$\tilde{U}_{\text{tot}}(t_0 + JT_c, t_0) = \exp\left\{i\omega_0\sigma_z J\sum_{n=1}^{N}(-1)^n t_n\right\}\exp\left\{\frac{\sigma_z}{2}\sum_k\left(\mu_k(N, T_c, J)e^{i\omega_k t_0}b_k^\dagger - h.c.\right)\right\} \tag{3.54}$$

with

$$\mu_k(N,T_c,J) \equiv \mu_k(N,T_c)\left(\sum_{j=0}^{J-1} e^{i\omega_k j T_c}\right) = \mu_k(N,T_c)\frac{1-e^{i\omega J T_c}}{1-e^{i\omega T_c}}. \tag{3.55}$$

Because this expression is similar to Eq.(1.29) and Eq.(3.18), this leads to a decoherence function given by

$$\Gamma(t) = \frac{1}{2}\sum_k |\mu_k(N,T_c,J)|^2 \coth\left(\frac{\hbar\omega_k}{2k_BT}\right). \tag{3.56}$$

In the continuum limit, the function above becomes

$$\Gamma(t) = \frac{1}{2}\int d\omega \frac{J(\omega)}{\omega^2}\left|\sum_{n=0}^{N}(-1)^n\left(1-e^{i\omega(\tau_{n+1}-\tau_n)T_c}\right)e^{i\omega\tau_n T_c}\right|^2 \frac{\sin^2\left(J\frac{\omega T_c}{2}\right)}{\sin^2\left(\frac{\omega T_c}{2}\right)}\coth\left(\frac{\hbar\omega_k}{2k_BT}\right) \tag{3.57}$$

where we have defined $\tau_n = t_n/T_c$ as the adimensional parameter that represents the localization of the nth pulse in the sequence. Defining the filter function

$$f(\omega T_c,N,J) = \frac{1}{2}\left|\sum_{n=0}^{N}(-1)^n\left(1-e^{i\omega(\tau_{n+1}-\tau_n)T_c}\right)e^{i\omega\tau_n T_c}\right|^2 \frac{\sin^2\left(J\frac{\omega T_c}{2}\right)}{\sin^2\left(\frac{\omega T_c}{2}\right)}, \tag{3.58}$$

we can write Eq.(3.57) as

$$\Gamma(t) = \int d\omega \frac{J(\omega)}{\omega^2} f(\omega T_c,N,J)\coth\left(\frac{\hbar\omega_k}{2k_BT}\right). \tag{3.59}$$

Using this decoherence function and filter function, we can investigate how the utilization of non-equidistant pulses can result in enhanced performances. Various approaches have been used to find the perfect pulse sequence and we will present below some interesting results.

3.2.1 Uhrig dynamical decoupling

In an article of 2007 [41], Götz S. Uhrig derived in a different manner the decoherence function of Eq.(3.59) and the filter function of Eq.(3.58). He was interested in optimizing a single cycle of N pulses and of total time T[1], which corresponds to the filter function of Eq.(3.58) for $J = 1$,

$$f_{\text{Uhrig}}(\omega T; N) = \frac{1}{2}|y(\omega T; N)|^2 \tag{3.60}$$

with

$$y(\omega T; N) = \sum_{n=0}^{N} (-1)^n \left(1 - e^{i\omega(\tau_{n+1}-\tau_n)T}\right) e^{i\omega\tau_n T}. \tag{3.61}$$

He then realized that $y(\omega T; N) = 0$ for $\omega T = 0$ and that the N free parameters τ_n enabled him to require his sequence to fulfill N conditions. His conditions were that the first N derivatives of $y(\omega T; N)$ with respect to ωT be equal to zero, that is

$$\frac{d^n}{dz^n} y(z; N) = 0 \quad n = 1, \dots N. \tag{3.62}$$

Solving the N equations above, one can find the optimal temporal location of the N pulses. This leads to the nice analytical solution

$$\tau_n = \sin^2\left(\frac{n\pi}{(2N+2)}\right). \tag{3.63}$$

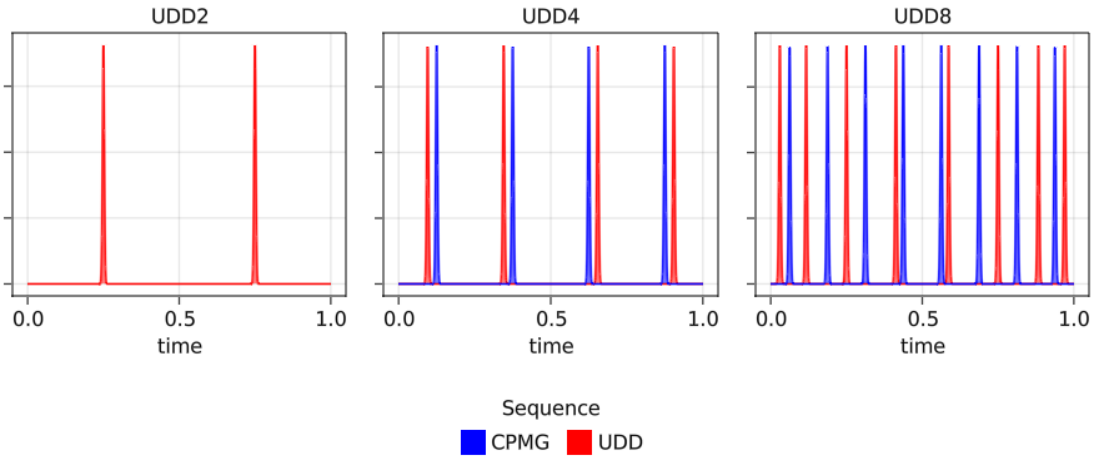

Figure 3.6: Pulses location $\{\tau_n\}$ for the UDD and CPMG sequence. Note that the CPMG sequence has been symmetrized such that the first pulse is applied at the time $\Delta t/2$ instead of Δt. This is done so that the sequence does not end with a pulse.

The result is thus a sequence of N pulses inter-spaced according to Eq.(3.63) called a *Uhrig Dynamical Decoupling* (UDD) sequence. We can summarize the sequence as

$$UDD_N(T) = U(t_1 - t_0)XU(t_2 - t_1)X \dots XU(t_N - t_{N-1})XU(T - t_N) \tag{3.64}$$

with $t_n = \tau_n T_c$ for $n = 1, \dots N$ and $U(t_n - t_{n-1})$ the free-evolution propagator in the time range $[t_{n-1}, t_n]$. Although one needs an even number of pulses in order to retrieve the initial state after the sequence, UDD also works with an odd number of pulses. In order to retrieve the initial state, one only needs to apply an

[1]Because the sequence is not constructed to be applied periodically, it makes sense to use the notation T instead of T_c.

additional pulse X at the end of the sequence. The UDD sequence for any number of pulses N (even or odd) is then defined by

$$UDD_N(T) = X^N U(t_1 - t_0) XU(t_2 - t_1) X \dots XU(t_N - t_{N-1}) XU(T - t_N). \tag{3.65}$$

As it was rigorously proved in Ref. [60], the UDD sequence is the sequence that achieves the highest decoupling order for a given number of pulses, which makes it optimal in this sense. It can be shown that a UDD sequence of N pulses (N being even or odd) achieves Nth order decoupling, which means that the terms of the Magnus expansion $\overline{H}^{(k)}$ for $k \leq N - 1$ are successfully eliminated by the decoupling procedure. In theory, it is thus possible to achieve arbitrary high-order decoupling by increasing the number of pulses N, with the number of pulses required only increasing linearly with the desired order.

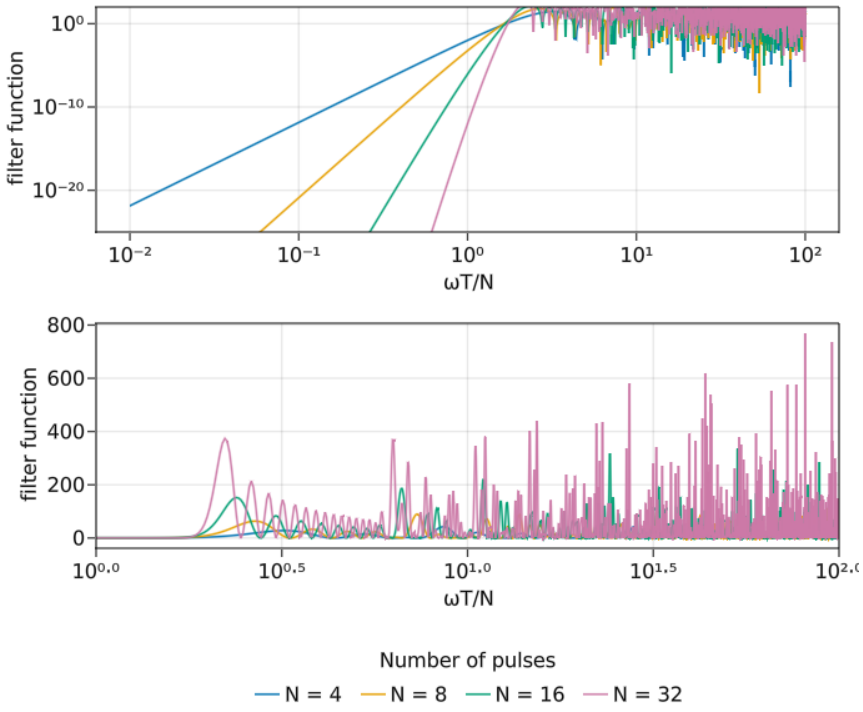

Figure 3.7: UDD filter function as a function of $\omega T_c/N$.

The UDD filter function for increasing number of pulses is plotted in Fig. 3.7 in order to see more clearly how the filtering is affected by the addition of more conditions as defined in Eq.(3.62). Two main behaviors appear when N is increased: (i) the filtering of low frequencies, i.e. $\omega T/N \lesssim 1$, is increased dramatically and (ii) the amplification of higher frequencies is overall higher when N is greater. This means that UDD sequences with a greater number of pulses will result in a better suppression of frequencies $\omega \lesssim N/T$ at the cost of amplifying the decoherence due to larger frequencies.

We can compare a UDD sequence with a sequence of equidistant pulses with the same number of pulses in order to see how the filtering is improved. This leads to Fig. 3.8 where we have plotted the filter function for 4, 8, 16 and 32 pulses using the CPMG and UDD scheme. One can clearly see how advantageous the UDD sequence is for filtering low frequencies. It produces however an overall greater amplification of higher frequencies. Having that in mind, one can assume that UDD is only advantageous over the CPMG sequence when the entire spectral density is located in the range of filtered frequencies. If a significant part of the spectral density is located beyond $\omega \sim N/T$, the greater amplification of the decoherence rate for those frequencies provided by the UDD scheme might lower its performance significantly. In order to study the

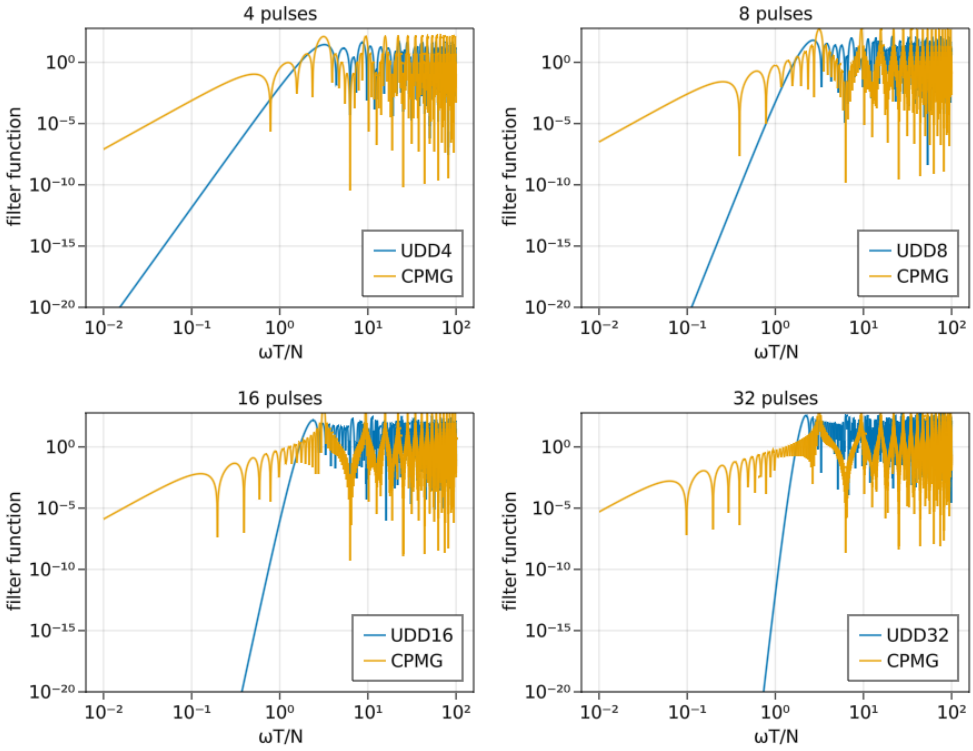

Figure 3.8: UDD and CPMG filter function for different number of pulses.

relative performance of the CPMG and UDD sequence, we constructed a plot similar to Fig. 3.4; we fixed the number of pulses N and calculated the coherence loss for a range $\omega_c T$ with T the duration of the N-pulses protocol, considering N equidistant pulses and N pulses applied according to the UDD scheme presented in Eq.(3.63).

The results are plotted in Fig. 3.9. It is clear that, for short duration protocols, it is highly advantageous to use the pulse intervals provided by the UDD schemes; for $N = 12$, coherence losses as low as $\sim 10^{-15}$ were calculated for $\alpha = 0.01$ for UDD while the CPMG sequence resulted in a coherence loss of $\sim 10^{-7}$ for the same coupling strength. However, as expected from the previous discussion, the performance provided by UDD for longer protocols is degraded and beyond a certain point CPMG becomes more advantageous. In order to see more clearly the regime where CPMG works best, we can re-scale the horizontal axis of Fig. 3.9, plotting the coherence loss as a function of $(2/N)\omega_c T$ instead of $\omega_c T$. This leads to Fig. 3.10 which shows that the CPMG sequence outperforms the corresponding UDD sequence for sequence's duration satisfying $(2/N)\omega_c T \gtrsim 0.4$, that is when the pulse interval of the CPMG sequence satisfies $\omega_c \Delta t \gtrsim 0.2$. It is worth to point out that increasing the number of pulses shifts the UDD-CPMG transition to the left, meaning that the regime where CPMG outperforms UDD extends to shorter duration as the number of pulses increases. For the number of pulses considered, however, the transition occurs around $(2/N)\omega_c T \sim 0.4$.

We plotted in Fig. 3.11 the filter functions corresponding to the UDD40, UDD4 and CPMG sequences as a function of $\frac{\omega}{\omega_c}$ for the sequences' duration satisfying $\frac{2}{N}\omega_c T = 0.4$ as well as the Ohmic spectral density. Around the frequency $\sim 10\omega_c$, the spectral density has decreased by a factor of the order of magnitude $\sim 10^{-3}$ compared to its maximal value, such that the spectral density beyond that point has no significant impact on the total decoherence rate when one integrates over all frequencies. At this frequency, while the CPMG sequence still corresponds to a filter function smaller than one, thus still providing some kind of filtering, the UDD filter functions are now in the amplification regime, with filter functions in the order of magnitude $f_{UDD4} \sim 1$ and $f_{UDD40} \sim 100$. This means that a range of frequency that do not significantly

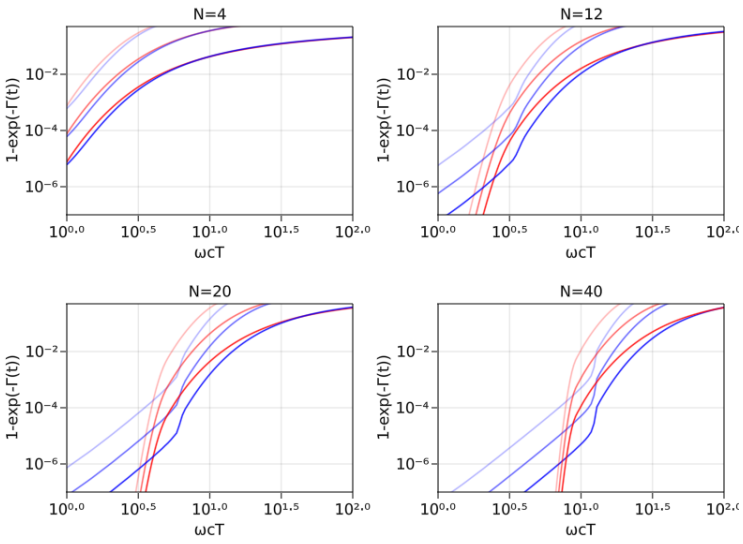

Figure 3.9: Coherence loss for fixed numbers of pulses as a function of the total sequence's duration for equidistant pulses (blue lines) and UDD pulses (red lines). Different values of the coupling strength were considered, namely $\alpha = 1.0$, 0.1 and 0.01 (from top to bottom).

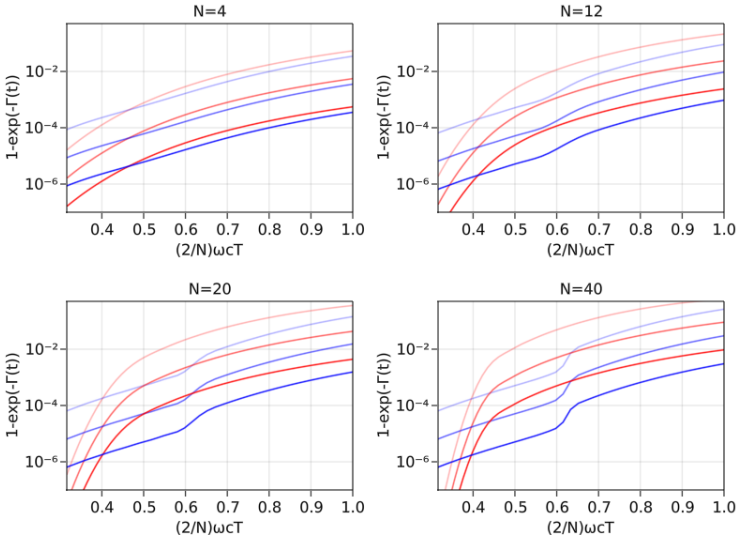

Figure 3.10: Coherence loss for fixed numbers of pulses as a function of $(2/N)\omega_c T$ for equidistant pulses (blue lines) and UDD pulses (red lines).

contribute to the total decoherence rate are sufficiently amplified, because of the UDD scheme, to become significant, thus lowering the advantage that UDD has over CPMG. For $\frac{2}{N}\omega_c T = 0.4$ and $N = 4$, as we can see from Fig. 3.10, this effect is not quite large enough to result in a UDD sequence less performing than the CPMG sequence. However, for $N = 40$, where the amplification is two orders of magnitude greater at the same frequency, the CPMG sequence becomes more performing than UDD.

We demonstrated in this section that the Uhrig dynamical decoupling sequence produces a better filtering of low frequencies at the expanse of producing a higher amplification of the higher frequencies. This means

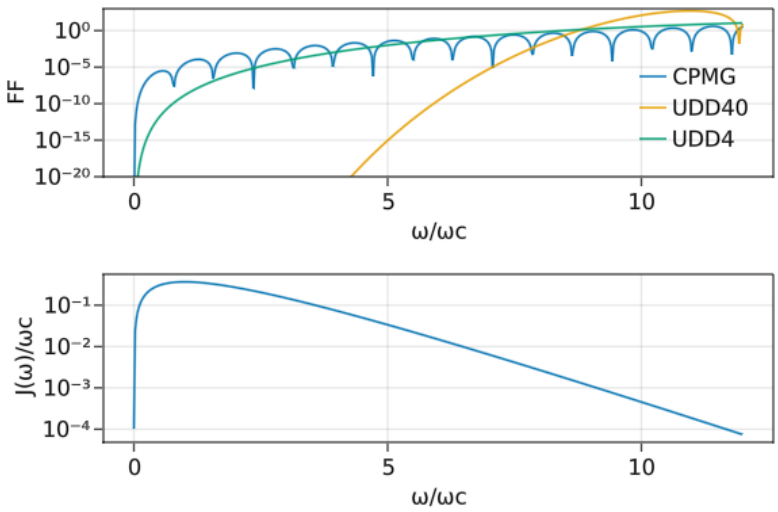

Figure 3.11: Filter function for UDD40, UDD4 and CPMG with the sequence's duration satisfying $\frac{2}{N}\omega_c T = 0.4$ (top) and Ohmic spectral density plotted in the logarithmic scale (bottom).

that the highest filtered frequency should be high enough such that, in the ideal case, the entirety of the spectral density is located in the filtered range of frequencies. When a significant enough part of the distribution is amplified by the filter, the UDD sequence will lose its efficiency and become less performing that the basic CPMG sequence. The superiority of the UDD sequence over the basic CPMG sequence was demonstrated experimentally on different types of qubit [54, 61–63].

3.2.2 Locally optimized dynamical decoupling

A different approach to DD optimization is presented in [54]. The idea is to fix the period T_c as well as the number of pulses N and let the pulses temporal location vary. The infidelity can then be computed as a function of the pulses temporal location as

$$f : \mathbb{R}^n \to [0,1] : (\tau_1, \ldots, \tau_N) \mapsto f(\tau_1, \ldots, \tau_N) \tag{3.66}$$

and the problem becomes a minimization problem that can be efficiently tackled by the *Nelder-Mead Simplex Algorithm* [64]. The infidelity can for example be computed using the analytical formula in Eq.(3.57) or using HOPS. If the infidelity is a physical quantity that we can measure with precision in an experimental set-up, it is *a priori* possible to perform the algorithm using experimental feedback. The sequences resulting from the minimization algorithm are called *Locally Optimized Dynamical Decoupling* (LODD) sequences.

In order to numerically calculate the LODD sequences, one needs to specify the spectral density and use a method capable of calculating the dynamics of the qubit with accuracy. For a single qubit undergoing pure dephasing, the analytical results introduced previously can be used. For more complex systems, one can possibly use HOPS or a relevant quantum master equation. However, when the spectral density is not known with accuracy, the LODD sequences must be calculated using experimental feed-back.

A fundamental issue of the LODD sequences is that they result from an N-dimensional optimization procedure. Nelder-Mead, or most optimization algorithm for that matter, does not perform well when N is too large. This prohibits the construction of many-pulses LODD sequences for long quantum memory application.

Four-pulses LODD sequences

We have implemented the Nelder-Mead algorithm in Julia in order to study the LODD sequences and replicate the results of [54]. The parameters of the Nelder-Mead algorithms were chosen according to [64], but we also allowed the utilization of the adaptive parameters introduced in [65] in order to tackle higher-dimensional problems more efficiently, which can be useful when a large number of pulses are involved. The infidelity function was implemented first using the decoherence function of Eq.(3.57), which enables the construction of locally optimized selective dynamical decoupling to overcome pure dephasing in the spin-boson model.

We first used the Nelder-Mead algorithm for four pulses using the Ohmic spectral density. The Nelder-Mead algorithm requires an initial guess for the pulses locations; the chosen initial guess is the *symmetrized* CPMG sequence[2] applied two times

$$\Delta t/2 - X - \Delta t - X - \Delta t - X - \Delta t - X - \Delta t/2, \tag{3.67}$$

i.e. the initial guess consists of equidistant pulses, but one could try other sequences as an initial guess, e.g. the UDD sequence. The LODD sequence was calculated for different values of the sequence's duration T, ranging from $0.2/\omega_c$ to $6/\omega_c$. For each value of $\omega_c T$, the algorithm returns a vector of dimension 4 containing the localization of each pulse of the sequence, i.e. the quantities $\{\tau_n = t_n/T\}$ which correspond to the pulses location in time $\{t_n\}$ scaled with respect to the sequence's duration T. Plotting $\{\tau_n\}$ as a function of $\omega_c T$, we can understand how the optimal placement of the pulses changes as the duration of the protocol increases. The resulting sequences are plotted in Fig. 3.12 and the corresponding coherence loss is plotted in Fig. 3.13.

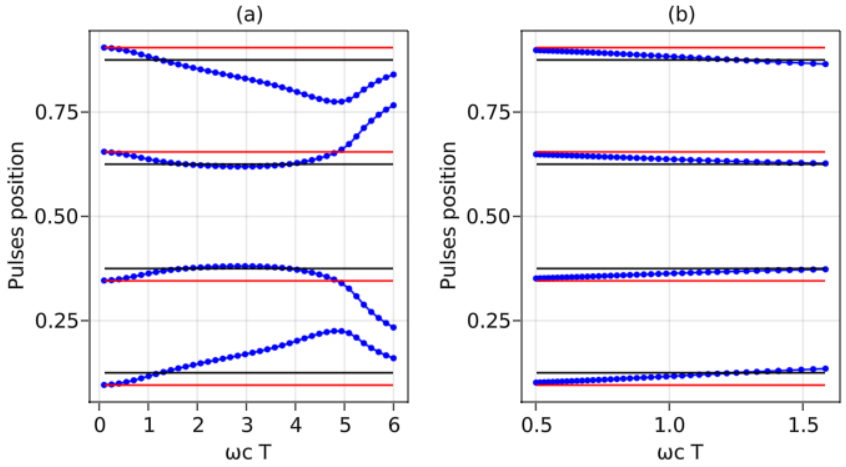

Figure 3.12: LODD sequences for four pulses for various values of $\omega_c T$ ranging from 0.2 to 6 (a) and from $10^{-0.7}$ (~ 0.2) to $10^{0.2}$ (b). The plot (b) is plotted in a logarithmic scale. The UDD and CPMG sequences are represented in red and black respectively.

As could be expected, as the protocol gets shorter, the pulses' localization asymptotically tends to the one given by the UDD sequence. This demonstrates that the Uhrig dynamical decoupling sequence is optimal, in some sense. However, as the duration of the protocol gets longer, the LODD sequences gradually move away from UDD. Although the LODD sequence may seem to correspond to the symmetrized CPMG sequence of Eq.(3.67) at $\omega_c T \sim 1.3$, a closer look reveals that the exact symmetrized CPMG sequence is never actually obtained and thus never corresponds to the optimal choice for pulses placement. The LODD sequences thus correspond to "unknown" sequences, in the sense that the placement of the pulses for those sequences has

[2]The symmetrized CPMG sequence is a reformulation of the classic CPMG sequence which makes it cyclic. It also corresponds to the UDD sequence for 2 pulses.

not been analytically derived and nor are they common choices or intuitive in any sense. These sequences are highly non-trivial and are constructed by a specific design of the filter function that takes into consideration how well the low frequencies are filtered as well as how much the higher frequencies are amplified. For a given duration $\omega_c T$, the LODD sequence is the perfect balance between high filtering of low frequencies and low amplification of high frequencies. For very short duration protocols, since the amplified frequencies correspond to a part of the spectral density with values close to zero, the LODD sequence only has to take into consideration how well low frequencies are filtered and it thus makes sense to recover the UDD sequence which is, by construction, the best filter for low frequencies.

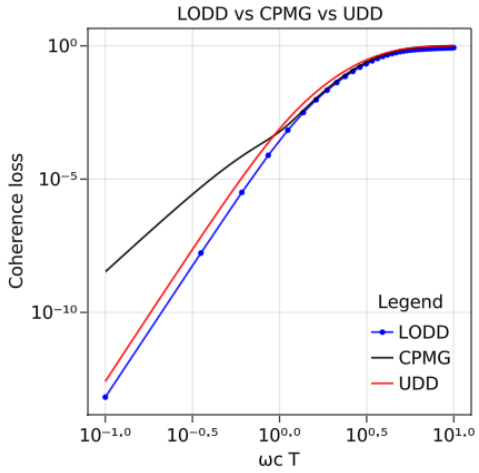

Figure 3.13: Coherence loss of the LODD sequences, compared to the CPMG and UDD sequences.

Using LODD, we can even demonstrate that UDD is the optimal filter by modifying a bit the Ohmic spectral density so that the cut-off is now represented by a Heavyside function,

$$J_0^{\text{modif.}}(\omega) = \alpha\omega\,\theta(\omega_c - \omega). \tag{3.68}$$

Using this spectral density and choosing a range of duration T for which the whole spectral density is being filtered[3], we can numerically compute the LODD sequence in order to find the sequence that provides the highest filtering of low frequencies. We computed the LODD sequences for $\omega_c T$ ranging from 1 to 2.54 (we can plot the filter function and show that the spectral density is localized entirely in the filtered range of frequency). The results are displayed in Fig. 3.14 and demonstrate that the highest possible filtering is provided by the UDD sequence as the results show that the LODD sequences are *exactly* equal to the UDD sequences.

Spectral density dependence of LODD

Because the infidelity is the quantity minimized by the Nelder-Mead algorithm, LODD sequences are expected to depend crucially on the spectral density. It is thus interesting to translate the results of Fig. 3.12 to the spectral densities presented in Fig. 1.5. The results can be found in Fig. 3.15 and show that the UDD sequence does not appear as optimal in the range of $\omega_c T$ considered and the CPMG sequence appears instead. This can be explained by the great amplification properties of UDD for the high frequencies; because the Lorentzian SD have a much softer cut-off $J_L \propto \frac{1}{\omega^2}$ than the Ohmic SD which exponentially decays to zero, the amplification of the higher frequencies will cause Uhrig dynamical decoupling to dramatically underperform.

[3]Notice that this is not possible using the Ohmic SD because the spectral density only *tends* to zero such that there is always some part of the spectrum that is amplified by the filter function. Because $\theta(\omega_c - \omega) = 0$ for $\omega > \omega_c$, the SD is *exactly* equal to zero beyond the cut-off.

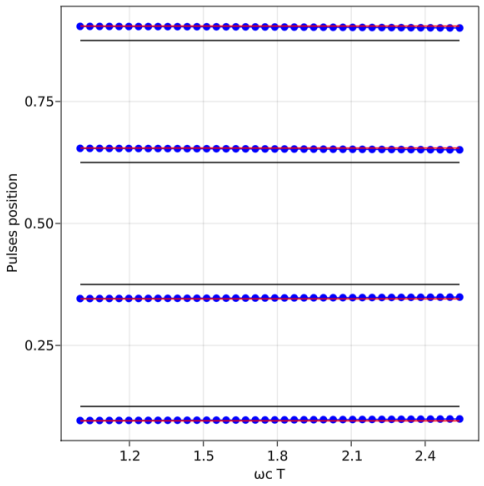

Figure 3.14: LODD sequences for the modified Ohmic spectral density defined in Eq.(3.68).

This should highlight one very important property of LODD: because of how the sequences are constructed, LODD provides ultimately the best DD sequence for a given spectral density at the cost of being very specific to the system considered.

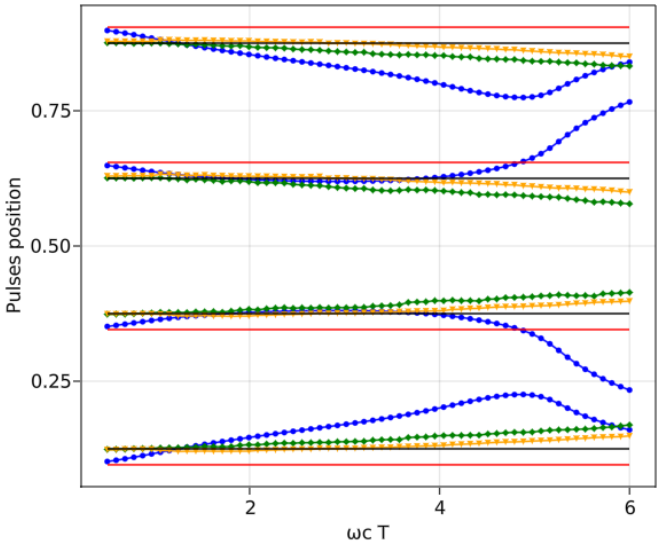

Figure 3.15: LODD sequences for the Ohmic SD (blue dots) and the two Lorentzian presented in Fig. 1.5 with the broader Lorentzian represented by the green diamonds and the thinner one represented by the yellow inverted triangles. The CPMG and UDD sequences are represented in black and red respectively.

Periodic application of LODD sequences

In the previous discussion, the goal was to create a sequence of specific duration T using a fixed number of pulses. However, for some applications, one may not know exactly for how long the qubit is wished to be protected. Instead, we may want to create a periodic sequence of pulses that we apply over and over again

until we no longer need to. In this context, one can wonder whether the sequences obtained in Fig. 3.12 are still the optimal ones. This question can be answered by using in the Nelder-Mead algorithm the decoherence function of Eq.(3.57) for different numbers of sequences, i.e. for different values of J. For a value of $J = 2$ for example, the algorithm calculates the coherence loss after the application of two sequences. The results are plotted in Fig. 3.16 for $J = 1$, 2, 5 and 10 and are quite interesting.

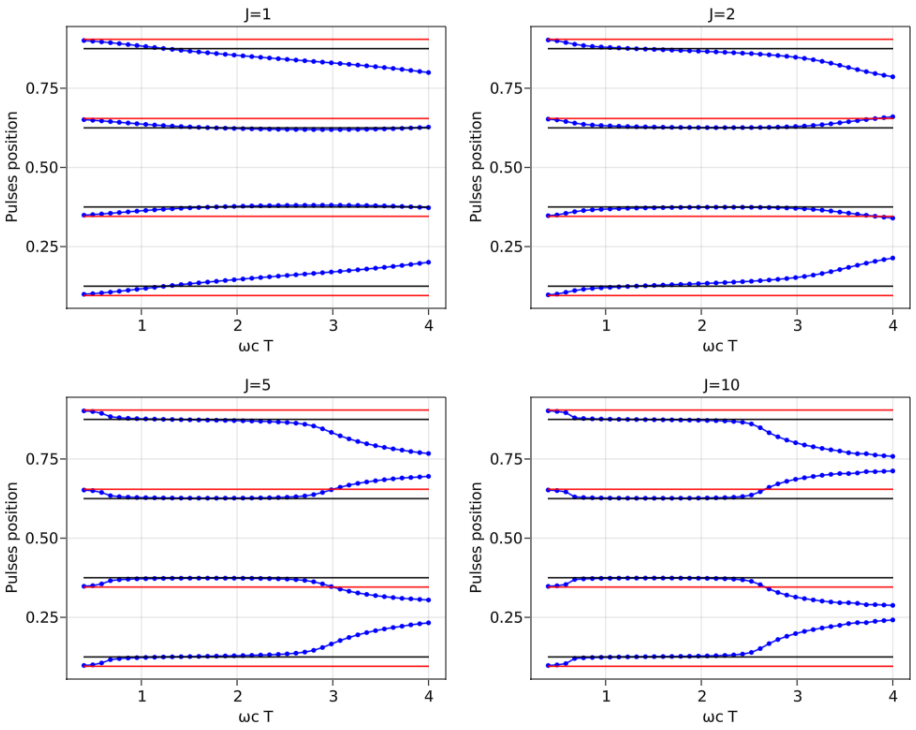

Figure 3.16: LODD sequences for different values of J. The CPMG and UDD sequences are once again represented in black and red respectively.

The results indicate that most LODD sequences of Fig. 3.12, when applied periodically, are no longer optimal. Instead of those complex sequences, the CPMG sequence actually becomes the better choice, which is quite unexpected because the CPMG sequence did not even appear as an optimal sequence in Fig. 3.12. Although UDD remains the best sequence for short duration protocols, we can see that LODD gradually (and slowly) converges to the CPMG sequence for shorter and shorter duration. We can distinguish three regimes that appear in Fig. 3.16 :

- the *UDD regime* for sequences of short duration $T \lesssim 0.6/\omega_c$, where the UDD sequence appears as the optimal sequence,
- the *LODD regime* for long sequences of duration $T \gtrsim 2.5/\omega_c$, where non-trivial sequences unique to LODD are optimal,
- and the *CPMG regime* which stands between them, where the CPMG sequence surprisingly appears as the optimal sequence.

It is interesting to focus on the range $\omega_c T \in [0.4, 0.9]$ where the UDD regime crosses the CPMG regime. The results plotted in Fig. 3.17 demonstrate that the CPMG regime gradually extends to the left, essentially taking over as the 'best' DD sequence. The LODD regime, on the other hand, is not of great interest because it accounts for sequences that result in high coherence losses, due to the fact that the period of those sequences

is essentially too great compared to the correlation time $\tau_c \sim 1/\omega_c$ to produce a satisfactory filter function. We generalized the results for 6 and 8 pulses; in the interest of not overcrowding the section, we decided to move this discussion to Appendix 4.

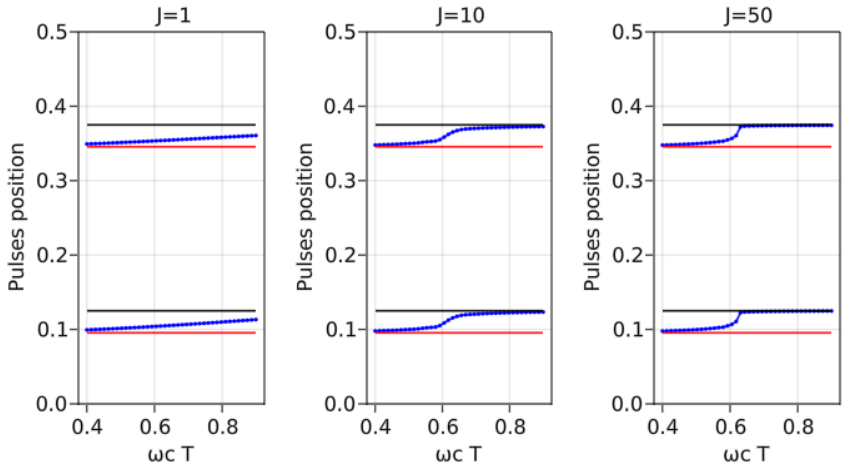

Figure 3.17: LODD sequences of different values of J.

The main result of the discussion above and of Appendix 4 is the following statement: "any dynamical decoupling sequence of non-equidistant pulses, when applied periodically a sufficiently large number of times, is believed to become less efficient that the corresponding sequence of equidistant pulses". Depending on the application in mind, it thus might be advantageous to trade those complex non-equidistant sequences for the basic CPMG sequence. Note that the calculations leading us to this conclusion cannot be considered as a proof of this statement and merely suggest that this extension of the CPMG regime appears for any number of pulses.

3.2.3 Optimized noise filtration through dynamical decoupling

Instead of minimizing the infidelity, which forces us to choose a spectral density and thus results in a sequence that depends greatly on this choice, one could decide to minimize the integral over the filter function of Eq.(3.58) only, leaving out the spectral density in order to create a spectrum-independent DD sequence. What should be minimized is therefore the area under the filter function. This approach leads to Optimized Noise Filtration through Dynamical Decoupling (OFDD) and was introduced in Ref. [66] as a way to create DD sequence that could prove more robust to errors in the environment model and to lower the dimension of the optimization problem in order to facilitate the construction of optimized sequence using experimental feed-backs.

In practice, we only try to minimize the integral over a range $\omega \in [0, \omega_D]$ with ω_D some cut-off frequency. This new parameter will later on be optimized for a given spectral density. The quantity to be minimized is thus

$$f(T, N, J) = \int_0^{\omega_D} f(\omega T, N, J) d\omega \tag{3.69}$$

with $f(\omega T, N, J)$ the filter function of Eq.(3.58). This function can be written as

$$f(\omega_D T, N, J) = \int_0^{\omega_D} f(\frac{\omega}{\omega_D} \omega_D T, N, J) d\omega \tag{3.70}$$

and a change of variable leads to

$$f(\omega_D T, N, J) = \omega_D \int_0^1 f(\tilde{\omega} \omega_D T, N, J) d\tilde{\omega} \tag{3.71}$$

where the integration is done with respect to the adimensional parameter $\tilde{\omega}$. Because the protocol duration T only appears through the adimensional parameter $\omega_D T$, we used the notation $f(\omega_D T, N, J)$ instead of $f(T, N, J)$ for the function to be minimized. Minimizing the function $f(\omega_D T, N, J)$ written as in Eq.(3.71) enables the construction of plots similar to FIG. 3.12 which are entirely independent of the frequency ω_D as it only appears as a scaling factor in front of the integral which we can omit without modifying the resulting sequences. Once again, the Nelder-Mead Simplex Algorithm can be used to minimize $f(\omega_D T, N, J)$.

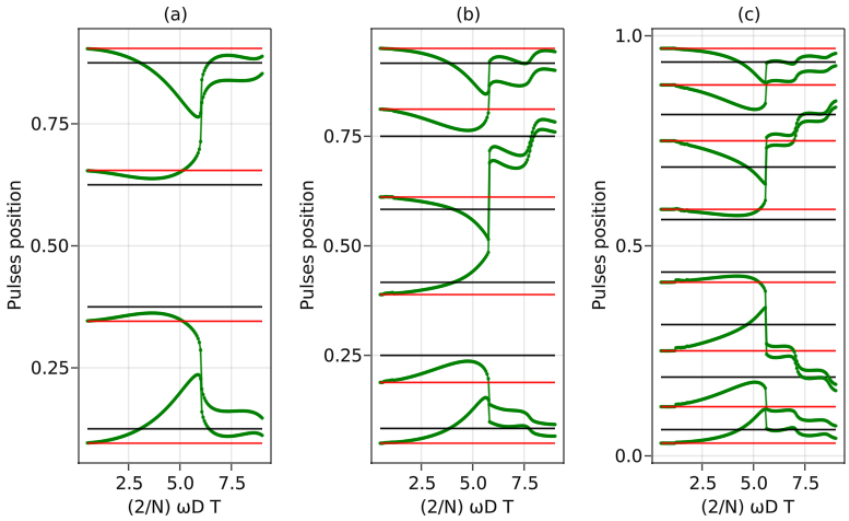

Figure 3.18: OFDD sequences for a number of pulses N equal to 4 (a), 6 (b) and 8 (c). The UDD and CPMG sequences are represented in red and black respectively.

Using Nelder-Mead on the position of the pulses for a given number of pulses N and $J = 1$, we computed the OFDD sequences over the range $\omega_D T \in \left[0.5\frac{N}{2}, 9.0\frac{N}{2}\right]$ (displayed in FIG.3.18). Because the pace at which Nelder-Mead converges depends greatly on the initial guess, we chose as the initial guess for $\omega_D T = 0.5\frac{N}{2}$ the UDD sequence. Then, for the highers value of $\omega_D T$, we chose as the initial guess the OFDD sequence of the slightely lower value of $\omega_D T$. This dramatically reduces the running time of the algorithm and increases its performance, because the algorithm starts running with an initial guess close to the optimal sequence. We see that the OFDD sequence tends to the UDD sequence for small enough $\omega_c T \frac{2}{N}$, similarly to the LODD sequence. Once again, the CPMG sequence does not appear. For large $\omega_D T \frac{2}{N} \gtrsim 6$, we observe a dramatic change in the pulses location that appears as a discontinuity. Although similar discontinuities are observed in the original paper [66], it should be noted that the algorithm did not converge at this particular point. Because the initial guess of the following iteration is the result of this unconverged iteration, and because the algorithm is very sensitive to the choice of the initial guess, our results after the discontinuity, despite their similarity to the results of Ref. [66], should not be trusted.

The sequences represented in FIG. 3.18 provide the optimal filter for each value of $\omega_D T$. In an experimental set-up, only one of those sequences correspond to the optimal OFDD sequence that should be applied for a given protocol duration; in order to find which OFDD sequence is best for a given spectral density, one has to fix the duration T of the protocol and find the parameter ω_D that provides the best filtering. This amounts to a one dimensional optimization procedure that can be realized with, once again, the Nelder-Mead Simplex Algorithm using either experimental feedback or a calculation of the coherence loss or the infidelity.

We have plotted in FIG. 3.19a the optimal OFDD sequences in the range $\omega_c T \in [0.5, 6]$ for 4 pulses using the Ohmic spectral density. For each value of $\omega_c T$, Nelder-Mead was used to find the parameter ω_D which results in the lowest coherence loss. The initial guess was initially chosen as $\omega_D = \omega_c$ for $\omega_c T = 0.5$, then the initial guess of the following iteration, i.e. for the next value of $\omega_c T$, was chosen as the value of ω_D from

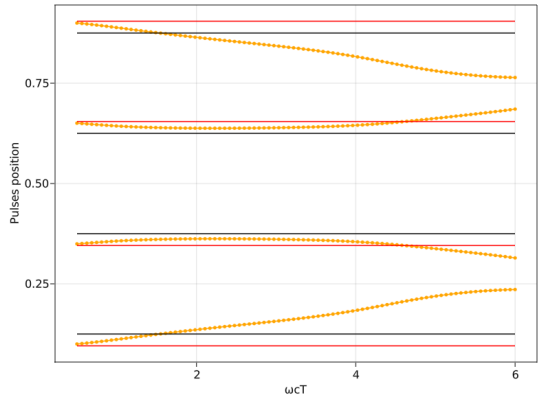

(a) OFDD sequences for the Ohmic spectral density.

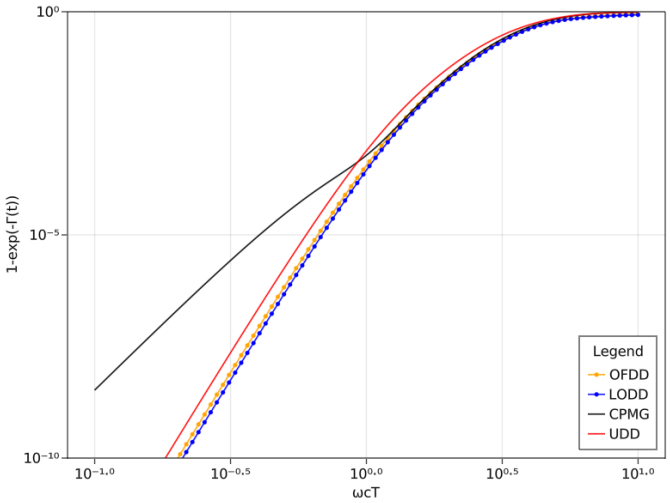

(b) Coherence losses of the OFDD, LODD, UDD and CPMG sequences for the Ohmic spectral density.

Figure 3.19

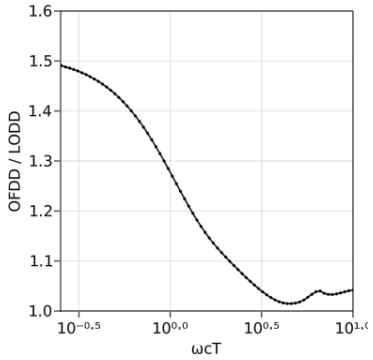

(c) Ratio of the coherence loss for the OFDD sequence over the coherence loss for the LODD sequence as a function of $\omega_c T$.

Figure 3.19

the previous iteration. We however realized after plotting ω_D as a function of $\omega_c T$ that an initial guess of $\omega_D = 5\omega_c$ for $\omega_c T = 0.5$ was a much better choice.

The corresponding coherence loss can also be found in FIG. 3.19b together with the coherence losses corresponding to the UDD, CPMG and LODD sequences. The OFDD sequence turns out to be almost as effective as the LODD sequences. We have plotted in FIG. 3.19c the ratio between the coherence loss for the OFDD and LODD sequences, showing that LODD outperforms OFDD by lowering the coherence loss by a factor of 1.5 for the shorter sequences.

3.2.4 Optimized bandwidth-adapted dynamical decoupling

In the last sections, we have introduced various approaches that aim at optimizing the temporal location of the pulses in the sequence. These approaches had the same objective, that is finding the "best" filter

function, but used different means to find the answer. These optimized sequences are summarized below:

UDD Uhrig optimized the filter function so that it provides the highest possible filtering for the frequencies lower than $\sim 2/T_c$. The weakness of this approach is that higher frequencies are greatly amplified such that the spectral density must be close to zero beyond $\sim 2/T_c$ for that approach to perform well.

LODD In order to overcome that problem, one can directly minimize the infidelity using an optimization algorithm, e.g. the Nelder-Mead Simplex algorithm. This approach requires a given duration T for the protocol and gives, ultimately, the best sequence for the number of pulses and the duration considered. The downside, in this case, is that the protocol is designed for a specific spectral density. One could decide to perform the optimization using experimental measurement of the infidelity instead of guessing the spectral density, but the hiccup is that, for N pulses, we have a N-dimensional optimization problem which can require a high number of iterations. Furthermore, the infidelity would need to be measured with high enough accuracy.

OFDD We can decide to use the optimization algorithm to minimize the integral over the filter function on the range $\omega \in [0, \omega_D]$, leaving out the spectral density. As in the LODD approach, one needs to fix the duration of the protocol T as well as the number of pulses and the algorithm gives as output the optimal location of the pulses for a specific value of $\omega_D T$. Then, the optimal choice for the parameter ω_D for a given spectral density can be found by using a one-dimensional minimization algorithm. The big advantage of this method is that it reduces the optimization problem from a N-dimensional to a one-dimensional optimization which is more easily tackled. This means that the infidelity must be measured or calculated less times. When the infidelity is computed with HOPS or measured experimentally, the lowering of the dimension of the optimization problem is very much appreciated.

However, none of the approaches described above have considered the fact that there could be some constraint on the minimum pulse separation. This is due to the fact that realistic pulses, as we shall discuss in the next section, have a finite duration which prohibits infinitely fast control. For a given system, we thus may find that the sequences given by the UDD, LODD and OFDD procedures for optimization are experimentally impossible to realize because they would require the application of pulses separated by a time interval smaller than the duration of a single pulse. This issue was addressed in Ref. [67] and K. Khodjasteh, T. Erdélyi and L. Viola came up with a solution with the introduction the Bandwidth-Adapted Dynamical Decoupling (BADD). The idea is to use an optimization algorithm on the infidelity, not unlike LODD, except that a constraint on the minimum separation of the pulses is added and that the number of pulses is not fixed. Basically, the algorithm takes as an input the spectral density, the total duration T and the minimum achievable pulse separation and the output consists of the number of pulses N and their location in the sequence $\{\tau_n\}$. The outcome of the procedure is the construction of the sequence that corresponds to the smallest value of the infidelity while satisfying the constraint that we imposed.

Studying the BADD sequences, they came to the sad conclusion that a dynamical decoupling procedure by itself is not able to extend the lifetime of a qubit to an arbitrary long time with an arbitrary low infidelity. The lowest possible infidelity achievable for a given protocol duration T will depend on the minimum pulse interval achievable. This statement from Ref. [67] basically leads to the conclusion that dynamical decoupling alone is not sufficient to achieve arbitrary long and accurate quantum computation.

3.3 Benchmarking HOPS in the context of dynamical decoupling

Because of the nice analytical solution for the decoherence function in the case of the purely dephasing qubit undergoing a series of spin-flips, it is possible to benchmark the results of the HOPS method in the context of dynamical decoupling. We considered a purely dephasing qubit as in Fig. 1.9, using the same spectral density parameters. Recall that those parameters had to satisfy the conditions $\kappa \ll \omega_c$ and $g \gg \omega_c^2/2\kappa$ in order to avoid the accumulation of the spurious dynamics generated by the non-physical negative frequencies used in HOPS. It is not yet clear whether the same conditions should be satisfied in the context of dynamical decoupling. However, as a starting point, it makes sense to use HOPS in the regime of validity derived

earlier. We have thus chosen the parameters $\kappa/\omega_c = 0.075$ and $g = 1.6\frac{\omega_c^2}{\kappa}$ which allowed us to match the simulation and the analytical results to a maximal time $t_f = 0.6/\Omega$ with $\Omega = g\frac{\kappa^2}{\omega_c^2}$. We should also keep similar simulation parameters and add a control field to the system Hamiltonian. The pulses were implemented using a time-dependent Hamiltonian of the form $H_{cf}(t) = \frac{\pi}{2}a(t)\sigma_x$ with $a(t)$ equal to a sum of a bunch of normalized Gaussian distributions of width σ localized at the timing of the pulses. The limiting case of the ideal pulses corresponds to the limit $\sigma \to 0$.

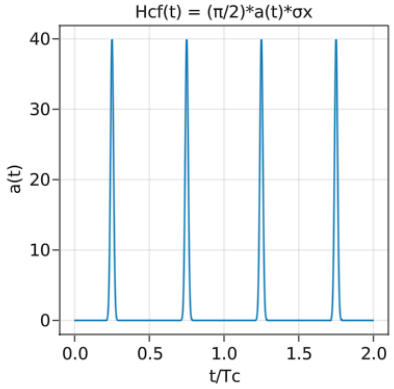

(a) Train of pulses as implemented in HOPS.

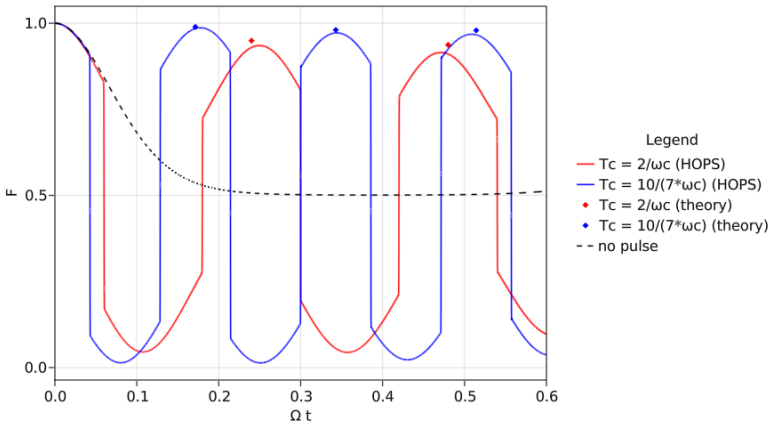

(b) Fidelity of a dephasing qubit when a CPMG sequence of period $\omega_c T_c = 2$ (red) and $\omega_c T_c = 10/7$ (blue) is applied. We also plotted the fidelity of the dephasing qubit without DD (dashed line). The initial state $|\psi\rangle = \frac{|0\rangle+i|1\rangle}{\sqrt{2}}$ was chosen. The simulation parameters were set at ($k_{\max}$, t_f/dt, n_{traj})=(7,20000,800).

Figure 3.20

We first intended to implement a sequence of equidistant pulses. We implemented the symmetrized CPMG sequence for different periods of the sequence and calculated the fidelity of the qubit using both HOPS and the analytical function. The results are plotted in Fig. 3.20b. The solid lines correspond to the evolution of the qubit as computed by the HOPS method. One can then see the evolution of the qubit within the sequence and observe sudden changes in the dynamics occuring when a pulses is applied. The dots correspond to the calculation of the coherence at the end of a DD sequence using the analytical solution. Qualitatively, the results match; we observe a dramatic decrease of the decoherence rate which is more significant when the period of the dynamical decoupling sequence is decreased. However, the exact value of the fidelity at the end of a period T_c does not match in a satisfactory way with the simulations from HOPS for either of the sequences considered. The simulation parameters $k_{\max}$ and n_{traj} were increased and the timestep dt was decreased but this did not result in a better agreement with the theoretical prediction. However, decreasing the width of the Gaussian increases the performance of the DD sequence and leads to a numerical calculation closer to the theoretical prediction. Note that decreasing the width of the Gaussian was followed by a decrease of the timestep dt for the numerical integration in order to make sure that the pulses were similarly integrated numerically.

Once again, calculating the fidelity of the qubit with the negative frequencies taken into account leads to a slight deviation from the exact solution (see Fig. 3.21). Because of our previous discussion on the impact of the negative frequencies on the HOPS method, we expect the simulation results to converge to the solution which considers negative frequencies in the integration when the width of the Gaussian is further reduced. This indicates that the regime of parameters chosen specifically to avoid the build up of spurious dynamics generated by negative frequencies does not prevent the issue from occurring in the context of studying a DD sequence.

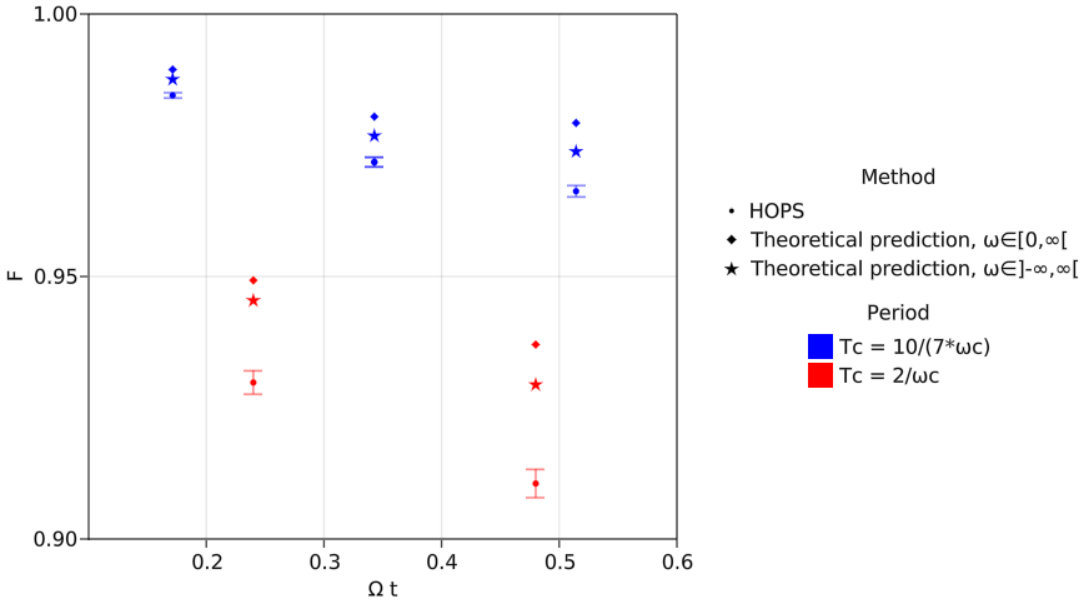

Figure 3.21: Fidelity of a qubit undergoing a CPMG sequence, calculated using the standard analytical derivation (diamonds), the analytical derivation with the negative frequencies considered (stars) and the HOPS method (dots). In the interest of making the plot more intelligible, only the values of the fidelity at the end of a cycle was kept.

3.3.1 Impact of the negative frequencies on the relative performances of DD sequences

As it has been stated previously, the regime of parameters chosen specifically to avoid undesirable effects of the non-physical negative frequencies in the HOPS simulation for the purely dephasing qubit does not prevent those same negative frequencies from influencing the dynamics of the same qubit undergoing a dynamical decoupling procedure. However, making accurate prediction on the fidelity of a qubit after applying a DD sequence is not necessary to obtain some interesting results. Instead, it may be interesting to compare the *relative* performances of two different dynamical decoupling sequences. If the negative frequencies of HOPS do not influence the relative performances, then it could *a priori* still be used as a tool to create DD sequences and compare different protocols.

In order to find out how useful HOPS can still be, we compared the UDD sequence of four pulses with the symmetrized CPMG sequence. The results can be found in Fig. 3.22. The periods and the two sequences were chosen such that the relative performance of the two sequences is alienated when the negative frequencies are considered. In other words, we chose to compare with the CPMG sequence a UDD sequence which is supposed to be more performing according to the exact solution, but appears less performing when the negative frequencies are taken into account. This is precisely what we observe in Fig. 3.22: according to the exact analytical solution, up to two applications of the UDD sequence yield a better fidelity than the CPMG sequence. After three cycles, UDD is outperformed by CPMG. However, when negative frequencies are taken into account, the UDD sequence is always outperformed by the CPMG sequence.

The HOPS results indicate that the UDD sequence is indeed less performing than the CPMG sequence. This supports the idea that HOPS accounts for the spurious dynamics generated by the negative frequencies in such a way that the relative performance of two sequences according to HOPS can differ from the theoretical prediction based on the exact analytical solution.

Note that the fact that the UDD sequence appears less performing because of the negative frequencies can be explained by the fact that the filter function is even with respect to the frequency ω, that is the value

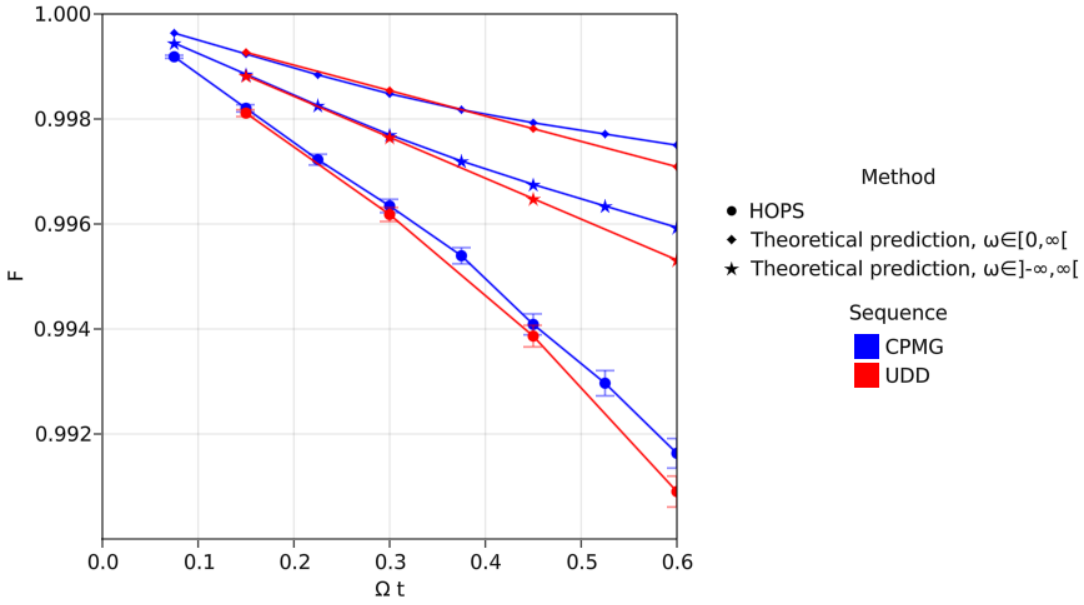

Figure 3.22: Time evolution of a qubit undergoing a UDD (red) and a CPMG (blue) sequence, calculated using the standard analytical derivation (diamonds), the analytical derivation with the negative frequencies considered (stars) and the HOPS method (dots). The simulation parameters were fixed at ($k_{\max}$, t_f/dt, n_{traj})=(7,10000,800).

of the filter function at ω is equal to its value at $-\omega$. It follows that the additional negative frequencies and the positive frequencies will be treated equally by the DD sequence and that we can construct an 'effective' spectral density

$$J_{eff}(\omega) = \frac{g\kappa}{2}\frac{\kappa}{\kappa^2 + (\omega - \omega_c)^2} + \frac{g\kappa}{2}\frac{\kappa}{\kappa^2 + (\omega + \omega_c)^2} \tag{3.72}$$

which is defined exclusively on the positive frequency domain (displayed in Fig.3.23a). This effective spectral density is the one implemented in HOPS and is constructed by adding two Lorentzians on top of each other, one centered at the frequency ω_c and the other centered at $-\omega_c$. It thus mean that the effective coupling to each frequency of the bath will be higher. In the range of frequencies where the UDD sequence out-performs, the higher coupling will tend to favor UDD over CPMG. Equivalently, in the range of frequencies where CPMG outperforms, the higher coupling will tend to favor CPMG over UDD. It is crucial to understand that this effective spectral density is **not** equal to the Lorentzian SD times a multiplicative factor. This means that the increase of the coupling is more significant in some range of frequencies. We plotted in Fig.3.23c the relative augmentation of the coupling strength for each frequency. In the low frequencies, i.e. the range of frequency where UDD performs best, the augmentation of the coupling strength rapidly drops from 100% to 0.1%. However, in the amplification regime, where UDD is dramatically outperformed by CPMG because of its amplification properties, the augmentation steadily increases. Because

$$\lim_{\omega\to\infty} \frac{J_{eff}(\omega) - J(\omega)}{J(\omega)} = \lim_{\omega\to\infty} \frac{\kappa^2 + (\omega - \omega_c)^2}{\kappa^2 + (\omega + \omega_c)^2} = 1, \tag{3.73}$$

the augmentation of the coupling strength keeps on increasing in the amplification regime. It essentially means that the effective spectral density has a softer cut-off. Because of the extreme amplification of high frequencies provided by UDD, we have already pointed out that UDD is extremely sensitive to the form of the spectral density beyond the cut-off; it is thus not surprising that the overall higher coupling will favor the CPMG sequence over UDD. That being said, one can understand how the issue of the negative frequencies prevent us from constructing DD sequences based on a careful design of the filter function.

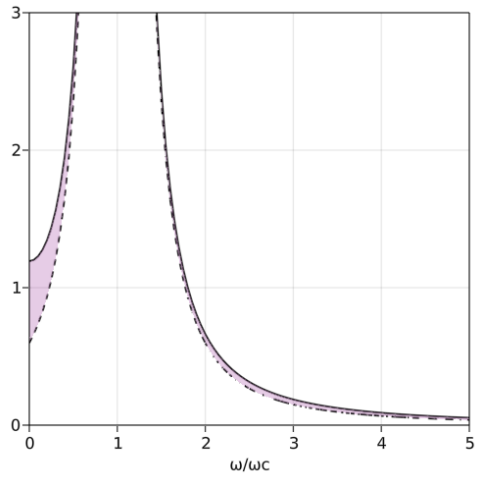

(a) The effective spectral density (solid line) and the Lorentzian spectral density (dashed line). The colored area between the two functions corresponds to the negative frequencies added to the Lorentzian in order to create the effective SD.

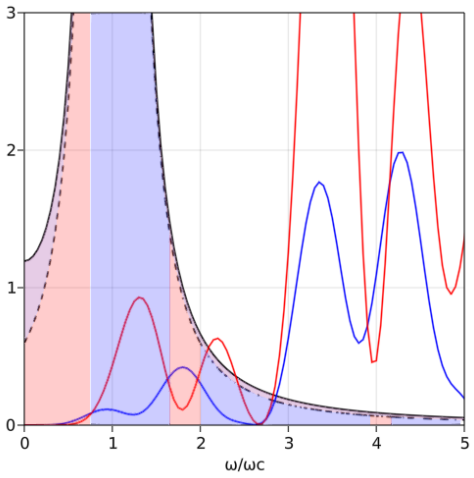

(b) To Fig.3.23a have been added the filter functions of the UDD (red) and the CPMG (blue) sequences used in HOPS to get Fig.3.22. The range of frequency where UDD (resp. CPMG) outperforms the other sequence is colored in red (resp. blue).

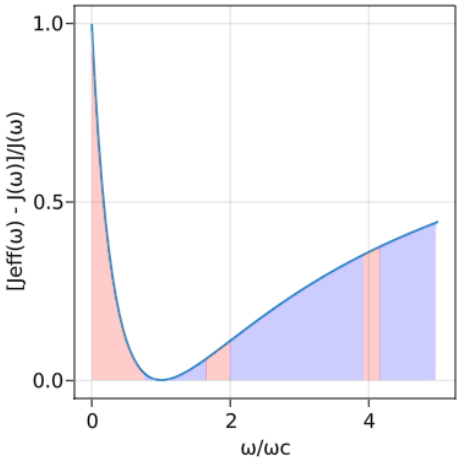

(c) The ratio $\frac{J_{eff}(\omega)-J(\omega)}{J(\omega)}$ indicates the relative augmentation of the coupling strength at the frequency ω.

Figure 3.23

Once again, it should be pointed out that the HOPS simulations slightly deviate from the theoretical predictions. Because decreasing the timestep did not help and neither did increasing the number of auxillliary states and the number of trajectories, this is most likely due to the finite duration of the pulses.

We therefore come to the conclusion that single-mode HOPS is not, at least in the regime of parameters considered, fitted to compare the relative performances of two dynamical decoupling protocols based on specific designs of the filter function. It is still not clear whether a regime of parameters that allows accurate analysis of dynamical decoupling protocols can be found. It is also not clear whether HOPS multi-modes can help in mitigating this issue through the introduction of modes of negative weight.

Chapter 4

Maximal Dynamical Decoupling

In the previous section, we introduced several SELDD sequences which, in the context of a purely dephasing qubit, are sufficient to increase the lifetime of said qubit to some extent. However, dissipation should at some point be taken into account. When dissipation is taken into account, as already mentioned, the decoherence process of a qubit can be considered as resulting from two relaxation processes, that is a *transverse relaxation* due to pure dephasing and a *longitudinal relaxation* due to dissipation [8]. These two processes are characterized by relaxation times T_1 and T_2 for the longitudinal and transverse relaxation respectively. Usually, T_2 is smaller than T_1, meaning that pure dephasing is the physical process that limits our ability to reliably store quantum information.

Using SELDD to eliminate pure dephasing, we have seen that the lifetime of the qubit can be extended by orders of magnitude. This amounts to increasing T_2 by orders of magnitude, such that at some point T_1 can become smaller than T_2, meaning that dissipation becomes the limiting physical process prohibiting the storage of quantum information; we arrive at a point where dissipation should be taken into account in order to extend the qubit's lifetime even further. This is where Maximal Dynamical Decoupling (MAXDD) strategies should be used instead of SELDD.

We have explained earlier than dissipative dynamics can be taken into account by adding an extra term in the Hamiltonian, this term being either a tunneling term $\Delta_0\sigma_x$ or an interaction Hamiltonian of the form $\hbar\sigma_x\sum_k\left(g_k b_k^\dagger + g_k^* b_k\right)$ or $\hbar\sum_k\left(g_k\sigma_- b_k^\dagger + g_k^*\sigma_+ b_k\right)$. One can easily check that the SELDD strategy considered in the previous section does not average out either of these terms, meaning that another decoupling group is needed to deal with dissipative behaviors. In this chapter, we will use as an interaction Hamiltonian the Hamiltonian presented in Eq.(1.98) (written again below for convenience) in order to account for dissipation and dephasing.

$$H_{SB}(\theta) = \hbar\big[\cos^2(\theta/2)\sigma_z + \sin^2(\theta/2)\sigma_x\big]\sum_k\left(g_k b_k^\dagger + g_k^* b_k\right), \tag{4.1}$$

We plotted in FIG. 4.1 and FIG. 4.2 the evolution of the qubit undergoing pure dissipation ($\theta = \pi$ in Eq.(4.1)) with and without a classic CPMG sequence of period $T_c = 1/(1.6\omega_c)$ applied, for two initial states $|\psi(0)\rangle = \frac{|0\rangle+|1\rangle}{\sqrt{2}}$ and $|\psi(0)\rangle = \frac{|0\rangle+i|1\rangle}{\sqrt{2}}$. This shows that decoherence is not prevented by the application of a CPMG sequence of spin-flips and more complex sequences are needed to deal with complex interaction Hamiltonian such as the one introduced in Eq.(4.1).

Remark. Because the pulses commute with the operator σ_x of the interaction Hamiltonian $H_{SB}(\theta = \pi)$, one could wonder why the dynamics of the qubit is modified by the sequence. This is explained by the effects of the CPMG sequence on the system Hamiltonian $H_S = \frac{\hbar\omega_0}{2}\sigma_z$. Because the pulses anti-commute with H_S, the system Hamiltonian is affected by the DD sequence. Accordingly, because the spontaneous decay of a two-level system depends not only on the interaction Hamiltonian but also on the system Hamiltonian (see the section on the James-Cummings model on resonance and the James-Cummings model with detuning in Ref. [11]), this means that the dynamics of the dissipative qubit undergoing a series of spin-flips is non-trivial.

We also observe that the choice of the initial state impacts the decoherence rate, the decoherence rate being greater for the initial state $|\psi(0)\rangle = \frac{|0\rangle+i|1\rangle}{\sqrt{2}}$.

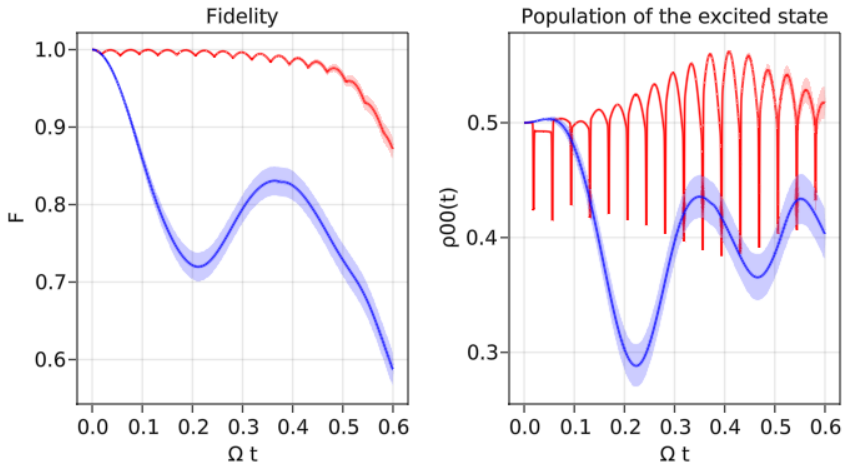

Figure 4.1: Fidelity and population of the excited state for $\theta = \pi$ with (red) and without (blue) a control field applying a CPMG sequence of spin-flips for the initial state $|\psi(0)\rangle = \frac{|0\rangle+|1\rangle}{\sqrt{2}}$. The simulation parameters were fixed at ($k_{\max}$, t_f/dt, n_{traj})=(6,5000,400).

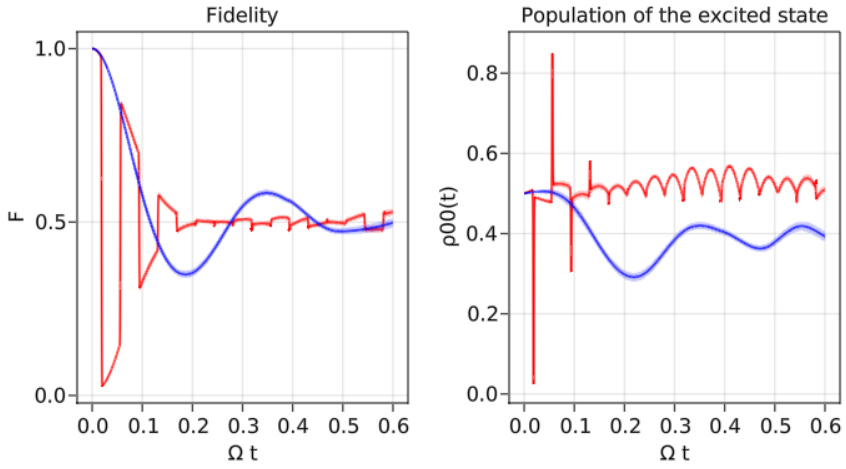

Figure 4.2: Fidelity and population of the excited state for $\theta = \pi$ with (red) and without (blue) a control field applying a CPMG sequence of spin-flips for the initial state $|\psi(0)\rangle = \frac{|0\rangle+i|1\rangle}{\sqrt{2}}$. The simulation parameters were fixed at ($k_{\max}$, t_f/dt, n_{traj})=(6,5000,400).

In this section, we will first present the XY4 sequence mentioned in Section 2.5. Then, we will present two more complex protocols that achieve higher-order decoupling, namely *Concatenated* and *Quadratic* dynamical decoupling.

4.1 XY4

The XY4 sequence has already been mentioned in Section 2.5; we showed in this previous section how to construct it by choosing the relevant decoupling group. It is however interesting to construct the sequence in another manner, using a method called *concatenation* which consists of merging two existing sequences in order to create a new one.

We now know that the decoupling group $\mathcal{G}_x = \{\mathbb{1}, \sigma_x\}$ averages out the operator σ_z as it was proven in Eq.(2.28) where we demonstrated that the symmetrization procedure on σ_z using $\mathcal{G}_x$ results in $\Pi_{\mathcal{G}_x}(\sigma_z) = 0$. One can easily see that swapping all the operators σ_x and σ_z in Eq.(2.28) still gives the same results. This would correspond to the symmetrization procedure $\Pi_{\mathcal{G}_z}(\sigma_x) = 0$ with $\mathcal{G}_z = \{\mathbb{1}, \sigma_z\}$. We now understand that, because $\mathcal{G}_x$ is a decoupling group for σ_z, $\mathcal{G}_x$ is a decoupling group for σ_x. The sequence of pulses is then given by the same sequence as CPMG but replacing the spin-flips $X = \sigma_x$ with phase-flips $Z = \sigma_z$. We thus have two protocols,

$$\begin{aligned} p_1 &= \Delta t - X - \Delta t - X \quad \text{for } \sigma_z, \\ p_2 &= \Delta t - Z - \Delta t - Z \quad \text{for } \sigma_x, \end{aligned} \tag{4.2}$$

which, separately, are sufficient to average out one of the unwanted terms of the Hamiltonian but not the other. By concatenating the two protocols, it is possible to create a single protocol that averages out both terms. Concatenation of DD procedure was first introduced in Ref. [55] and consists in replacing the free-evolution of a sequence by another sequence. For example, concatenating p_1 and p_2 leads to the sequence

$$\begin{aligned} p_{1\to 2} &= p_1 - Z - p_1 - Z \\ &= \Delta t - X - \Delta t - X - Z - \Delta t - X - \Delta t - X - Z \\ &= \Delta t - X - \Delta t - Y - \Delta t - X - \Delta t - Y \end{aligned} \tag{4.3}$$

where we have used $Y = XZ$. The same derivation can be done using $p_3 = \Delta t - Y - \Delta t - Y$ which is a sequence that also averages out σ_x and this would lead to

$$p_{1\to 3} = \Delta t - X - \Delta t - Z - \Delta t - X - \Delta t - Z \tag{4.4}$$

which is precisely the sequence that was found in Section 2.5 that achieves maximal dynamical decoupling. The protocols $p_{1\to 3}$ and $p_{1\to 2}$ are actually equivalent as they correspond to the same decoupling group $\mathcal{G} = \{\mathbb{1}, \sigma_x, \sigma_x\sigma_z, \sigma_z\}$.

In order to illustrate the efficacy of this XY4 sequence compared to the classic CPMG sequence of spin-flips, we computed the fidelity and population of the excited state when both sequences are applied, using an interaction Hamiltonian consisting of both dissipative and dephasing terms, $H_{SB}(\theta = 1.2)$. The results are displayed in Fig.4.3. Note that in order to make the results more intelligible, we removed the evolution of the qubit within the sequence and only plotted the fidelity and the population of the excited state at the end of each cycle. The period of the XY4 sequence was set to $T_c = 1/(1.6\omega_c)$ and the period of the CPMG sequence was set to $2T_c$ in order to obtain the same pulse interval Δt between each pulse.

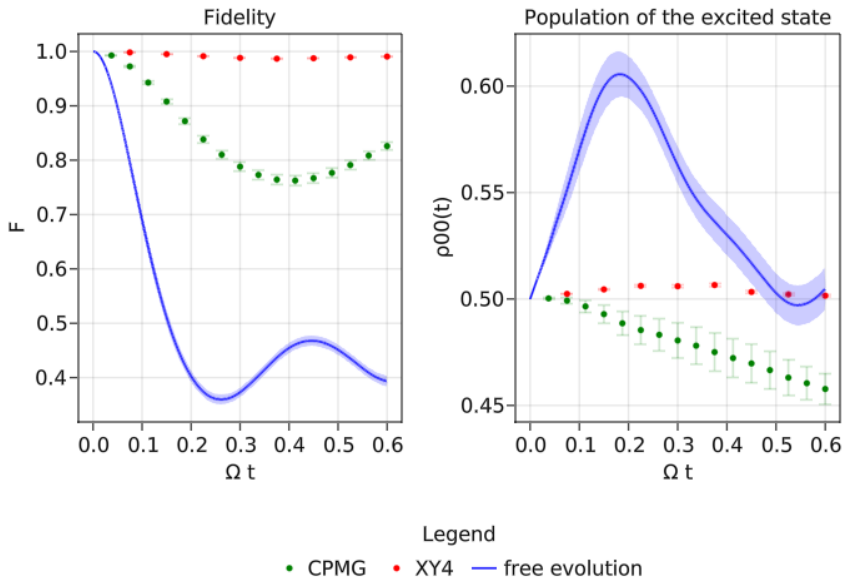

Figure 4.3: Fidelity and population of the excited state with the interaction Hamiltonian $H_{SB}(\theta = 1.2)$ with a CPMG sequence (green), a XY4 sequence (red) and no sequence (blue) applied. The initial state is $|\psi(0)\rangle = \frac{|0\rangle+i|1\rangle}{\sqrt{2}}$ and the simulation parameters were fixed at $(k_{\max}, t_f/dt, n_{\text{traj}}) = (6,10000,300)$.

4.2 Concatenated dynamical decoupling

The simplest sequences, such as CPMG and XY4 for example, can only decouple a qubit up to the first order of the Magnus expansion. This means that the errors resulting from higher-order terms will eventually build up as we keep applying the sequence periodically. In order to avoid that, one must seek more advanced DD sequences that achieve higher-order decoupling. One way to increase the order of the decoupling is to concatenate the simplest sequence, the same way we have done in the last section to create the XY4 sequence, thus resulting in *Concatenated Dynamical Decoupling* (CDD) sequences [55]. The concatenation process for the XY4 sequence is rather simple: writing the sequence at the 0th level of concatenation as

$$p^{(0)} \equiv U(\Delta t)XU(\Delta t)ZU(\Delta t)XU(\Delta t)Z \tag{4.5}$$

with $U(\Delta t)$ the free-evolution propagator that has the exact same meaning as the notation $-\Delta t-$ which was used in the last section, we can define the sequence at the $(l+1)$th level of concatenation by

$$p^{(l+1)} \equiv p^{(l)}Xp^{(l)}Zp^{(l)}Xp^{(l)}Z, \quad n = 0, 1, \ldots \tag{4.6}$$

In such a sequence, each level l of the concatenation will average the term of order $l+1$ of the Magnus expansion. In theory, one can then eliminate the undesired Hamiltonian up to an arbitrary high order of the Magnus expansion simply by repeating the concatenation procedure described above. Concatenation can be done on any sequence with any number of pulses; one can think about successive concatenation of OFDD, LODD or UDD sequences for example.

It is important to point out that, although arbitrary high-order decoupling can be achieved in theory, physical constraint will eventually limit the level of concatenation that can be attained. First, the number of pulses in the sequence increases exponentially with the level of concatenation, such that in order to achieve $(l+1)$th order decoupling by concatenating XY4 sequences successively, one would need a total of $N \lesssim 4^{(l+1)}$ pulses in the sequence. Then, all of those pulses are separated by a pulse interval Δt, which makes the total duration of the sequence $T_c \lesssim 4^{(l+1)}\Delta t$. This means that if the total duration of the sequence is fixed, i.e.

we need to protect the qubit for a specific duration, the pulse interval decreases as $\Delta t \gtrsim T_c/4^{(l+1)}$; the minimum pulse interval decreases exponentially with the level of concatenation. Because the minimum pulse interval achievable by an experimental set-up is not zero, this results in a maximum level of concatenation for a given experimental set-up and duration.

One can wonder why we wrote $N \lesssim 4^{(l+1)}$ instead of $N = 4^{(l+1)}$. At first sight, it might seem like each level of concatenation multiplies the number of pulses by exactly four. However, one finds that some of the additional pulses will correspond to the identity operator. These pulses can then be left out. It is interesting to illustrate this by explicitly calculate the concatenated XY4 sequence up to the first level of concatenation, that is $p^{(1)}$ in Eq.(5.5). One finds that the corresponding sequence is

$$\begin{aligned} & p^{(0)} \equiv X - Z - X - Z \\ \Rightarrow \quad & p^{(1)} \equiv X - Z - X - ZX - X - Z - X - ZZ - X - Z - X - ZX - X - Z - X - ZZ \end{aligned} \tag{4.7}$$

where we left out the free-evolution propagator $U(\Delta t)$ between the pulses in order to avoid an unnecessary long formula (each dash $-$ corresponds to a free evolution $U(\Delta t)$). We can replace ZX by the pulse Y as they are equal up to a phase factor (Y being defined as $Y = XZ$). Now notice that the pulse ZZ appears two times in the sequence. Because Z is unitary and hermitian, ZZ is nothing but the identity operator. We can thus leave these two identity pulses out and write the final sequence as

$$C^{(1)}XY4 \equiv X - Z - X - Y - X - Z - X - X - Z - X - Y - X - Z - X \tag{4.8}$$

which is a 14 pulses sequence instead of a 16 pulses sequence as one could have expected. We introduced here the notation $C^{(l)}XY4$ for the concatenated XY4 sequence with lth level of concatenation. The fidelity of a qubit undergoing the $C^{(1)}XY4$ and $XY4$ sequences is plotted in FIG.4.4 in order to illustrate the superiority of this new sequence.

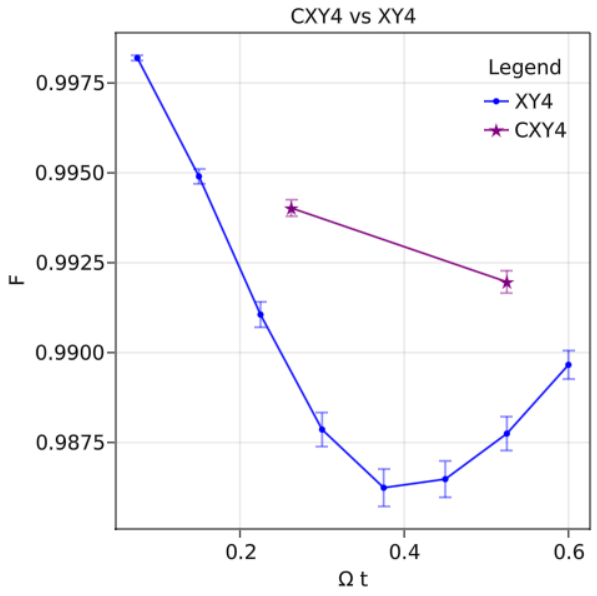

Figure 4.4: Relative performance of the $C^{(1)}XY4 \equiv CXY4$ and $XY4$ sequences for the Hamiltonian $H_{SB}(\theta = 1.2)$. In order to ensure a fair comparison, we used for both sequences the same pulse interval Δt. The duration of the XY4 sequence is set to $T_c = \frac{1}{1.6\omega_c}$. In the interest of making the results more intelligible, we only plotted the value of the fidelity at the end of a period. The simulation parameters were fixed at ($k_{\max}$, t_f/dt, n_{traj}) = (6,10000,700).

4.3 Quadratic dynamical decoupling

Throughout Chapter 3, we presented many SELDD sequences constructed by optimizing the pulses placement in the sequence and one can wonder whether similar sequences can be constructed when different types of pulses are considered. LODD sequences can easily be constructed, provided that calculating the infidelity is possible using either HOPS or a non-Markovian quantum master equation. However, because no analytical development is possible in this case and thus no filter function can be defined, it is *a priori* not trivial to generalize OFDD and UDD. Similar sequences can however be obtained by concatenation, using the exact same method as in Section 4.1 but using OFDD or UDD sequences instead of the CPMG sequence.

Quadratic Dynamical Decoupling [51, 68, 69] is a sequence constructed by concatenation of two UDD sequences. As a reminder, the UDD sequence introduced previously is given by

$$UDD_N(T_c) \equiv U((\tau_1 - 0)T_c)XU((\tau_2 - \tau_1)T_c)X \dots XU((\tau_N - \tau_{N-1})T_c)XU((1 - \tau_N)T_c) \tag{4.9}$$

with $\{\tau_n\}$ are the temporal localization of the pulses in the sequence and are given by

$$\tau_n = \sin^2\left(\frac{n\pi}{2N+2}\right), \quad n = 1, \dots, N \tag{4.10}$$

and $U(\Delta t)$ corresponds to the free-evolution propagator for a duration Δt. A more convenient way to write this sequence is

$$UDD_N(T_c) \equiv U(\delta_1 T_c)XU(\delta_2 T_c)X \dots XU(\delta_N T_c)XU(\delta_{N+1} T_c) \tag{4.11}$$

defining the pulses separations $\{\delta_n\}$ as

$$\delta_n = \sin^2\left(\frac{n\pi}{2N+2}\right) - \sin^2\left(\frac{(n-1)\pi}{2N+2}\right), \quad n = 1, \dots, N+1. \tag{4.12}$$

This sequence was constructed using spin-flips X in order to eliminate pure dephasing of a qubit, but that same sequence can be constructed using phase-flips Z to eliminate dissipation. In order to differentiate the two sequences, we define

$$\begin{aligned} X_{N_1}(T_c) &\equiv U(\delta_1 T_c)XU(\delta_2 T_c)X \dots XU(\delta_{N_1} T_c)XU(\delta_{N_1+1} T_c), \\ Z_{N_2}(T_c) &\equiv U(\delta_1 T_c)ZU(\delta_2 T_c)Z \dots ZU(\delta_{N_2} T_c)ZU(\delta_{N_2+1} T_c). \end{aligned} \tag{4.13}$$

Concatenation the two sequences as we have done in the previous section, we find

$$QDD_{N_1,N_2}(T_c) = X_{N_1}(\delta_1 T_c)ZX_{N_1}(\delta_2 T_c)Z \dots ZX_{N_1}(\delta_{N_2} T_c)ZX_{N_1}(\delta_{N_2+1} T_c) \tag{4.14}$$

the resulting QDD sequence composed of an inner and outer UDD sequence of N_1 and N_2 pulses respectively. Because the inner sequence appears N_2+1 times, the total number of X pulses is equal to $N_1(N_2+1)$ whereas the total number of Z pulses is equal to N_2. In this sequence, the location of the Z pulses of the outer sequence is given by

$$\tau_n^z = \sin^2\left(\frac{n\pi}{2N_2+2}\right) \quad \forall n = 1, \dots N_2. \tag{4.15}$$

On the other hand, the location of the X pulses of the nth inner sequence is given by

$$\tau_m^{x,n} = \tau_{n-1}^z + \sin^2\left(\frac{m\pi}{2N_1+2}\right)(\tau_n^z - \tau_{n-1}^z) = \tau_{n-1}^z + \sin^2\left(\frac{m\pi}{2N_1+2}\right)\delta_n^z \quad \forall m = 1, \dots N_1 \tag{4.16}$$

with $\tau_0^z = 0$.

Because a UDD sequence of N pulses achieves $(N-1)$th order decoupling on the error it is designed to suppress, the QDD sequence achieves $(N_1 - 1)$th order decoupling on the errors $\{\sigma_y, \sigma_z\}$ and $(N_2 - 1)$th order decoupling on the errors $\{\sigma_y, \sigma_x\}$, such that decoherence is entirely eliminated to the order $\min\{(N_1+1), (N_2+1)\}$. The rigorous proof of this statement was done in Ref. [51] for $N = N_1 = N_2$ and

generalized for any N_1, N_2 in Ref. [68]. Using $N_2 = N_1 = N$, we can then achieve $(N-1)$th order maximal decoupling using a total number of $N(N+1) + N = N^2 + 2N \propto N^2$ pulses.

QDD can then achieve arbitrary high-order decoupling using a number of pulses which increases quadratically with the order. This result is particularly interesting when compared with the CDD sequence described in the previous section as we observe an exponential gain on the number of pulses needed to achieve the same order of decoupling. An extensive analysis of the QDD sequence can be found in Refs. [68, 69] and shows that QDD works best with $N_1 = N_2$.

We plotted the HOPS results for the fidelity of a qubit undergoing QDD with $N_1 = N_2 = 4$ (which amounts to a 20 pulses sequence) in FIG.4.5. In order to proceed to a fair comparison between the QDD and XY4 sequences, we fixed the duration T of the QDD sequence to be equal to five times the duration of the XY4 sequence. This means that after a duration T, either 20 pulses are applied according to the QDD sequence or 5 sequences of 4 pulses are applied according to XY4.

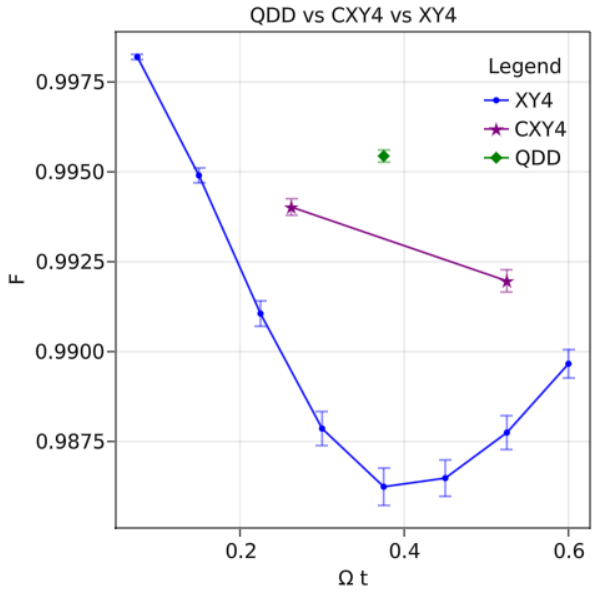

Figure 4.5: Relative performance of the XY4, CXY4 and $\text{QDD}_{4,4}$ sequences for an Hamiltonian $H_{SB}(\theta = 1.2)$. The simulation parameters were fixed at $(k_{\max}, t_f/dt, n_{\text{traj}}) = (6,10000,700)$.

Remark. This comparative figure was reproduced for different values of n_{traj} and t_f/dt in Appendix E in order to make sure that the results are converged with respect to the simulation parameters.

Chapter 5

Some Important Results in the Field of Dynamical Decoupling

In this chapter, we will go through some important results in the field of dynamical decoupling that we have not mentioned until now. These results will each be introduced in the context of solving a particular problem that comes either directly from dynamical decoupling theory or from the experimental implementation of DD. This chapter will essentially focus on the consequences of the utilization of *realistic pulses*. That is, the pulses are neither ideal (in the sense that they are not infinitely short and of infinite strength) nor perfectly implemented by a given experimental set-up.

5.1 Dynamical decoupling using bounded control strength

So far the approximation of unbounded and infinitely fast pulses has been made. However, δ-pulses are not physically implementable because, for a given experimental set-up, a pulse will only be able to reach a finite maximum strength and last for a finite, non-zero, duration. The approximation made earlier stating that the interaction Hamiltonian is equal to zero during the pulses will thus not be valid. It is thus interesting to spend some time reflecting on Section 2: we showed how the relevant symmetrization procedure could create an averaged out Hamiltonian and effectively decouples the system from the bath, but we have made the approximation of the ideal δ-pulses a bit early in the derivation and one can wonder whether the results still hold in the case of bounded strength control. The issue was addressed in Ref. [58] where it was shown that symmetrization could still occur using non-ideal pulses assuming that an *Eulerian* DD sequence is used. In the next subsection, we will work out the proof of this previous statement. The demonstration is rather similar to the one made in Section 2 in the case of ideal pulses.

5.1.1 Proof that dynamical decoupling occurs with non-ideal pulses

At the end of the derivation of Section 2, we proved that by choosing a decoupling group $\mathcal{G} = \{g_j,\, j = 1, \ldots |\mathcal{G}|\}$, one could construct the following symmetrization procedure:

$$\Pi_{\mathcal{G}} : \mathcal{B}(\mathcal{H}_S) \to \mathcal{B}(\mathcal{H}_S) : S \mapsto \overline{S} = \Pi_{\mathcal{G}}(S) = \frac{1}{|\mathcal{G}|} \sum_{g_j \in \mathcal{G}} g_j^\dagger S g_j. \tag{5.1}$$

By choosing a relevant decoupling group, one can then average out the unwanted operators, thus removing unwanted effects from the system's dynamics. We showed that this operation can be implemented by the right sequence of pulses and that such sequence can be found by choosing some cyclic path on the Cayley graph $G(\mathcal{G}, \Gamma)$ where $\Gamma = \{\gamma_\lambda\}$ is a generating set of $\mathcal{G}$. In the derivation, however, we used ideal pulses P_j to instantaneously flip the evolution Hamiltonian from $\tilde{H}_{j-1} = g_{j-1}^\dagger H g_{j-1}$ to $\tilde{H}_j$. In this section, we will use a

smooth transition from $\tilde{H}_{j-1}$ to $\tilde{H}_j$ in order to remove discontinuities. Using smooth transition, implemented by bounded strength pulses of undetermined shapes, it is possible to implement the symmetrization procedure if a specific path is used along the Cayley graph $G(\mathcal{G},\Gamma)$: an Eulerian cycle [58,59]. An Eulerian cycle consists of a cyclic path that uses each edge exactly once such that from each vertex, there is exactly one departing edge of each color, resulting in a sequence of total length $L = |\Gamma||\mathcal{G}|$ [58]. An example of Eulerian cycle for the maximal decoupling of 1 qubit is given in FIG. 5.1. We will now dive into a derivation similar to the one of Section 3 and show that the main result of the previous derivation can be obtained in the case of bounded control when a Eulerian path is used.

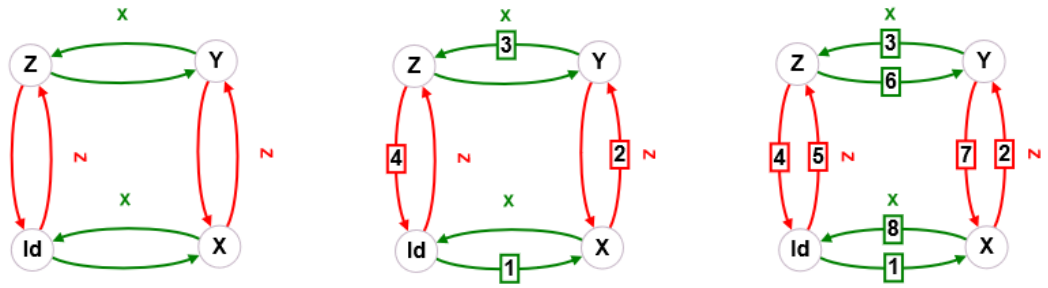

Figure 5.1: Cayley graph of $\mathcal{G} = \{\mathbb{1}, X, Y, Z\}$ with respect to $\Gamma = \{X, Z\}$ (a). A non-Eulerian and Eulerian path are represented in (b) and (c) respectively.

First, let us consider a decoupling group $\mathcal{G} = \{g_j\}$ and its (not unique) generating set $\Gamma = \{\gamma_\lambda\}$, $\lambda = 1, \dots |\Gamma|$. We consider a path that forms an Eulerian cycle on the Cayley graph $G(\mathcal{G},\Gamma)$ and we assume that we are able to implement each generator with the use of a control Hamiltonian over a finite time interval Δt as

$$\gamma_\lambda = \mathcal{T}_{\leftarrow} \exp\left\{-\frac{i}{\hbar}\int_0^{\Delta t} dt' h_\lambda(t')\right\} \quad \forall \lambda \in \{1, \dots, |\Gamma|\} \tag{5.2}$$

with $h_\lambda(t)$ an implementable control Hamiltonian. Our sequence will consist of $L = |\mathcal{G}||\Gamma|$ intervals of duration $\Delta t = \frac{T}{|\mathcal{G}||\Gamma|}$. The corresponding graph will possess L edges $p_l \in \Gamma = \{\gamma_\lambda\}$ and the Eulerian cycle will follow the path $p_1 \to p_2 \to \cdots \to p_L$, visiting the different vertices in the order $g_0 \to g_1 \to \cdots \to g_{L-1} \to g_L = g_0$ starting from the identity ($g_0 = \mathbb{1}$). During the lth subinterval, the Hamiltonian $h_l(t)$ will ensure a smooth transition of the propagator $U_{cf}(t)$ from g_{l-1} to g_l by smoothly implementing p_l. In other words, the pulse p_l is now implemented during the lth subinterval whereas, in the case of ideal δ-pulses, it was implemented instantaneously at the end of the lth subinterval (or equivalently 'between' the lth and $(l+1)$th subintervals because of the infinitesimally small duration of the pulse). A visual representation is displayed in FIG.5.2, taking the basic CPMG sequence as an example.

In the δ-pulse case scenario, we would have had a propagator $U_{cf}(t)$ given by

$$U_{cf}(l\Delta t + t) = p_l U_{cf}((l-1)\Delta t), \quad t \in [0, \Delta t[, \quad l = 1, \dots |\Gamma||\mathcal{G}| \tag{5.3}$$

with $U_{cf}(l\Delta t + t) = g_l$, $U_{cf}((l-1)\Delta t) = g_{l-1}$ and $p_l = g_l g_{l-1}^\dagger$ the lth δ-pulse, as expressed in Eq.(2.21) and Eq.(2.23) and represented in FIG. 2.1 . In the present case, this translates to

$$U_{cf}((l-1)\Delta t + t) = u_l(t) U_{cf}((l-1)\Delta t), \quad t \in [0, \Delta t[, \quad l = 1, \dots |\Gamma||\mathcal{G}| \tag{5.4}$$

with $u_l(t) = \mathcal{T}_{\leftarrow} \exp\left\{-\frac{i}{\hbar}\int_0^t dt' h_l(t')\right\}$ and $U_{cf}((l-1)\Delta t) = g_{l-1}$. Equation (5.2) ensures that $u_l(\Delta t) = p_l$ such that $U_{cf}(l\Delta t) = p_l g_{l-1} = g_l$. Now that we have an expression for the action of the control field $U_{cf}(t)$,

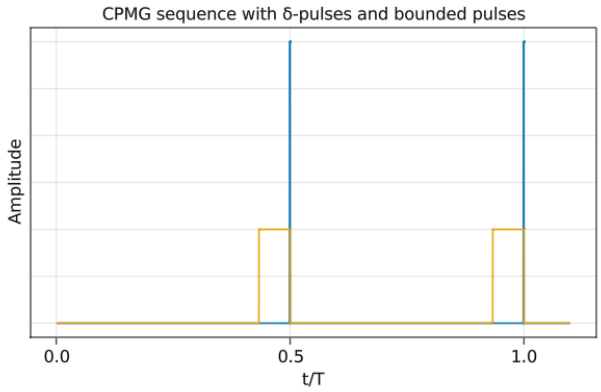

Figure 5.2: CPMG sequence with δ-pulses (blue) and bounded pulses (orange). In the case of the CPMG sequence, one can easily see by drawing the Cayley graph that the original sequence $\Delta t - X - \Delta t - X$ is Eulerian. A rectangular shape was chosen for the pulses for the sake of simplicity, but there is no constraint on the shape, leaving the possibility for pulse shaping.

we can calculate the average Hamiltonian at first order as defined in Eq. (2.13a),

$$\begin{aligned}
\hbar\overline{H}^{(0)} &= \frac{1}{T}\int_0^T dt U_{cf}^\dagger(t) H_0 U_{cf}(t) \\
&= \frac{1}{T}\sum_{l=1}^{L}\int_0^{\Delta t} dt U_{cf}^\dagger((l-1)\Delta t) u_l^\dagger(t) H_0 u_l(t) U_{cf}((l-1)\Delta t) \\
&= \frac{1}{T}\sum_{l=1}^{L} U_{cf}^\dagger((l-1)\Delta t)\left[\int_0^{\Delta t} dt u_l^\dagger(t) H_0 u_l(t)\right] U_{cf}((l-1)\Delta t) \\
&= \frac{1}{T}\sum_{l=1}^{L} g_{l-1}^\dagger\left[\int_0^{\Delta t} dt u_l^\dagger(t) H_0 u_l(t)\right] g_{l-1}.
\end{aligned}$$

Because the sequence is Eulerian, we can now separate the sum $\sum_{l=1}^{L}$ as a double-sum over the different colors λ and vertices g_j and use $T = \Delta t|\mathcal{G}||\Gamma|$ in order to obtain the expression

$$\hbar\overline{H}^{(0)} = \frac{1}{|\mathcal{G}|}\sum_{j=1}^{|\mathcal{G}|} g_{j-1}^\dagger\left[\frac{1}{|\Gamma|}\sum_{\lambda=1}^{|\Gamma|}\frac{1}{\Delta t}\int_0^{\Delta t} dt u_\lambda^\dagger(t) H_0 u_\lambda(t)\right] g_{j-1} \equiv \mathcal{Q}_{\mathcal{G}}(H_0) \tag{5.5}$$

where we have defined the quantum operation $\mathcal{Q}_{\mathcal{G}}(\cdot)$. We recognize in this expression the quantum dynamical symmetrisation Eq.(2.16) and define the quantum operation $F_\Gamma(\cdot)$

$$F_\Gamma : \mathcal{B}(\mathcal{H}_S) \to \mathcal{B}(\mathcal{H}_S) : S \mapsto F_\Gamma(S) = \frac{1}{\Delta t|\Gamma|}\sum_{\lambda=1}^{|\Gamma|}\int_0^{\Delta t} dt u_\lambda^\dagger(t) S u_\lambda(t) \tag{5.6}$$

such that

$$\hbar\overline{H}^{(0)} \equiv \mathcal{Q}_{\mathcal{G}}(H_0) \equiv \Pi_{\mathcal{G}}[F_\Gamma(H_0)]. \tag{5.7}$$

I will now prove that in the situation considered, $\mathcal{Q}_{\mathcal{G}}(H_0) = \Pi_{\mathcal{G}}(H_0)$, following the work from Ref. [58]. Recall that $\mathcal{C}_S$ is the control algebra of the decoupling group $\mathcal{G}$ and that $\Pi_{\mathcal{G}}$ is the projector onto the commutant of $\mathcal{C}_S$, which we will call $\mathcal{C}_S'$. The proof consists of two steps.

(i) We have assumed that $h_\lambda(t) \in \mathcal{C}_S$ for all $\lambda \in \{1, \dots |\Gamma|\}$ and $t \in [0, \Delta t[$, which leads to $u_\lambda \in \mathcal{C}_S$ as well. This means that every element Y in the commutant of $\mathcal{C}_S$, that is $Y \in \mathcal{C}'_S$, will satisfy $F_\Gamma(Y) = Y$, which is straightforward to prove because of the form of F_Γ in Eq. (5.6) : since Y commutes with $u_\lambda(t) \in \mathcal{C}_S$, we can permute the two operators and realize that $u_\lambda^\dagger(t)u_\lambda(t) = \mathbb{1}$ because they are unitary operators.

(ii) Now, let us consider any $X \in \mathcal{B}(\mathcal{H}_S)$. Calculating $\mathcal{Q}_\mathcal{G}[\mathcal{Q}_\mathcal{G}(X)]$, we see that

$$\begin{aligned}\mathcal{Q}_\mathcal{G}[\mathcal{Q}_\mathcal{G}(X)] &= \Pi_\mathcal{G}[F_\Gamma[\Pi_\mathcal{G}[F_\Gamma(X)]]] \\ (*) \quad &= \Pi_\mathcal{G}[\Pi_\mathcal{G}[F_\Gamma(X)]] \\ (**) \quad &= \Pi_\mathcal{G}[F_\Gamma(X)] = \mathcal{Q}_\mathcal{G}(X).\end{aligned}$$

In order to get (*), we realized that, $\Pi_\mathcal{G}$ being a projector onto $\mathcal{C}'_S$, (i) implies that $F_\Gamma[\Pi_\mathcal{G}[F_\Gamma(X)]] = \Pi_\mathcal{G}[F_\Gamma(X)]$. Also, since $\Pi_\mathcal{G}$ is a projector, $\Pi_\mathcal{G}[\Pi_\mathcal{G}(X)] = \Pi_\mathcal{G}(X)$ which leads to (**). The conclusion of this derivation is that $\mathcal{Q}_\mathcal{G}(X)$ is a projector since $\mathcal{Q}_\mathcal{G}[\mathcal{Q}_\mathcal{G}(X)] = \mathcal{Q}_\mathcal{G}(X)$. The definition of $\mathcal{Q}$ leads to it being a projector onto a subspace of $\mathcal{C}'_S$. It follows that $\mathcal{Q}_\mathcal{G} = \Pi_\mathcal{G}$ if and only if $\mathcal{Q}_\mathcal{G}$ and $\Pi_\mathcal{G}$ have identical actions on $\mathcal{C}'_S$. Since we proved in (i) that $\mathcal{Q}_\mathcal{G}(Y) = \Pi_\mathcal{G}(Y)$ for all $Y \in \mathcal{C}'_S$, it is clear that $\mathcal{Q}_\mathcal{G} = \Pi_\mathcal{G}$.

5.1.2 Discussion

We demonstrated above that the symmetrization procedure capable of generating averaged out Hamiltonian can be implemented using non-ideal pulses, that is pulses of bounded control strength and finite non-zero duration. The only constraint imposed is that the DD sequence must follow an Eulerian cycle on the Cayley graph. For a given decoupling group, an Eulerian DD sequence can be found by tracing a Cayley graph for a given generating set and construct the sequence of pulses accordingly. When tracing the Cayley graph is a painful process, one can also find an Eulerian DD sequence by the knowledge of a non-Eulerian sequence. This can be done by taking the non-Eulerian sequence and adding to the sequence the hermitian adjoint of the initial sequence. For the XY4 sequence, for example, this gives

$$\begin{aligned}XY4 &\equiv \Delta t - X - \Delta t - Z - \Delta t - X - \Delta t - Z \\ (XY4)^\dagger &\equiv (\Delta t - X - \Delta t - Z - \Delta t - X - \Delta t - Z)^\dagger \\ &= \Delta t - Z - \Delta t - X - \Delta t - Z - \Delta t - X \\ (XY4)(XY4)^\dagger &\equiv \Delta t - X - \Delta t - Z - \Delta t - X - \Delta t - Z - \Delta t - Z - \Delta t - X - \Delta t - Z - \Delta t - X\end{aligned}$$

which is precisely the sequence represented in Fig. 5.1c.

In the demonstration, no heavy constraint was imposed on the shape of the pulses. This leaves the possibility for *pulse shaping* [70], that is designing the shape of the pulses to improve performance. This also allows for the development of a new field of dynamical decoupling where we do not attempt to create short and strong pulses but quite the opposite: the objective is to apply a continuous field over the sequence. We then talk of *Continuous Dynamical Decoupling*. A framework for the design of continuous dynamical decoupling sequences was developed in [71]. In this interesting article, they introduce a geometrical perspective of dynamical decoupling, where the interaction Hamiltonian can be seen as an error vector in $\mathbb{R}^N$, with $N = n^2 - 1$ and n the dimension of the Hilbert space of the system. For example, for a single qubit for which $\dim(\mathcal{H}_S) = 2$, the error vector is a three dimensional vector $\vec{S} \in \mathbb{R}^3$. In this framework, a DD sequence has the effect of rotating the error vector such that, by choosing a sequence for which the rotation occurs on a plane that contains the error vector, it is possible average out the error vector with the rotating wave approximation if the rotation is fast enough (that is if the DD sequence is of sufficiently short duration). δ-pulses dynamical decoupling, which is sometimes called '*bang-bang*' dynamical decoupling, can be recovered as a limiting case in that framework by considering infinitely fast π rotations. Using this framework, designing a DD sequence is done by calculating the error vector and finding the operator that performs a rotation on the relevant plane.

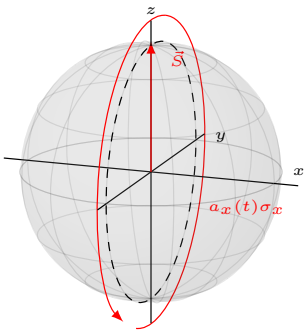

Figure 5.3: Representation of the error vector $\vec{S}$ for the purely dephasing qubit. Applying a control field corresponding to an Hamiltonian $H_{ctrl}(t) = a_x(t)\sigma_x$ corresponds to a rotation around the x axis. The CPMG sequence corresponds to the limiting case of two infinitely fast π rotations around the x axis.

5.2 Errors in the control field

Another problem that affects the performance of a dynamical decoupling strategy is the errors in the control field due to imperfect control at the experimental level. The actual propagator of a realistic pulse will then differ from the desired pulse propagator corresponding to the ideal pulse, therefore affecting the performance of DD schemes. Because of the errors induced by the DD sequence, it can even create more errors than it corrects. The issue of imperfect control is not unique to dynamical decoupling; great efforts have been made to overcome this issue in the field of quantum control. In the field of dynamical decoupling, the response to the problem of imperfect control has been the development of *robust* dynamical decoupling.

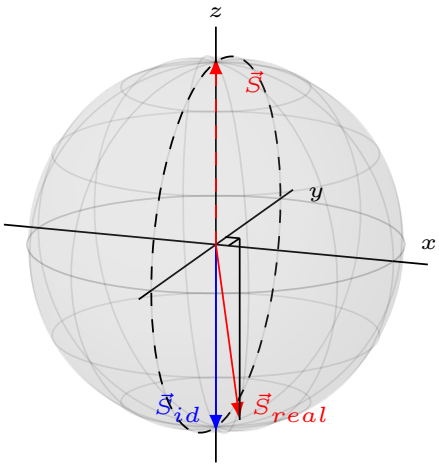

(a) Representation of the error vector after an ideal pulse (blue) and after an imperfect pulse (red).

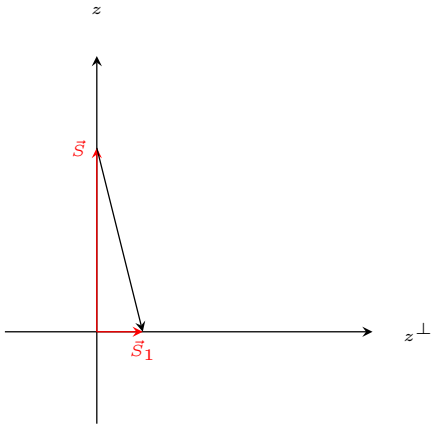

(b) If the CPMG sequence is applied with a sufficiently high frequency, performing the rotating wave approximation leads to the z component of the error vector being averaged out. This can be seen as a projection of the error vector on the $z^\perp$ plane. However, using imperfect pulses, the projection is imperfect and the resulting error vector has a non-zero component on the $z^\perp$-plane.

Figure 5.4: Geometric representation of the effect of an imperfect CPMG sequence on the error vector.

In order to illustrate the issue, we can take the CPMG sequence and use the geometric perspective

introduced previously. Two kinds of imperfection can occur due to the CPMG sequence [30]. First, a pulse can over-rotate or under-rotate the error vector. This kind of error is usually referred to as a *flip-angle error*. Secondly, the pulse can have a small undesirable component $\epsilon_z\sigma_z$ or $\epsilon_y\sigma_y$ which leads to a small rotation around another axis. This is referred to as an *axis-misspecification*. After several imperfect pulses, the errors eventually build up. The objective of robust DD sequences is to prevent the errors introduced by the individual pulses from building up. A visual representation of flip-angle and axis-misspecification errors in a CPMG sequence is presented in FIG.5.4.

A first technique to mitigate errors due to imperfect control is to use a maximal decoupling strategy instead of a selective one. Take the geometric representation of the CPMG sequence (see FIG. 5.4a), for example. Without control field, the error vector has a non-zero component on the z axis only. In order to average this component, the CPMG sequence performs a rotation around the x axis. However, because of imperfect control, the application of a pulse induces a non-zero component of the error vector on the x axis. The CPMG sequence alone is not able to correct this error. However, the application of a XY4 sequence solves this issue as the phase-flip sequence will average out the error component induced by the spin-flip sequence on the x axis. In conclusion, each individual sequence of the XY4 sequence partially corrects the imperfection caused by the other one. We can say that the XY4 have some self-correcting properties, in a sense.

In order to improve the self-correcting properties of the XY4 sequence, one can concatenate a bunch of XY4 sequence on top of each other [55]. In a similar way as to how each layer of the XY4 sequence corrects the imperfection of the other layer, each level of concatenation will correct the errors created by the lower levels. The effect of the XY4 sequence on the error vector as well as the effect of the concatenated XY4 sequence to the first level of concatenation are represented in FIG. 5.5. Because concatenation can be repeated an arbitrary number of times, it is possible to design sequences with arbitrary high robustness.

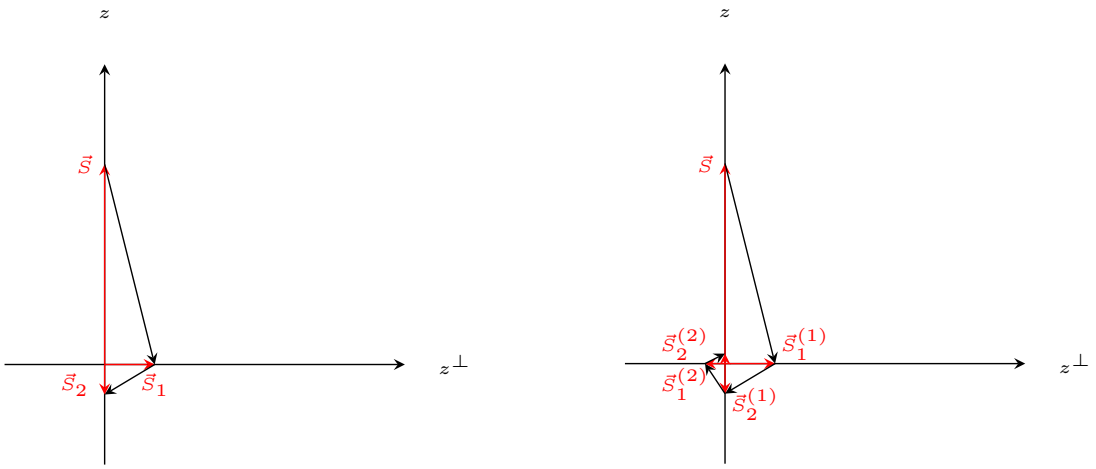

(a) Effect of the XY4 sequence on the error vector. $\vec{S}_1$ represents the effect of the first layer of the XY4 sequence on the error vector, while $\vec{S}_2$ represents the effect of the second layer of the XY4 sequence on $\vec{S}_1$.

(b) Effect of the concatenated XY4 sequence on the error vector to the first level of concatenation. $\vec{S}_2^{(1)}$ is the error vector resulting from the first level of concatenation while $\vec{S}_2^{(2)}$ is the error vector resulting from the second level.

Figure 5.5: Effects of imperfect XY4 and CXY4 sequences on the error vector.

As stated previously when concatenation was presented, concatenating sequences increases exponentially the number of pulses in the sequence and it is thus an inefficient way to treat control errors. Fortunately, other schemes have been developed. One such scheme is called *Knill Dynamical Decoupling* (KDD). The idea is to replace a pulse by a so-called *composite pulse* [72]. The composite pulse effectively implements the original pulse, but does so through the implementation of five different pulses. Let us illustrate this for the X pulse. As stated earlier, this pulse implements a π rotation around the x axis; in the context of

KDD, we then use the notation $\pi_x \equiv X$. More generally, we call π_ϕ the pulse that implements a π rotation around the axis forming an angle ϕ with the x axis and belonging to the (x, z) plane (see FIG.5.6 for a visual representation of the corresponding rotational plane). The strategy introduced in Ref. [73] consists in replacing this single π pulse by a series of π pulses around tilted axis. This ultimately gives

$$\pi_0 \mapsto \pi_{\pi/6} - \pi_0 - \pi_{\pi/2} - \pi_0 - \pi_{\pi/6} \tag{5.8}$$

where π_0 is the original X pulse. More generally, any pulse π_ϕ can be replaced by the corresponding composite pulse

$$\pi_\phi \mapsto K_\phi \equiv \pi_{\phi+\pi/6} - \pi_\phi - \pi_{\phi+\pi/2} - \pi_\phi - \pi_{\phi+\pi/6} \tag{5.9}$$

where K_ϕ can be referred to as a *Knill pulse* around the ϕ axis. These composite pulses are constructed such that systematic errors in the individual pulses can be compensated at the end of the protocol.

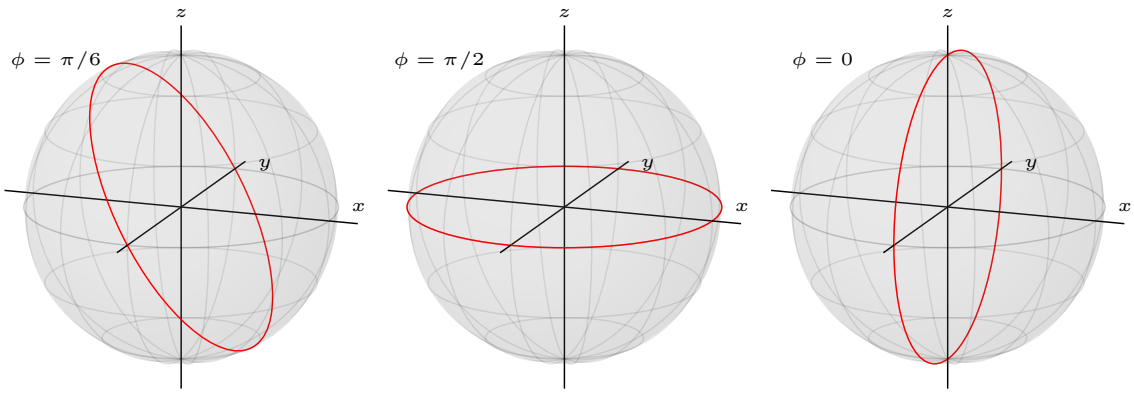

Figure 5.6

It follows that the CPMG sequence can be replaced by the *selective* KDD[1] sequence of 10 pulses

$$SELKDD \equiv K_0 - K_0 \tag{5.10}$$

with

$$K_0 = \Delta t/2 - \pi_{\pi/6} - \Delta t - \pi_0 - \Delta t - \pi_{\pi/2} - \Delta t - \pi_0 - \Delta t - \pi_{\pi/6} - \Delta t/2 \tag{5.11}$$

where $\Delta t = T/10$ if T is the total duration of the SELKDD sequence. The CPMG sequence of 2 pulses have then been traded with a 10 pulses sequence which is supposed to be more robust.

It follows that the XY4 sequence can be modified in a similar way, which results in the 20 pulses KDD sequence presented for the first time in Ref. [74],

$$KDD \equiv K_0 - K_{\pi/2} - K_0 - K_{\pi/2}. \tag{5.12}$$

The performance of this sequence was demonstrated experimentally in Refs. [73, 75]. It was constructed in the context of creating a sequence more robust to *systematic* over and under-rotation in the individual pulses, that is systematic flip-angle errors.

In order to illustrate the superiority of KDD in terms of control error suppression, we introduced a systematic flip-angle error in the pulses implemented in HOPS. The flip-angle error is implemented by replacing the ideal σ_i-pulse Hamiltonian $H^{\text{ideal}}_{\text{pulse}} = \frac{\pi}{2}\sigma_i\delta(t - t_{\text{pulse}})$ by

$$H^{\text{FA}}_{\text{pulse}} \equiv \frac{\pi}{2}(1 + \epsilon)\sigma_i\delta(t - t_{\text{pulse}}) \tag{5.13}$$

[1]The CPMG sequence of composite pulse is not commonly used in literature such that it does not really have a name. In the original article [73], the notation "CP Robust 180" was used to present the sequence. We decided to refer to this sequence as SELKDD instead.

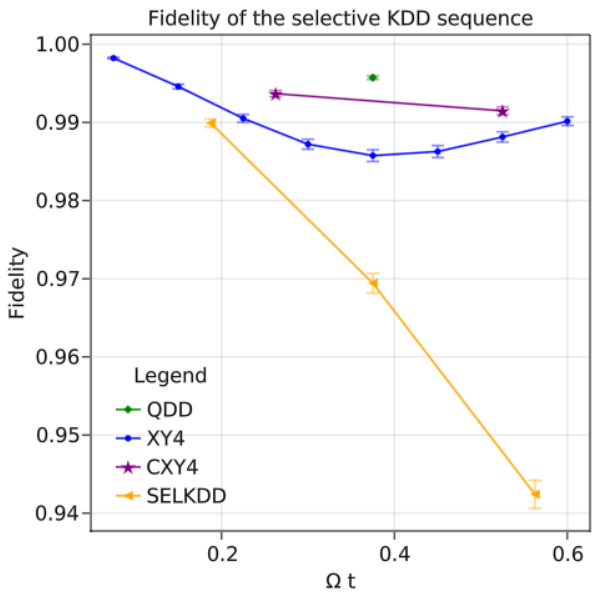

Figure 5.7: Performance of the XY4, CXY4, $\text{QDD}_{4,4}$ and SELKDD sequences for $H_{SB}(\theta = 1.2)$. We see that SELKDD is not sufficient to suppress decoherence as efficiently as the other sequences because dissipative effects are taken into account.

where FA stands for "flip-angle" [30]. The parameter ϵ indicates the amplitude of the error. The relative performance of the XY4 and KDD sequences for different values of ϵ can be found in FIG.5.9. It illustrates that the introduction of flip-angle errors in the control field lowers greatly the performance of the XY4 sequence, whereas the KDD sequence is not affected as much, thus revealing its robustness to over and under-rotations. The robustness of the CXY4 sequence was also considered in FIG.5.10; it shows that the CXY4 sequence proves more effective than KDD in the timescale considered. However, because the fidelity seems to drop more rapidly for the CXY4 sequence, it seems that the flip-angle errors build up faster such that one could expect KDD to outperform CXY4 if we keep applying the sequences periodically.

Having that in mind, we can now realize that the phase ϕ of the pulses is a new parameter that can be tuned. One can then construct a sequence of N π-pulses

$$\pi_{\phi_1} - \pi_{\phi_2} - \cdots - \pi_{\phi_N} \tag{5.14}$$

and consider the phases $\{\phi_k\}$ as parameters that can be optimized. An approach was presented in Ref. [76] in order to find the optimal robust sequence in the context of a purely dephasing qubit undergoing flip-angle errors and leads to a sequence known as *Universally Robust Dynamical Decoupling* (URDD). the URDD sequence is given by the formula

$$URDD_N \equiv \pi_{\phi_1} - \pi_{\phi_2} - \cdots - \pi_{\phi_N} \tag{5.15}$$

for even $N \geq 4$ and with the phases $\{\phi_k\}$ given by

$$\phi_k = \frac{(k-1)(k-2)}{2}\Phi^{(N)} + (k-1)\phi_2 \quad \forall k = 2, \ldots N. \tag{5.16}$$

such that ϕ_1 and ϕ_2 are free parameters that are commonly set to 0 and $\pi/2$ respectively [30] and $\Phi^{(N)}$ is given by

$$\Phi^{(N)} = \begin{cases} \frac{\pi}{m} & \text{if } N = 4m \\ \frac{2m\pi}{2m+1} & \text{if } N = 4m+2. \end{cases} \tag{5.17}$$

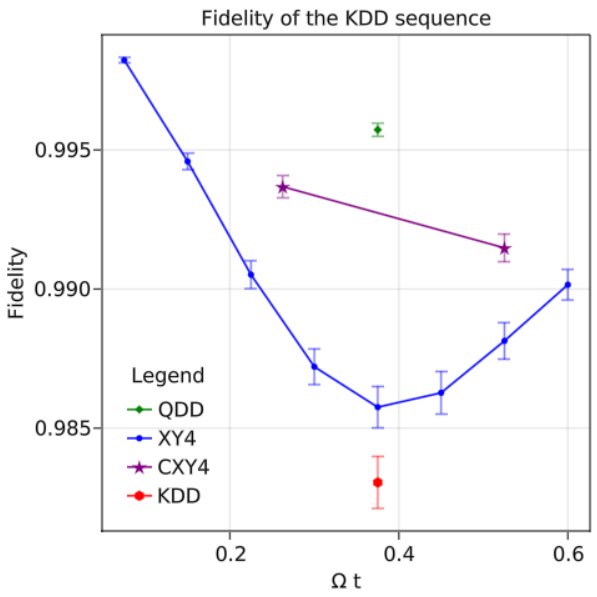

Figure 5.8: Performance of the XY4, CXY4, $\text{QDD}_{4,4}$ and KDD sequences for $H_{SB}(\theta = 1.2)$. KDD does not seem to provide additional suppression properties. This is because no control errors were artificially added to the simulation: the addition of systematic errors should lower the performances of the other sequences enough to reveal the superiority of KDD in terms of control error suppression. According to Ref. [30], KDD only outperforms the other sequences in a regime where the flip-angle error dominates; in a system with slow decoherence but high flip-angle error, the KDD sequence would be the appropriate choice.

This sequence, once again, proves robust to systematic over and under-rotation errors because these systematic errors in the net rotation of each of the pulses compensate at the end of the sequence. A similar approach is presented in Ref. [77] in order to increase the robustness of continuous DD sequences; in that case, the phase is a continuous parameter and the authors used some machine learning to solve the optimization problem.

Another fundamentally different way to increase robustness of a sequence is by *pulse shaping*. With pulse shaping, the robustness can be increased at the level of the individual pulse. An interesting approach to pulse shaping is presented in Ref. [70] and uses a Quantum Optimal Control algorithm to shape the pulse.

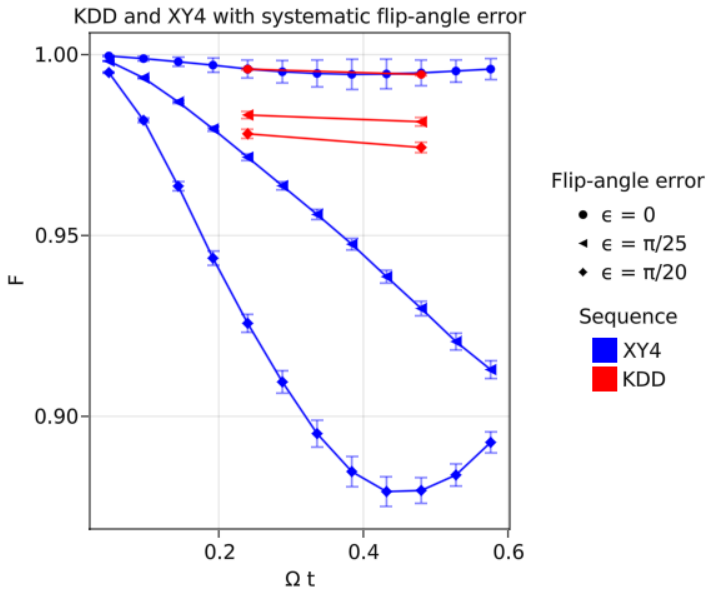

Figure 5.9: Effects of systematic flip-angle errors in the DD pulses on the performance of the sequence. The period of the XY4 sequence was set to $T = \frac{1}{2.5\omega_c}$ and the period of the KDD sequence was chosen equal to $5T$ such that the same number of pulses are applied for the same duration for each sequence, in order to provide a fair comparison between the two sequences.

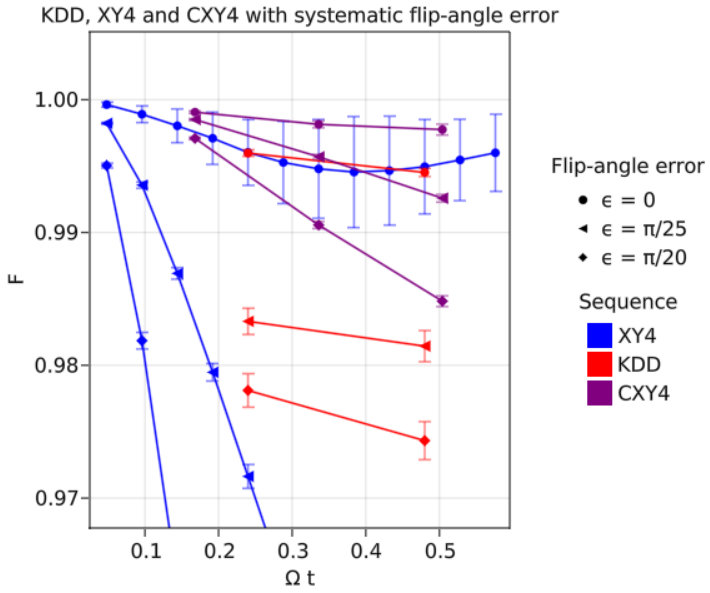

Figure 5.10: Effects of systematic flip-angle errors in the DD pulses on the performance of the XY4, CXY4 and KDD sequences. The duration of the CXY4 sequence was fixed such that the pulse interval of the CXY4 sequence is equal to the pulse interval of the KDD and XY4 sequences.

Conclusion

Summary

The aim of this Master's thesis was to provide a state of the art on dynamical decoupling and to benchmark the HOPS method in this context.

In the first chapter, we have presented a particularly useful model for studying decoherence in a single qubit, namely the spin-boson model. The spin-boson model consists of a two-level system interacting with a bosonic field. Depending on the form of the interaction Hamiltonian, different methods have been presented to study decoherence. When the interaction Hamiltonian caused pure dephasing without dissipation of energy, an exact analytical solution was derived. When it involved a term responsible for dissipation, a method based on a stochastic Schrödinger equation was presented, called the HOPS method. In this chapter, we first studied pure dephasing using the analytical results. This enabled us to introduce the timescale of the decoherence process as well as the different spectral densities used throughout the thesis. Then, we intended to use the analytical results in order to validate the HOPS method in the context of a decohering qubit. This task unexpectedly led to an interesting discussion on the regime of validity of the HOPS method as well as the impact of the non-physical negative frequencies which appear in the HOPS equation. We demonstrated that the negative frequencies introduced by the Lorentzian distribution, as small as they can be, bear a significant impact on the dynamics in the relevant timescale. In order to overcome that problem, we derived a regime of parameters that prevents the negative frequencies to build up enough importance in this timescale. Finally, using this regime of parameters, we could validate the HOPS method in the context of a purely dephasing qubit and calculate the time evolution of said qubit when including dissipative behaviors.

In this second chapter, we followed the work of Ref. [21] and presented the theory of dynamical decoupling. We showed how, using a sequence of pulses, it is possible to implement a quantum operation that effectively averages out the unwanted operators of an Hamiltonian. We also showed how to construct the relevant sequence based on the form of the undesired system-bath interaction Hamiltonian and illustrated the process with two simple examples.

In the next chapter, we focused on *selective* dynamical decoupling protocols which aim at averaging out the term responsible for pure dephasing. We analytically derived the time evolution of the qubit undergoing pure dephasing and a series of spin flips. Using this analytical derivation, we first presented the most basic DD sequence, namely the CPMG sequence. We then presented a few procedures aiming at optimizing the position of the pulses in order to increase the performance of a dynamical decoupling sequence. Altogether, four sequences were presented and tested, namely the CPMG, UDD, LODD and OFDD sequences, each having their respective advantages and disadvantages. Another sequence called BADD was introduced briefly in the context of presenting the fundamental limit of dynamical decoupling resulting from the finite width of the pulses. In this chapter, we then used the exact analytical derivation to validate the results obtained with HOPS. Our results first demonstrated that HOPS captures well the effects of a DD protocol on the Hamiltonian such that it could be used to demonstrate the efficacy of DD. However, the negative frequencies introduced by HOPS were showed to prohibit the replication of the exact analytical results. This prevents us from making arbitrarily accurate prediction. Moreover, a fair comparison of the performances of different sequences is also prohibited because of those same negative frequencies; it was shown that a more performing sequence can appear as less performing according to the HOPS method.

In Chapter 4, we introduced several sequences aiming at suppressing dissipative effects as well as dephasing effects. We first constructed the most basic sequence, called XY4, using a concatenation method. The same concatenation method was then used to add several levels of concatenation to the XY4 sequence, creating a so-called *Concatenated* DD sequence which results in a higher order of decoupling. We then introduced another sequence which aimed at providing the same order of decoupling as CDD but using a lower number of pulses. This scheme, called *Quadratic* DD, was created in much the same way XY4 was constructed, but using a UDD sequence as the building block instead of CPMG. The three sequences introduced in this section were compared using HOPS.

Finally, in the last chapter, we addressed, in the context of dynamical decoupling, a fundamental problem in the field of Quantum Control, that is the issue of dealing with realistic control fields. In the context of dynamical decoupling, the first problem to address was to prove validity of the theory when non-ideal pulses are considered. This led to the conclusion that the utilization of an *Eulerian* dynamical decoupling sequence was sufficient to ensure the implementation of the averaging operation with non-ideal pulses. Afterwards, we addressed the issue of errors in the control field. This led to the definition of the *phase* of a pulse, a new parameter that can be optimized to increase the robustness of a sequence to errors in the control field. Two sequences were introduced in this context, namely the *Knill* DD sequence and the *Universally Robust* DD sequence. We then introduced systematic control errors in the Hamiltonian and demonstrated the superiority of KDD over XY4 in terms of robustness to control errors.

Perspectives

Although dynamical decoupling has been studied for over two decades, the field still has much to offer. In this section, we provide some perspectives on two problematics in the field of dynamical decoupling which have not yet been extensively studied.

Dynamical decoupling on qudits

A wide variety of dynamical decoupling protocols have been developed in order to decouple a single qubit from its environment. This includes the bang-bang DD sequences presented in this Master's thesis, the continuous dynamical deocupling sequences introduced in Ref. [71] or even feedback-based strategies [78]. For multi-qubit systems, a method was presented in Ref. [79] which consists of *nesting* single-qubit dynamical decoupling sequences in a manner similar to the concatenation method. In the last decade, various sequences have been implemented experimentally.

However, not as much work has been done on the design and optimization of *qudit* dynamical decoupling. While qubits are the most common elementary quantum systems considered for quantum information storage and processing, elementary quantum systems with more than two levels, i.e. qudits, are currently considered to enable better performance in some quantum technologies. Some rapidly evolving fields such as quantum cryptography [80, 81], quantum metrology [3, 82] and quantum computing [83] could benefit greatly from trading qubits with qudits. This recent interest for qudit systems calls for the development of new techniques to protect quantum information and entanglement in those more complex systems. We thus expect a renewed interest in the field of dynamical decoupling in the following years, as the field of qudit dynamical decoupling had not yet been fully explored and could potentially be of great interest for the developing quantum technologies.

In theory, the framework presented in Ref. [71] should help in the construction of qudit DD sequences, although not much work, to the extent of our knowledge, has followed up on this article. Some works have only recently started to focus on this subject. The CPMG sequence was generalized in Ref. [84] for a qudit system. A method for protecting an arbitrary quantum operation on a 3-level system, i.e. a *qutrit*, based on continuous DD was presented in Ref. [85] and was extended to the case of a d-level system. Only in 2022 has the first experimental implementation of dynamical decoupling on a 3-level system been reported [86]. In the APS march meeting of this year, a presentation was dedicated to the development of a new formalism for robust qudit dynamical decoupling and Hamiltonian engineering [87]. The corresponding paper was only

very recently published and presents a geometrical formalism constructed for the purpose of facilitating the design of qudit DD sequences satisfying some robustness requirements.

The optimization procedures mentioned in this Master's thesis have not yet been extended to the qudit systems. This is, however, not surprising. The UDD sequences and the OFDD sequences, for example, are constructed by an optimal design of the filter function, for which the expression is known from the analytical derivation made in Section 3.2. Because no such analytical solution is known in the context of a qudit undergoing a DD sequence, it is not trivial to repeat these two optimization procedures. The LODD sequences, on the other hand, can be obtained if the infidelity of a qudit undergoing DD can be computed using some non-Markovian method. However, in order to compute LODD sequences, one would need a sufficiently accurate method. Because the algorithm can converge slowly for a high number of pulses, it would also be preferable that said method enables fast calculation of the infidelity. No one has so far focused on qudit-LODD, but the idea of generalizing it to the d-level system is exciting. In particular, since the LODD sequences presented in Section 3.2.2 are shown to converge to the UDD sequence for short duration protocols, generalizing LODD to qudit-systems could possibly lead to the generalization of Uhrig Dynamical Decoupling in the context of qudit DD.

Reconciling quantum control and dynamical decoupling

As we have briefly stated earlier, quantum control and dynamical decoupling might seem fundamentally incompatible at first sight. The effect of a dynamical decoupling sequence can be seen as a projection of the system operators appearing in the Hamiltonian onto a subspace of $\mathcal{B}(\mathcal{H}_S)$ called the *commutant* of the control algebra $\mathcal{C}_S$. Using the right control algebra, projecting an unwanted Hamiltonian onto the commutant of $\mathcal{C}_S$ can result in a effective suppression of said Hamiltonian. However, this has the side effect of reducing greatly the control that we possess over the system; the operators that we can still use for computation purposes are now all included in the commutant of $\mathcal{C}_S$. For a single qubit undergoing the CPMG sequence, for example, the only (non-trivial) remaining operation is the spin-flip. For the same qubit undergoing a XY4 sequence, the commutant of $\mathcal{C}_S$ merely consists of the identity operator.

In order to overcome this issue, it is possible to encode a logical qubit into several physical qubits [88]. If this interaction Hamiltonian has certain symmetries, it is *a priori* possible to perform dynamical decoupling and design enough quantum gates that commute with the control algebra such that enough control remains over the system. Another strategy introduced in Ref. [56] consists of introducing additional pulses in a sequence such that the DD sequence effectively implements an arbitrary quantum operation on top of protecting the system against potential errors. Those sequences are called *Dynamically Error-Corrected Gates* (DECG). This strategy is extremely interesting but involves a great number of pulses. Moreover, it is not trivial to incorporate optimized sequences such as KDD and UDD in the formalism. Instead, in order to increase the self-correcting properties of the quantum gate, DECG can be concatenated in a manner similar to the one presented in Section 4.2. However, because the number of pulses increases exponentially with the level of concatenation, this means that concatenation will only be possible up to a certain level in an experimental set-up.

A recent article has proposed a new exciting formalism for the design of error-corrected quantum gates [85]. Instead of adding additional pulses to a bang-bang DD sequence, the authors decided to use the framework of continuous dynamical decoupling in order to come up with a formalism for the design of arbitrary quantum gates protected from general noise. This formalism is extremely convenient as it can be extended to the design of qudit quantum operations. However, the process of designing a continuous sequence for a given system and desired quantum gate following this formalism is absolutely not trivial.

We strongly believe that this last strategy should be investigated more deeply in the context of designing state preparation protocols. The objective of a state preparation protocol is to bring a quantum system from an initial quantum state to a target state. This problem is not easily solved for some highly non-classical states, such as the d-level anticoherent states considered for quantum metrology [3], and some highly non-trivial control fields need to be designed. Various techniques have been developed in order solve this quantum control problem. One such technique is called Quantum Optimal Control [89] and consists of a set of methods designed to find the optimal control field that solves a particular quantum control problem.

Because robustness constraints can be added in certain QOC algorithms, it is possible to design a control field which has some robustness to implementation errors. However, on top of errors in the control field, decoherence should also be taken into account. Because the framework introduced in Ref. [85] aims at designing a control field that decouples a system from its environment while performing an operation on the system, it seems perfectly suitable to increase the robustness of a state preparation protocol to decoherence.

General conclusion

As stated in the introduction of this Master's thesis, the objective of this work was twofold. First, we attempted to write a review of the current state of the art in the field of dynamical decoupling. Secondly, we intended to benchmark the HOPS method in the context of dynamical decoupling.

Throughout this master's thesis, we introduced various optimization procedures aiming at increasing the performance of a given sequence. One procedure was based on the optimization of the pulses location inside the sequence. This led to the presentation of the UDD, OFDD and LODD sequences (see Tab. 5.1 for a summary of the respective advantages and disadvantages of each sequence). Another procedure consisted in concatenating DD sequences on top of each other. Thus lead to the introduction of the QDD sequence, believed to be the best analytical DD sequence up to date [30], in the sense that it provides the highest order of maximal decoupling for a given number of pulses. Finally, we briefly introduced another optimization protocol based on an optimal choice of the pulses phase. The KDD and URDD sequences were presented in this context.

At first, our intentions with HOPS was to replicate the analytical results in order to validate the method in the context of dynamical decoupling. Because the method is fairly new, no work on dynamical decoupling had previously used the HOPS method for simulating the performance of a DD sequence, to the extent of our knowledge. We also hoped to use the method to calculate the LODD sequences in the context of maximal dynamical decoupling. However, manipulating HOPS revealed to be a much harder endeavor than expected.

The first problem occurred when studying the purely dephasing qubit model, a system which has been used extensively to study decoherence properties throughout the years. Studying this supposedly simple system, we found that the analytical results did not match with the HOPS results as they should. After much work, we found that the issue came from negative frequencies which build up enough significance over time to alienate the results from HOPS. We then intended to find the timescale at which these negative frequencies become significant and this led to the calculation of an appropriate regime of parameters for studying pure dephasing with HOPS.

Having finally obtained satisfying results with HOPS, we intended to use this method in the context of dynamical decoupling. We expected that keeping the same regime of parameters would allow for an accurate replication of the analytical results. However, we found that the negative frequencies once again played an important role in the dynamics of the system undergoing DD such that we were not able to obtain a satisfactory match with the analytical function. This time, we were not able to find an appropriate regime of parameters. Having given up on the possibility to make accurate prediction of the fidelity of a qubit undergoing DD, we intended to check whether two DD sequences could still be accurately compared. We thus computed the fidelity with HOPS, using the UDD and CPMG sequence and found that the normally underperforming sequence was showed to outperform the other according to HOPS. This led to the unfortunate conclusion that the problem of the negative frequencies seems to prohibit a fair comparison of two DD sequences.

Although problematic when the objective is to compare two sequences, we should point out that HOPS still captures well the effect of a dynamical decoupling sequence on a quantum system. Using HOPS, we were still able to replicate qualitative results about the CPMG sequence. We could show that increasing the frequency of the spin-flips resulted in a better suppression of the dephasing process and that the CPMG sequence alone could not suppress dissipative effects. HOPS also captured well the decoupling properties of the MAXDD strategies XY4, CXY4 and $\text{QDD}_{4,4}$. In this regime of parameters, although the negative frequencies seemingly prohibit an accurate analysis of the performance of the sequence, HOPS can still be used to demonstrate the decoupling properties of sequences. It is then possible to use HOPS to demonstrate

the efficiency of non-trivial DD protocols on qudit systems. Moreover, it is possible to include control field errors. The results of Chapter 5 indicate that the robustness of the KDD sequence to flip-angle errors is well taken into account; HOPS can then be used to analyse the robustness of a DD sequence to errors in the control field. The model for control field errors introduced in Chapter 5 only took flip-angle errors into account, but axis-misspecification errors can also be added quite easily.

Future work should be dedicated to the analysis of the regime of validity of the HOPS method and the impact of the negative frequencies. The first step should be to verify whether HOPS multi-mode suffers from the same issue as its single-mode counterpart. If the problem persists, one could then try to overcome the issue in the context of dynamical decoupling by deriving an appropriate regime of parameters where HOPS predicts well enough the dynamics of the dephasing qubit undergoing SELDD. However, it is not clear whether this regime of parameters could be relevant for dissipative systems or qudit systems; it would solve the issue in a very particular context without solving the underlying problem, just as the regime of parameters for the analysis for decoherence did not help in the context of dynamical decoupling.

In the context of dynamical decoupling, future work should focus on the development of optimized DD sequences for qudit systems. The first step would be to derive basic DD sequences using the frameworks of Refs. [71, 87]. Using HOPS, it is possible to verify that the sequences decouple the system from its environment. Using concatenation methods, MAXDD sequences could then be constructed from simple SELDD sequences, and tested using HOPS. In order to optimize the pulses location, different methods could be investigated. First, more efforts could be made in order to derive an analytical function describing the dynamics of a qudit undergoing a simple DD sequence. If we are to find such a solution, the UDD, OFDD and LODD sequences could be generalized simply by repeating the optimization procedures described in this thesis. If an analytical solution is not possible, one can try to compute the LODD sequences using HOPS or any other method which describes the dynamics of a qudit undergoing DD. As stated previously, a generalized LODD sequence for qudit could lead us to the generalization of the UDD sequence. This could then lead to the generalization of the QDD sequence.

More work should also concentrate on the utilization of dynamical decoupling in the context of implementing a high-fidelity quantum gate or state preparation protocol. This should be done by making use of the frameworks of Refs. [56, 85], each providing an exciting formalism for the construction of error-corrected quantum operations. Because HOPS captures the decoupling properties of a DD sequence and because any time-dependent Hamiltonian can be implemented in the solver, it is possible to use this method to verify some theoretical results.

Sequence	CPMG	UDD	LODD	OFDD
Pulses location	Equidistant pulses	Pulses location given by an analytical formula	Pulses location obtained by running an optimization algorithm to minimize the infidelity.	Sequences obtained by running an optimization algorithm to minimize the area of the filter function on a range $[0, \omega_D]$. Pulses then obtained by running a second optimization algorithm on the parameter ω_D to minimize the infidelity.
Parameters required	The period of the sequence	The duration of the protocol and the number of pulses	The duration of the protocol, the number of pulses and the spectral density	The duration of the protocol, the number of pulses and the spectral density (for the second optimization algorithm)
Pro's	• Simple scheme • Can be repeated periodically • Optimal for Lorentzian SD	• Simple scheme • Best filtering for low frequencies • Optimal sequence for short duration protocols with a high number of pulses	• Ultimately the most optimal sequence	• Near optimal • 1-dimensional algorithm for the infidelity instead of N-dimensional
Con's	• Only optimal for SD with a soft cut-off	• Progressively decreases in performance when applied periodically	• Requires a N-dimensional optimization algorithm on the infidelity • Depends greatly on the SD • Not optimal for periodic applications of DD	• Requires a N-dimensional algorithm on the filter function • Depends on the SD (although less than LODD [67])

Table 5.1: Summary of the SELDD sequences introduced in Chapter 3.

Appendix A

Moving to the Rotating Frame

Suppose that an Hamiltonian $H(t)$ governs the dynamics of a quantum system. In order to find the wave function $|\psi(t)\rangle$, one would need to solve the Schrödinger equation

$$i\hbar\frac{d}{dt}|\psi(t)\rangle = H(t)\,|\psi(t)\rangle\,. \tag{A.1}$$

However, this equation is often very complex and some tricks are sometimes needed to simplify the equation. One of those tricks consists in moving to the *rotating frame*. It consists of defining a unitary operator $R(t)$ that will account for a certain dynamic of the system. Having defined such unitary operator, we will define a new state $|\phi(t)\rangle$ as

$$|\phi(t)\rangle = R(t)\,|\psi(t)\rangle \tag{A.2}$$

or equivalently

$$|\psi(t)\rangle = R^\dagger(t)\,|\phi(t)\rangle \tag{A.3}$$

because the operator is unitary. In order to retrieve the state $|\psi(t)\rangle$ (which is the objective of the procedure), one now needs to find the time evolution of the new state $|\phi(t)\rangle$. Taking the time derivative of Eq.(A.2) leads to

$$i\hbar\frac{d}{dt}|\phi(t)\rangle = i\hbar\bigg(\frac{d}{dt}R(t)\,|\psi(t)\rangle + R(t)\frac{d}{dt}|\psi(t)\rangle\bigg). \tag{A.4}$$

We can use Eq.(A.1) and then replace all $|\psi(t)\rangle$ using Eq.(A.3) to end up with the equation

$$i\hbar\frac{d}{dt}|\phi(t)\rangle = \bigg[i\hbar\frac{d}{dt}R(t)R^\dagger(t) + R(t)H(t)R^\dagger(t)\bigg]\,|\phi(t)\rangle \tag{A.5}$$

which is nothing more than Schrödinger's equation for the state $|\phi(t)\rangle$ with the effective Hamiltonian $\tilde{H}(t) = \big[i\hbar\frac{d}{dt}R(t)R^\dagger(t) + R(t)H(t)R^\dagger(t)\big]$. By moving to the rotating frame, we thus constructed an effective Hamiltonian $\tilde{H}(t)$ which governs the time evolution of a state $|\phi(t)\rangle$. Then by applying $R^\dagger(t)$ to the state $|\phi(t)\rangle$, it is possible to find the state $|\psi(t)\rangle$ for which the time evolution is governed by the Hamiltonian $H(t)$. By choosing the appropriate unitary operator $R(t)$, it is sometimes possible to greatly simply the Schrödinger equation.

In particular, let us consider the Hamiltonian $H(t) = H_0(t) + H_1(t)$. The Schrödinger equation with respect to this Hamiltonian may be hard to solve and it might be simpler, in some cases, to consider the Hamiltonians $H_0(t)$ and $H_1(t)$ separately. This can be done by using the unitary operator

$$R(t) = U_0^\dagger(t, t_0) \tag{A.6}$$

with $U_0^\dagger(t, t_0)$ the time-evolution operator that corresponds to the dynamics generated by $H_0(t)$, which thus satisfies

$$i\hbar\frac{d}{dt}U_0(t, t_0) = H_0(t)U_0(t, t_0). \tag{A.7}$$

Having defined $R(t)$, we can calculate the effective Hamiltonian constructed by this rotation and we find that

$$\tilde{H}(t) = i\hbar\frac{d}{dt}U_0^\dagger(t,t_0)U_0(t,t_0) + U_0^\dagger(t,t_0)[H_0(t) + H_1(t)]U_0(t,t_0). \tag{A.8}$$

Using the equation equivalent to Eq.(A.7) for $U_0^\dagger(t,t_0)$ in order to simply the first term on the right-hand side of the equation above, we find that the first term cancels out with part of the second one, resulting in

$$\tilde{H}(t) = U_0^\dagger(t,t_0)H_1(t)U_0(t,t_0). \tag{A.9}$$

The problem was thus translated from the Schrödinger equation with the Hamiltonian $H(t)$ to the Schrödinger equation

$$i\hbar\frac{d}{dt}\left|\phi(t)\right\rangle = \tilde{H}(t)\left|\phi(t)\right\rangle \tag{A.10}$$

with $\tilde{H}(t) = U_0^\dagger(t,t_0)H_1(t)U_0(t,t_0)$.

Appendix B

Exponential of Pauli Operators

Let us consider $\vec{n}$ a unitary vector and $\vec{\sigma} = (\sigma_x, \sigma_y, \sigma_z)$ a vector containing all Pauli operators. Using the properties of the Pauli operators, one can calculate explicitly the exponential $\exp\{i\theta(\vec{n}\cdot\vec{\sigma})\}$ for any θ and any unit vector $\vec{n}$. Since the operator $\vec{n}\cdot\vec{\sigma}$ commutes with itself, the exponential can be expanded as follows

$$\exp\{i\theta(\vec{n}\cdot\vec{\sigma})\} = \sum_{n=0}^{\infty} \frac{i^n\theta^n}{n!}(\vec{n}\cdot\vec{\sigma})^n. \tag{B.1}$$

Since the Pauli operator are Hermitian and unitary, they satisfy the properties

$$\begin{aligned}(\vec{n}\cdot\vec{\sigma})^{2n} &= \mathbb{1}\\ (\vec{n}\cdot\vec{\sigma})^{2n+1} &= \vec{n}\cdot\vec{\sigma}\end{aligned}$$

for all $n \in \mathbb{N}$. Because of these properties, it makes sense to separate in Eq.(B.1) the odd and even terms, which leads to

$$\begin{aligned}\exp\{i\theta(\vec{n}\cdot\vec{\sigma})\} &= \sum_{n=0}^{\infty} \frac{i^{2n}\theta^{2n}}{(2n)!}(\vec{n}\cdot\vec{\sigma})^{2n} + \sum_{n=0}^{\infty} \frac{i^{2n+1}\theta^{2n+1}}{(2n+1)!}(\vec{n}\cdot\vec{\sigma})^{2n+1}\\ &= \sum_{n=0}^{\infty} \frac{(-1)^n\theta^{2n}}{(2n)!}\mathbb{1} + i\sum_{n=0}^{\infty} \frac{i^{2n}\theta^{2n+1}}{(2n+1)!}(\vec{n}\cdot\vec{\sigma}).\end{aligned} \tag{B.2}$$

Now the only remaining thing to do is to recognise that

$$\sum_{n=0}^{\infty} \frac{(-1)^n\theta^{2n}}{(2n)!} = \cos(\theta) \tag{B.3}$$

$$\sum_{n=0}^{\infty} \frac{i^{2n}\theta^{2n+1}}{(2n+1)!} = \sin(\theta) \tag{B.4}$$

which straightforwardly leads to the identity

$$\exp\{i\theta(\vec{n}\cdot\vec{\sigma})\} = \cos(\theta)\mathbb{1} + i\sin(\theta)(\vec{n}\cdot\vec{\sigma}). \tag{B.5}$$

Appendix C

Magnus Expansion

When confronted with a differential equation

$$\dot{U}(t) = A(t)U(t), \quad U(0) = U_0 \tag{C.1}$$

with $A(t)$ a $n \times n$ matrix, the solution

$$U(t) = e^{\int_0^t A(t')dt'} U_0 \tag{C.2}$$

no longer holds true in general when $n > 1$. In fact, it only does when the matrices $A(t)$ at different times commute, that is when $A(t_1)A(t_2) = A(t_2)A(t_1)\ \forall t_1, t_2$. In the most general scenario, the solution is then

$$U(t) = \mathcal{T}_{\leftarrow} e^{\int_0^t A(t')dt'} U_0 \tag{C.3}$$

with $\mathcal{T}_{\leftarrow}$ the time-ordering operator. The Magnus expansion expresses the solution of Eq.(C.3) as

$$U(t) = e^{\Omega(t)} \quad \text{with} \quad \Omega(t) = \sum_{k=0}^{\infty} \Omega_k(t). \tag{C.4}$$

and with the first terms of the Magnus series given by [90]

$$\begin{aligned}
\Omega_0(t) &= \int_0^t dt_1 A(t_1), \\
\Omega_1(t) &= \frac{1}{2} \int_0^t dt_1 \int_0^{t_1} dt_2 [A(t_1), A(t_2)], \\
\Omega_2(t) &= \frac{1}{6} \int_0^t dt_1 \int_0^{t_1} dt_2 \int_0^{t_2} dt_3 ([A(t_1), [A(t_2), A(t_3)]] + [A(t_3), [A(t_2), A(t_1)]]).
\end{aligned}$$

As one can see, the first term of the Magnus series is the argument of the exponential in Eq.(C.3), while the additional terms are corrections involving commutators of the Hamiltonian at different times. One can easily verify that if they commute, the solution of Eq.(C.3) is retrieved. A more extensive introduction to Magnus expansion can be found in Ref. [90].

Appendix D

Locally Optimized Dynamical Decoupling for More than Four Pulses

We showed in Section 4.3.2 the emergence of three regimes as we increase the number of applied sequences J, namely the *CPMG*, *UDD* and *LODD regime*. The data indicated that the CPMG regime shifts to smaller duration when J is increased, essentially extending onto the former UDD regime. Physically, that would mean that an optimal sequence of non-equidistant pulses, when applied periodically, eventually becomes less optimal than the CPMG sequence of equidistant pulses. The CPMG sequence, which did not appear as optimal originally, that is when a single sequence was consider, becomes an optimal choice over a wide range of protocol duration T when we wish to apply a DD sequence periodically. These results were obtained for four pulses, but it is interesting to take more than four pulses into consideration in order to generalize the results a bit more.

In order to do that, the first step is to construct once again FIG. 3.12 for different numbers of pulses N. We chose to focus on $N = 4$, 6 and 8 because increasing the number of pulses even more becomes more challenging computational-wise. The results are plotted in FIG. D.1. Notice that the horizontal axis had to be scaled as a function of the number of pulses because, as we kept increasing the number of pulses, the whole structure shifted to the right. This is of course easily explained by the fact that increasing the number of pulses increases the range $\omega_c T$ over which the sequence is effective, essentially shifting each LODD sequence to the right side of the plot, i.e. to a larger duration $\omega_c T$. Another adjustment that we made is the choice of the initial guess required by the algorithm; because Nelder-Mead is very sensitive to the initial guess, especially for high-dimensional optimization problems, choosing the CPMG sequence as the initial guess over the whole range $\frac{2}{N}\omega_c T$ lead to convergence issues in both extremities of the range. In order to avoid that, we chose the initial guess for the first iteration, i.e. for the smallest value of $\frac{2}{N}\omega_c T$, to be equal to the UDD sequence. For the following iterations, we chose as the initial guess the output of the previous iteration, i.e. the optimal sequence for a slightly shorter protocol duration. This prevents convergence issues and increases the efficiency of the algorithm.

Analyzing FIG. D.1, we can first notice that the LODD sequences as a function of $\frac{2}{N}\omega_c T$ for $N = 6$ and 8 exhibit a behavior similar to the one observed for $N = 4$: LODD asymptotically tends to UDD for short duration protocols, and as the duration increases the pulses tend to move closer to the center of the sequence while pairing up with one of its neighbour. At one point, the pulses, still paired up, start to move away from the center. For $N = 6$, we observe a breakdown of the symmetry of the control field; the two pulses closest to the center, still paired up, start to move away from the center by choosing a specific 'direction'. However, another run of the algorithm with slightly different parameters showed the pair choosing the other direction which leads us to believe that this is essentially an artefact probably caused by the finite accuracy of the integration over all frequencies in the definition of the decoherence function. Because the initial guess for the sequence is the output of the previous iteration, a significant enough fluctuation of the middle-pulses position due to numerical error can lead the following iterations to favor one direction over the other. Similar behaviors were observed in studying OFDD sequences in Section 4.3.3.

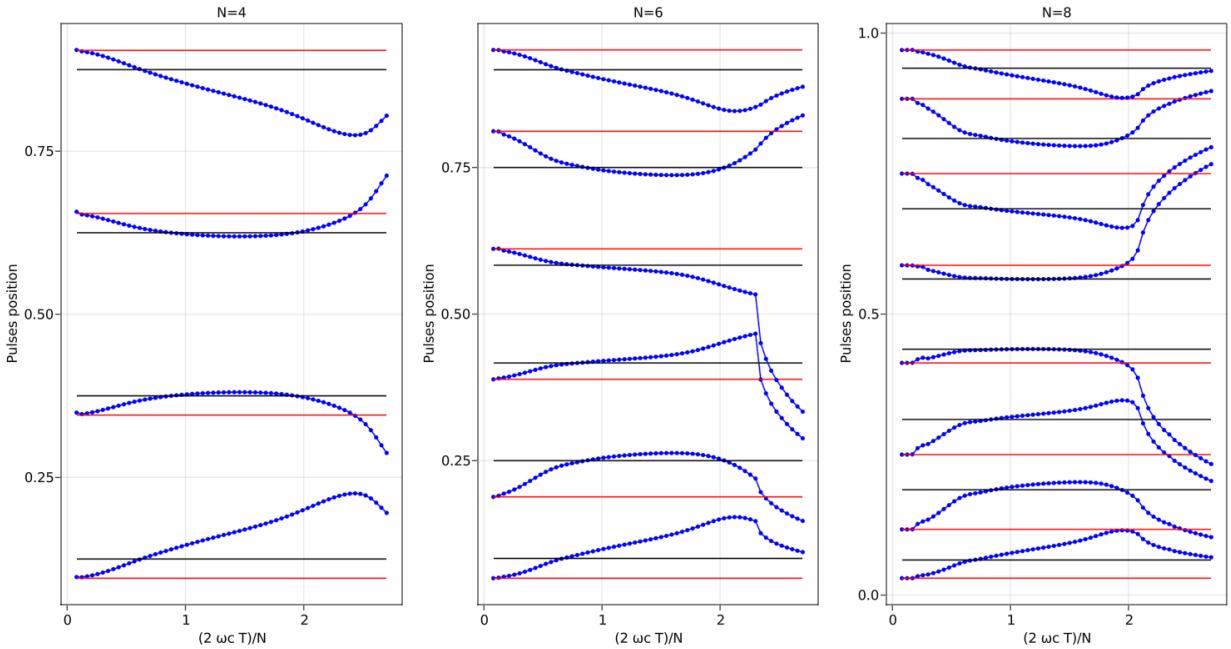

Figure D.1: LODD sequences for $N = 4$, 6 and 8. The horizontal axis has been scaled according to the number of pulses as $\frac{2}{N}\omega_c T$ and the vertical axis corresponds to the pulses location in time scaled with respect to the sequence's duration.

We plotted in Fig. D.2 our results for $\frac{2}{N}\omega_c T$ ranging from 0.08 to 0.9. The adaptive parameters[1] introduced in Ref. [65] were used for $N = 6$ and 8 in an attempt to increase the algorithm's performances.

We can now replicate the plot Fig. 3.17 for different number of pulses. Our results are plotted in Fig. D.3 for $N = 4$ (a), 6 (b) and 8 (c). The values of J chosen were $J = 1$, 5 and 25. Unfortunately, fine tuning the parameters and optimization of the initial guess as explained previously has not prevented the algorithm from suffering small fluctuations, likely due to numerical accuracy, for short duration sequences, especially for $J = 25$ and $N = 8$. Although the plots for $J = 5$ and $J = 25$ seem very similar for 6 and 8 pulses, a closer look on the data reveals that the sequences (for all periods T) keep moving from the UDD line to the CPMG line as J increases. These results indicate that the extension of the CPMG regime to the left occurs for larger numbers of pulses and we can now infer that this result can be generalized for any number N of pulses.

However, for the same value of J, the CPMG regime seems to shift to the right when N increases which seems to indicate that the UDD sequences are more "stable" when the number of pulses is larger. In other words, when applying a UDD sequence of 4 pulses J times might lead to a less efficient protocol than $4J$ equidistant pulses separated by Δt, applying a UDD sequence of $N > 4$ pulses J times can be more efficient than applying NJ equidistant pulses separated by the same Δt.

The conclusion of this Appendix is the following: any DD sequence of non-equidistant pulses, when applied periodically a sufficient number of times, is believed to become less efficient that the corresponding sequence of equidistant pulses, making the symmetrized CPMG sequence optimal when the DD sequence must be applied an unknown number of times. However, when the number of pulses in the sequence increases, the non-equidistant sequences are more stable in the sense that a greater number of sequences must be applied for the CPMG sequence to perform better. Although the analysis presented above is not a proof of the

[1]The adaptive parameters consists of a fine tuning of the Nelder-Mead parameters for which the values of these parameters change with the dimension of the optimization problem. According to Ref. [65], these parameters are expected to improve the algorithm's performance, which it did.

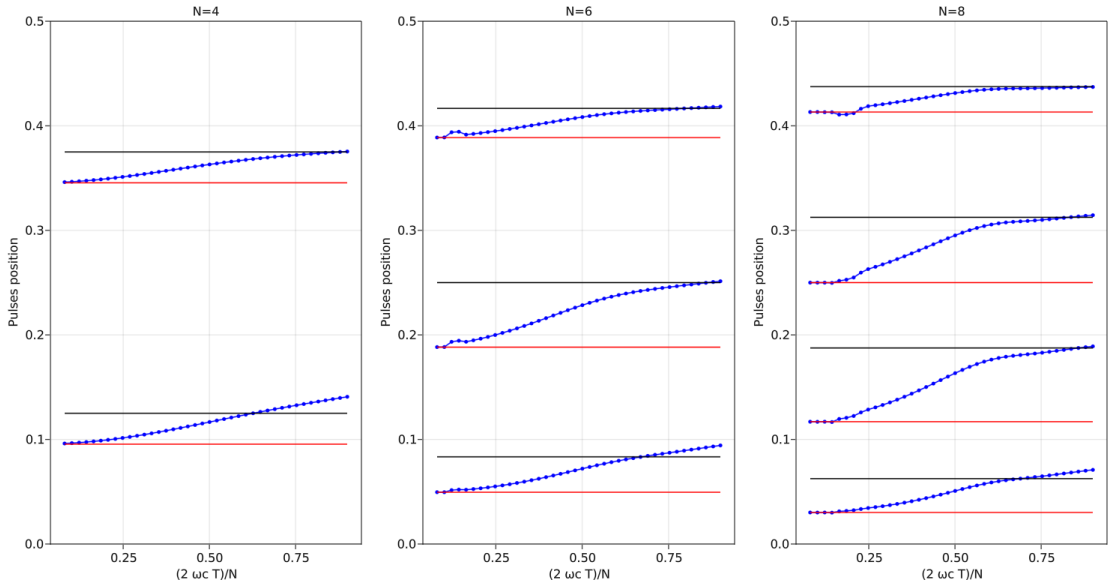

Figure D.2: LODD sequences for $N = 4$, 6 and 8.

previous statement, our results suggest that it is true for any number of pulses in the case of the SELDD sequence of decoupling group $\mathcal{G} = \{\mathbb{1}, \sigma_x\}$.

It could be interesting to do a similar analysis for MAXDD sequences, but a few complications have to be taken into account. The analytical derivation used to compute the coherence loss cannot be generalized for the case of the MAXDD protocol which means that more complex methods are necessary to compute the function to be minimized (coherence loss or infidelity). One can think about the state-of-the-art HOPS method which can be used to study complex DD sequences. However, because the HOPS method is stochastic and the infidelity is computed as a statistical mean over a finite number of iterations, the Nelder-Mead algorithm is likely to suffer from more convergence issues due to unsatisfactory accuracy. This would make the plots Fig. D.3 harder to construct as highly demanding simulation parameters would need to be chosen to obtain the sufficient accuracy. The other solution is to use a deterministic Quantum Master Equation (QME). However, QME for non-Markovian systems are considerably harder to derive.

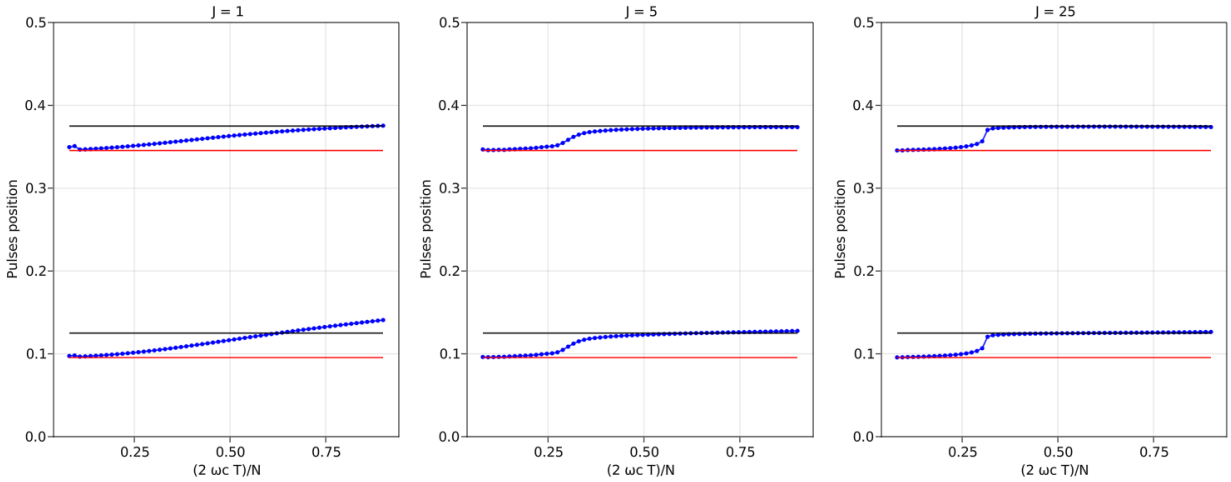

(a)

Figure D.3: LODD sequences for increasing number of pulses for 4 pulses (a), 6 pulses (b) and 8 pulses (c).

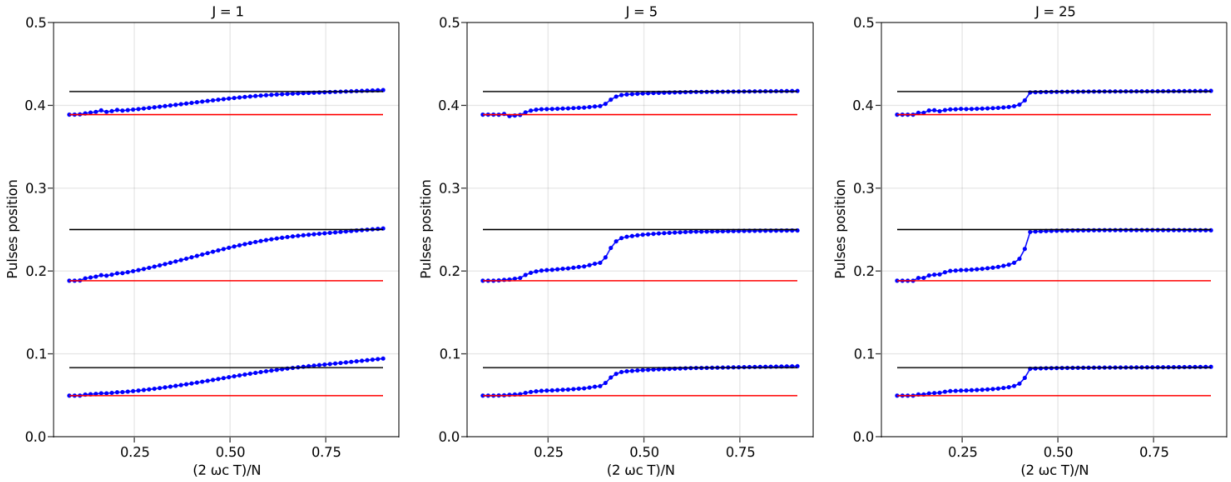

(b)

Figure D.3: LODD sequences for increasing number of pulses for 4 pulses (a), 6 pulses (b) and 8 pulses (c).

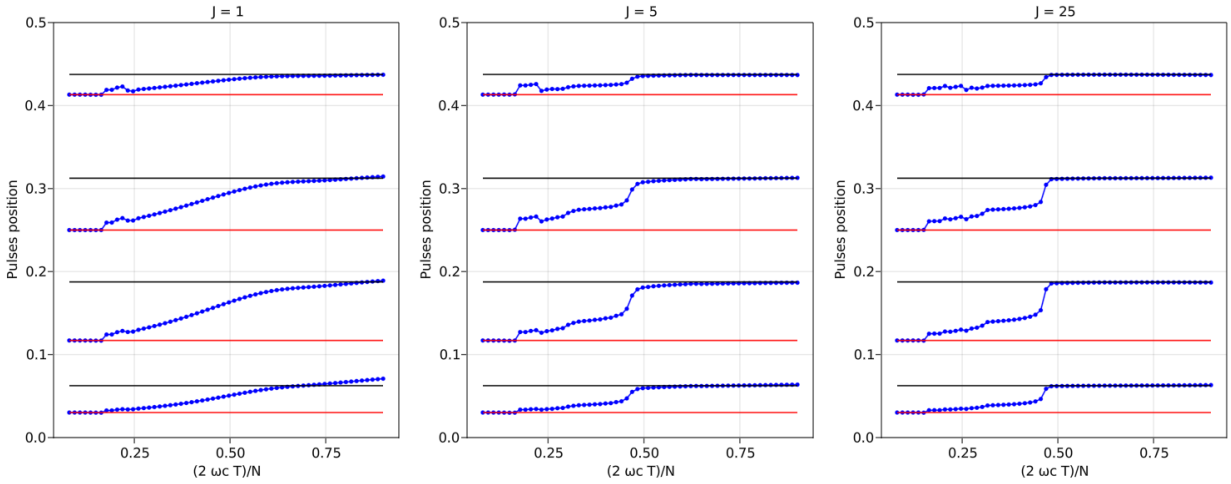

(c)

Figure D.3: LODD sequences for increasing number of pulses for 4 pulses (a), 6 pulses (b) and 8 pulses (c).

Appendix E

Convergence of the HOPS Method

As stated in Section 1.5.1, the numerical calculations performed using HOPS require three simulation parameters to be set, namely

- the number of auxiliary states $k_{\max}$,
- the number of timesteps for the numerical integration t_f/dt
- and the number of trajectories n_{traj}.

Before using the results obtained via the HOPS method, it is thus necessary to make sure that the results are converged with respect to these simulation parameters. The parameters are then chosen high enough to ensure a converged solution but as low as possible in order to lower the computational cost of the simulation. Such a convergence analysis can be found below for the dephasing qubit as well as the qubit undergoing the MAXDD sequences XY4, CXY4 and QDD.

E.1 Dephasing qubit

Firstly, we decided to fix the number of auxiliary states to $k_{\max} = 6$. This initial choice was based on some preliminary results indicating that six auxiliary states were enough to ensure a converged solution with respect to this parameter. We then converged the solution with respect to the three simulation parameters as follows:

(i) We set the number of timesteps to $t_f/dt = 6000$ and varied the number of trajectories. For each value of n_{traj}, we calculated the fidelity and the population of the excited state, which is supposed to stay constant. We then fixed n_{traj} accordingly.

(ii) We then varied the number of timesteps and calculated once again the fidelity and population of the excited state. We then fixed t_f/dt accordingly.

(iii) Finally, we varied the number of auxiliary states.

The results of the steps (i), (ii) and (iii) are presented in Figs. E.1a, E.1b and E.1c respectively. The results of (i) show that the number of trajectories seem already converged up to 10^{-2} for $n_{\text{traj}} = 700$. For the following calculations, we however decided to set n_{traj} equal to 1100. The results of (ii) indicate that the the number of timesteps can be fixed to 8000, which guarantee a converged solution up to 10^{-2} as well. We however decided to set t_f/dt equal to 10000. Finally, the results of (iii) demonstrate that the initial guess of $k_{\max} = 6$ ensures a converged solution with respect to the number of auxiliary states.

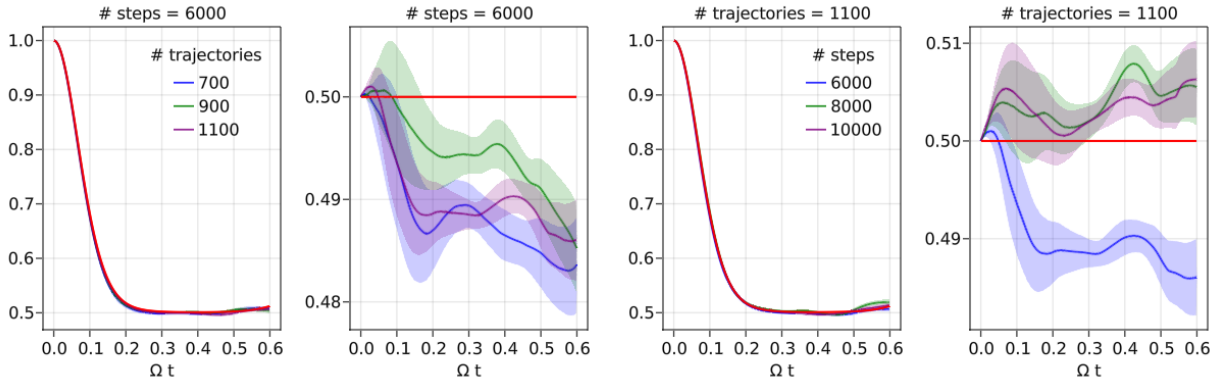

(a) Convergence on the number of trajectories

(b) Convergence on the number of timesteps

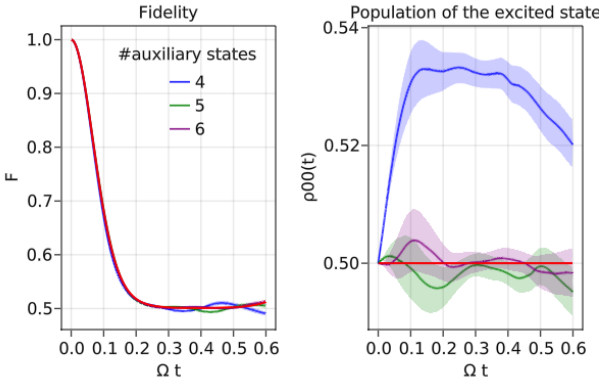

(c) Convergence on the number of auxiliary states

Figure E.1: Convergence of the HOPS results for the purely dephasing qubit. The exact analytical prediction is represented by a solid, red line.

E.2 Maximal dynamical decoupling sequences

We decided to fix the number of auxiliary states to $k_{\max} = 6$, as previous results indicated that six auxiliary states were sufficient to account for the non-Markovian dynamics of a dynamical decoupling sequence. Preliminary results also indicated that the number of trajectories $n_{\text{traj}} = 300$ already ensured a convergence of the solution. We thus decided to study the convergence with respect to the number of timesteps first. The results (displayed in Fig. E.2) indicate that the solution is converged up to 10^{-3} for a number of timesteps equal to 10000 for the XY4 sequence, whereas the solution is already converged to that order for a number of timesteps equal to 9000 for the other two sequences. We then fixed $t_f/dt = 10000$ and varied the number of trajectories (results displayed in Fig. E.3). While a number of trajectories equal to 500 is necessary to converge the solution up to 10^{-3} for the XY4 sequence, $n_{\text{traj}} = 300$ already ensures a convergence up to 10^{-3} for the CXY4 and QDD sequences.

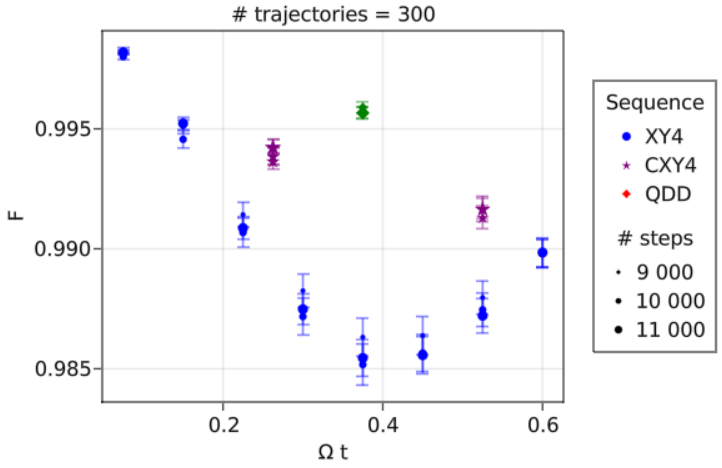

Figure E.2: Convergence on the number of timesteps.

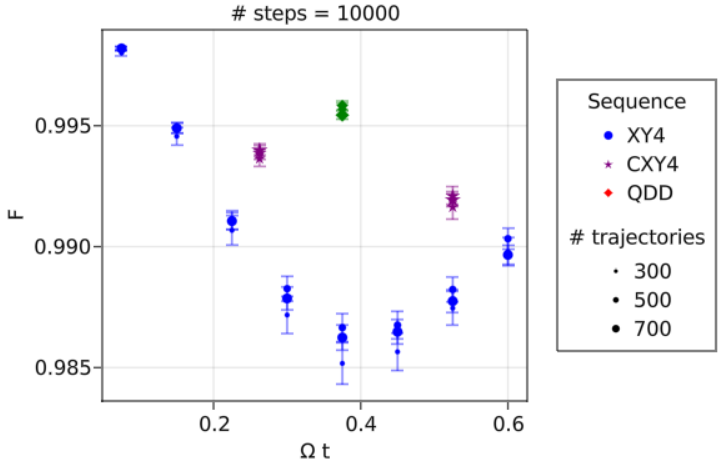

Figure E.3: Convergence on the number of trajectories.

Bibliography

[1] I. H. Deutsch, PRX Quantum **1**, 020101 (2020).

[2] J. P. Dowling and G. J. Milburn, Phil. Trans. R. Soc. A. **361**, 1655–1674 (2003).

[3] J. Martin, S. Weigert, and O. Giraud, Quantum **4**, 285 (2020).

[4] C. Chryssomalakos and H. Hernández-Coronado, Phys. Rev. A **95**, 052125 (2017).

[5] A. R. Shlyakhov *et al.*, Phys. Rev. A **97**, 022115 (2018).

[6] C. Portmann and R. Renner, Rev. Mod. Phys. **94**, 025008 (2022).

[7] K. M. Erhard M. and Z. A., Nat Rev Phys **2**, 365–381 (2020).

[8] M. A. Nielsen and I. L. Chuang, *Quantum Computation and Quantum Information: 10th Anniversary Edition* (Cambridge University Press, 2010).

[9] M. Schlosshauer, Physics Reports **831**, 1 (2019).

[10] M. Schlosshauer, Rev. Mod. Phys. **76**, 1267 (2005).

[11] H.-P. Breuer and F. Petruccione, *The Theory of Open Quantum Systems* (, 2002).

[12] G. Popkin, Science **354**, 1090 (2016), https://www.science.org/doi/pdf/10.1126/science.354.6316.1090.

[13] D. Gottesman, Stabilizer codes and quantum error correction, 1997.

[14] J. Roffe, Contemporary Physics **60**, 226 (2019), https://doi.org/10.1080/00107514.2019.1667078.

[15] B. M. Terhal, Rev. Mod. Phys. **87**, 307 (2015).

[16] E. T. Campbell, B. M. Terhal, and C. Vuillot, Nature **549**, 172 (2017).

[17] S. Kais, editor, *Quantum Information and Computation for Chemistry* (John Wiley & Sons, Inc., 2014).

[18] R. Babbush *et al.*, Phys. Rev. X **8**, 041015 (2018).

[19] B. A. Jung and M. Weigel, Journal of Magnetic Resonance Imaging **37**, 805 (2013), https://onlinelibrary.wiley.com/doi/pdf/10.1002/jmri.24068.

[20] L. Viola and S. Lloyd, Phys. Rev. A **58**, 2733 (1998).

[21] L. Viola, E. Knill, and S. Lloyd, Phys. Rev. Lett. **82**, 2417 (1999).

[22] J. Zhang and D. Suter, Phys. Rev. Lett. **115**, 110502 (2015).

[23] B. Naydenov *et al.*, Phys. Rev. B **83**, 081201 (2011).

[24] C. Piltz, B. Scharfenberger, A. Khromova, A. F. Varón, and C. Wunderlich, Phys. Rev. Lett. **110**, 200501 (2013).

[25] M. J. Biercuk *et al.*, Nature **458**, 996 (2009).

[26] S. S. Roy, T. S. Mahesh, and G. S. Agarwal, Phys. Rev. A **83**, 062326 (2011).

[27] X. Peng, D. Suter, and D. A. Lidar, Journal of Physics B: Atomic, Molecular and Optical Physics **44**, 154003 (2011).

[28] V. Tripathi *et al.*, Phys. Rev. Appl. **18**, 024068 (2022).

[29] M. Schlosshauer, The quantum-to-classical transition and decoherence, 2014.

[30] N. Ezzell, B. Pokharel, L. Tewala, G. Quiroz, and D. A. Lidar, Dynamical decoupling for superconducting qubits: a performance survey, 2022.

[31] D. Suess, A. Eisfeld, and W. T. Strunz, Phys. Rev. Lett. **113**, 150403 (2014).

[32] A. J. Leggett *et al.*, Rev. Mod. Phys. **59**, 1 (1987).

[33] F. Otterpohl, P. Nalbach, and M. Thorwart, Phys. Rev. Lett. **129**, 120406 (2022).

[34] D. P. DiVincenzo and D. Loss, Phys. Rev. B **71**, 035318 (2005).

[35] D. Porras, F. Marquardt, J. von Delft, and J. I. Cirac, Phys. Rev. A **78**, 010101 (2008).

[36] M. L. *et al.*, Nature Communications **9** (2018).

[37] A. Lemmer *et al.*, New Journal of Physics **20**, 073002 (2018).

[38] A. Cesa, (2019).

[39] Y.-C. Liang *et al.*, Reports on Progress in Physics **82**, 076001 (2019).

[40] B. Schumacher, Phys. Rev. A **51**, 2738 (1995).

[41] G. S. Uhrig, Phys. Rev. Lett. **98**, 100504 (2007).

[42] Ibm quantum lab, `https://quantum-computing.ibm.com`, Accessed : 13/04/2023.

[43] J. Larson and T. Mavrogordatos, *The Jaynes–Cummings Model and Its Descendants* (IOP Publishing, 2021).

[44] L. Dió si, N. Gisin, and W. T. Strunz, Physical Review A **58**, 1699 (1998).

[45] B. Hall, Journal of Functional Analysis **122**, 103 (1994).

[46] C. P. Robert and G. Casella, *Monte Carlo Integration* (Springer New York, New York, NY, 1999), pp. 71–138.

[47] L. Dió si, N. Gisin, and W. T. Strunz, Physical Review A **58**, 1699 (1998).

[48] T. Ma, Y. Chen, T. Chen, S. R. Hedemann, and T. Yu, Physical Review A **90** (2014).

[49] P. Zanardi, Physics Letters A **258**, 77 (1999).

[50] W. Yang, Z.-Y. Wang, and R.-B. Liu, Frontiers of Physics **6**, 2 (2010).

[51] J. R. West, B. H. Fong, and D. A. Lidar, Phys. Rev. Lett. **104**, 130501 (2010).

[52] M. J. Biercuk, A. C. Doherty, and H. Uys, Journal of Physics B: Atomic, Molecular and Optical Physics **44**, 154002 (2011).

[53] H. Uys, M. J. Biercuk, and J. J. Bollinger, Phys. Rev. Lett. **103**, 040501 (2009).

[54] M. J. Biercuk *et al.*, Nature **458**, 996 (2009).

[55] K. Khodjasteh and D. A. Lidar, Phys. Rev. Lett. **95**, 180501 (2005).

[56] K. Khodjasteh and L. Viola, Phys. Rev. Lett. **102**, 080501 (2009).

[57] J. R. West, D. A. Lidar, B. H. Fong, and M. F. Gyure, Phys. Rev. Lett. **105**, 230503 (2010).

[58] L. Viola and E. Knill, Physical review letters **90 3**, 037901 (2003).

[59] L. Viola, *Introduction to quantum dynamical decoupling* (Cambridge University Press, 2013), p. 105–125.

[60] W. Yang and R.-B. Liu, Phys. Rev. Lett. **101**, 180403 (2008).

[61] S. S. Roy, T. S. Mahesh, and G. S. Agarwal, Physical Review A **83** (2011).

[62] M. J. Biercuk *et al.*, Phys. Rev. A **79**, 062324 (2009).

[63] D. J. Szwer, S. C. Webster, A. M. Steane, and D. M. Lucas, Journal of Physics B: Atomic, Molecular and Optical Physics **44**, 025501 (2010).

[64] S. Singer and J. Nelder, Scholarpedia **4**, 2928 (2009), revision #91557.

[65] F. Gao and L. Han, Computational Optimization and Applications **51**, 259 (2012).

[66] H. Uys, M. J. Biercuk, and J. J. Bollinger, Phys. Rev. Lett. **103**, 040501 (2009).

[67] K. Khodjasteh, T. Erdélyi, and L. Viola, Phys. Rev. A **83**, 020305 (2011).

[68] W.-J. Kuo and D. A. Lidar, Physical Review A **84** (2011).

[69] G. Quiroz and D. A. Lidar, Phys. Rev. A **84**, 042328 (2011).

[70] X. Yang, Y. Ge, B. Zhang, and J. Li, Phys. Rev. Appl. **18**, 054075 (2022).

[71] P. Chen, Phys. Rev. A **73**, 022343 (2006).

[72] M. H. Levitt, *Composite Pulses* (John Wiley Sons, Ltd, 2007), , https://onlinelibrary.wiley.com/doi/pdf/10.1002/9780470034590.emrstm0086.

[73] A. M. Souza, G. A. Álvarez, and D. Suter, Phys. Rev. Lett. **106**, 240501 (2011).

[74] A. M. Souza, G. A. Álvarez, and D. Suter, Phys. Rev. Lett. **106**, 240501 (2011).

[75] D. Farfurnik *et al.*, Phys. Rev. B **92**, 060301 (2015).

[76] G. T. Genov, D. Schraft, N. V. Vitanov, and T. Halfmann, Phys. Rev. Lett. **118**, 133202 (2017).

[77] M. Cai and K. Xia, Phys. Rev. A **106**, 042434 (2022).

[78] F. Ticozzi and L. Viola, Phys. Rev. A **74**, 052328 (2006).

[79] G. A. Paz-Silva, S.-W. Lee, T. J. Green, and L. Viola, New Journal of Physics **18**, 073020 (2016).

[80] Z. Ji, P. Fan, and H. Zhang, Security proof for qudit-system-based quantum cryptography against entanglement-measurement attack, 2021, 2012.14275.

[81] T. Durt, D. Kaszlikowski, J.-L. Chen, and L. C. Kwek, Phys. Rev. A **69**, 032313 (2004).

[82] A. R. Shlyakhov *et al.*, Phys. Rev. A **97**, 022115 (2018).

[83] Y. Wang, Z. Hu, B. C. Sanders, and S. Kais, Frontiers in Physics **8** (2020).

[84] N. V. Vitanov, Phys. Rev. A **92**, 022314 (2015).

[85] R. d. J. Napolitano, F. F. Fanchini, A. H. da Silva, and B. Bellomo, Phys. Rev. Res. **3**, 013235 (2021).

[86] X. Yuan *et al.*, Phys. Rev. A **106**, 022412 (2022).

[87] H. Zhou *et al.*, Robust hamiltonian engineering for interacting qudit systems, 2023, 2305.09757.

[88] J. R. West, D. A. Lidar, B. H. Fong, and M. F. Gyure, Phys. Rev. Lett. **105**, 230503 (2010).

[89] Koch, Christiane P. *et al.*, EPJ Quantum Technol. **9**, 19 (2022).

[90] S. Blanes, F. Casas, J. A. Oteo, and J. Ros, European Journal of Physics **31**, 907 (2010).